GC-MS analysis of PFOA to investigate soil partitioning behavior and biodegradability under methane oxidizing conditions

Mats Ippach

Thesis submitted for the degree of
Master in Environmental Geoscience
60 credits

Institute of Geosciences
Faculty of mathematics and natural sciences

UNIVERSITY OF OSLO

Autumn 2021

GC-MS analysis of PFOA to investigate soil partitioning behavior and biodegradability under methane oxidizing conditions

Mats Ippach

GC-MS analysis of PFOA to investigate soil partitioning behavior and biodegradability under methane oxidizing conditions

1 Abstract

The objective of this study was to investigate the partitioning behaviour and potential biodegradability of perfluorooctanoic acid (PFOA) in different soils under laboratory conditions. An analysis of PFOA by gas chromatography mass spectrometry (GC-MS) was applied instead of the more expensive analysis by liquid chromatography tandem mass spectrometry (LC-MS/MS). The sample soils were examined regarding sedimentological and mineralogical characteristics, before abiotic partitioning experiments were performed to relate differences in the phase distribution of the contaminant to soil properties. Subsequently the resulting partitioning coefficients were applied for the evaluation of microcosmic biodegradation experiments in closed systems to investigate, if the recalcitrant pollutants can be degraded co-metabolically alongside the aerobic respiration of methane induced by indigenous microorganisms. The sampled soils were analyzed regarding their grain size distribution using a laser diffraction particle size analyzer, the content and composition of organic matter by dry combustion, and the mineralogical composition by performance of a powder X-ray diffraction analysis. Resulting soil properties were related to results of abiotic the partitioning experiments.

Two partitioning experiments were conducted, whereby one intended to investigate the phase distribution in one soil with increasing PFOA concentrations, while for the other one replica of the different soil samples were contaminated with equal concentrations. These latter concentrations correspond to the concentrations used in the biotic incubation experiments, whereby both setups are co-contaminated with perchloroethylene (PCE). This organic pollutant is known to be degraded cometabolically by aerobic methane oxidation. The co-contaminant PCE was analyzed by direct headspace injection into a GC-MS system. To analyse the PFAS concentrations, the porewater was extracted from the closed system experiments. Subsequently the chemical composition of the porewater was analyzed by ion chromatography and inductively coupled plamsa mass spectrometry. To be able to analyze PFOA using GC-MS, the contaminats were pre-analytically derivatized to the corresponding PFOA-anilide (after Li and Sun, 2020). During the incubation experiments the headspace composition was monitored by an automized gas chromatography system, to observe the content of methane and carbon dioxide.

Results of the study showed a successfull analysis of PFOA employing the GC-MS analysis with minor adjustments and implications for further improvement. A reliable quantification of biologically induced mass reduction was restricted by variations of derived equations for the partitioning behaviour. The variation were attributed to methodological compromises due to limited sample material. However, the results indicated reduced concentrations of PFOA for one biotic soil sample treated with methane compared to the corresponding abiotic and biotic control experiments. The attribution of the decreased concentrations due to abiotic or biotic processes was uncertain, but further investigation under application of suggested improvements for the methodological and analytical approach would be of interest.

2   Acknowledgement

Contents

List of Figures

8

9

List of Tables

3 Introduction

3.1 PFAS

Poly- and perfluoroalkylic substances (PFAS) describe a large and diverse group of synthetic chemicals with over 4000 known compounds (Sunderland et al., 2019), whose contamination of environmental compartments are of emerging global concern. Threats to the human health, the aquatic and the terrestrial environment arising from this group of organic pollutants in combination with their ubiquitous distribution indicate the urge for a final and sustainable remediation strategy (Sunderland et al., 2019; Teaf, Garber, Covert, & Tuovila, 2019; ITRC, 2021; Shahsavari et al., 2021). Their ubiquitous appearance results from unique phyico-chemical properties, which are also the cause for their wide variety of industrial and commercial applications since the early middle of the last century (Prevedouros, Cousins, Buck, & Korzeniowski, 2006). These properties desired in macroscopic applications are mainly attributed to their molecular structure - in particular the characteristic carbon-fluorine bonds. Hereafter, the physico-chemical properties and the resulting range of applications of the anthropogenic compounds are described and linked to their dynamic behaviour in the environment. Subsequentially the potential threats to humans and the environment together with recent regulations and proposed remediation approaches are depicted.

3.1.1 Nomenclature

PFAS are alkylic structures with at least one perfluorinated carbon atom and a polar head group. Structures in which all hydrogen atoms are substituted by fluorine atoms are referred as perfluorinated compounds and the ones with incompletely substituted alkylic chains are called polyfluorinated compounds (Sunderland et al., 2019; Teaf et al., 2019). The non fluorinated bonds in polyfluorinated compounds typically contain hydrogen or oxygen atoms covalently bonded in the carbon chain (Teaf et al., 2019). The hydrophobic carbon chain of varying length forms the non-polar moiety and the hydrophilic head group the polar moiety of these molecules. The carbon chain length of typical PFAS varies from 4 to 16 C-atoms with the characteristic C-F bonds (Sunderland et al., 2019). This covalent bond is the strongest in organic chemistry with a dissociation energy of $450 \frac{kJ}{mol}$ (Huang & Jaffé, 2019; Shahsavari et al., 2021). A consequence of the contrary (non-)polar properties of the chain and the head group is the amphiphilic character of the compounds (Shahsavari et al., 2021), which is one major aspect of their practical applicability, e.g. as surfactants and emulsifiers (Teaf et al., 2019). The high solubility in water and the formation of ions according to the functionality of the headgroup promotes their usage as surface active substances. Thereby, the ionic character of the head group is significant regarding the surface active behaviour. It determines, if the compounds can be protonated and form positively charged cations or deprotonates and form negatively charged anions, when in solution. A potential cationic functionality could be formed by the protonation of an ammonia group, while anionic head groups like from dissociated (deprotonated) sulfonic or carboxylic acid are more common in application and therefore more relevant (Wang, Cousins, Scheringer, Buck, & Hungerbühler, 2014; Shi et al., 2015;

Wang, Boucher, Scheringer, Cousins, & Hungerbuhler, 2017). The molecular structures for perfluorinated compounds with typical headgroups are depicted in Table 1.

Table (1)   Chemical structure perfluorinated compounds with typical headgroups.

carboxyl

sulfonic

sulfonamide
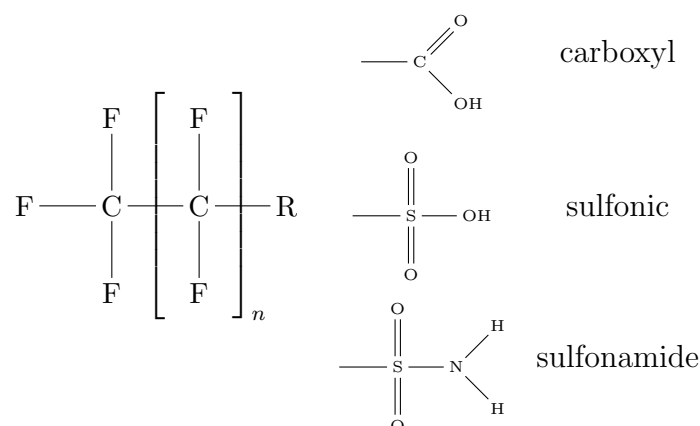
Most research has been focused on perfluorinated compounds with carboxylic or sulfonic headgroups (Sunderland et al., 2019), especially on perfluorooctanoic acid (PFOA) and perfluorooctane sulfonic acid (PFOS) (Teaf et al., 2019). A common classification of the numerous members of the PFAS family is introduced in the ITRC report from 2020, suggesting an organization regarding polymeric or non-polymeric structures, per- or poly-fluorinated chains, functionality of the headgroups and further heterofunctionalities (e.g. alcohol, ether) with a parallel classification as potential precursors. An overview of the classification scheme is illustrated in Figure 1.
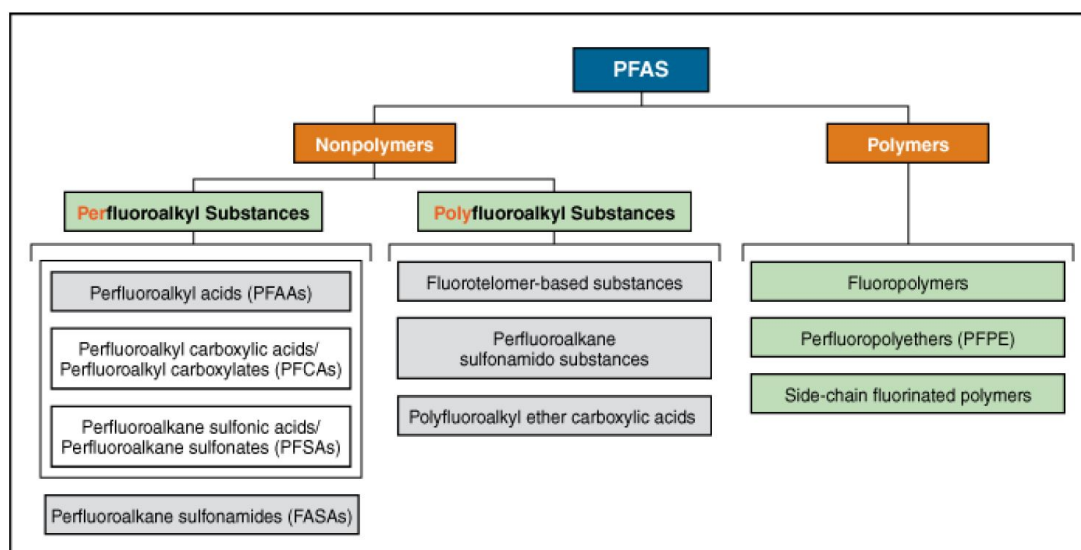
Figure (1)   Overview of the PFAS family with the corresponding nomenclature after Buck et al. 2011 (from ITRC report 2021, Figure 2-2; after Buck et al. 2011 and Wang, DeWitt et al. 2017).

The most studied classes of perfluorinated carboxylic acids (PFCA) and perfluorinated sulfonic acids (PFSA) are further distinguished by their length of the carbon chain. Both groups are differentiated in short-chained and long-chained compounds, whereby PFCA with $C \geq 7$, and PFSA with $C \geq 6$ are considered long-chained PFCA, respectively PFSA. Compounds with less total carbon atoms are considered short-chained.

For these a general sumformula of $C_nF_{2n+1} - R$ results, whereby the length of the carbon chain is indicated by n and R represents the head group. Additionally to the strong co-valent C-F bonds in the chain group, the carbon atoms are sterically shielded by the free electron pairs of the fluorine atoms, which cause a high thermal, chemical and biological resistance compared to non-fluorinated analogue hydrocarbons (Parsons, Sáez, Dolfing, & De Voogt, 2008; Montagnolli et al., 2017). The steric shielding prevents spatial proximity of potential reactants needed for biotic or abiotic chemical reactions. The consequen-tial persistance shows in required temperatures for thermal degradation up to 900 - 1100 °C, chemical inertness against conventional acids, bases, oxidants, reductants as well as resistance against photolytic, hydrolytic degradation, atmospheric photooxidation, and major biological metabolic degradation processes (Parsons et al., 2008; Teaf et al., 2019; Shahsavari et al., 2021). These major characteristics of PFAS are on the one hand their main qualities for the broad spectrum of applicability, but on the other hand also the key factor regarding their inertness against degradation, detoxification, and remediation leading to global accumulation in diverse environmental compartments (Ahrens, Hedlund, Dürig, Tröger, & Wiberg, 2016; Sunderland et al., 2019).

3.1.2   Sources and applications

After the group of PFAS was discovered in the 1930's, their production via electrochemical fluorination started in the late 1950's, followed by the increasing appearance in the in-dustry, consumer products, and thus in the environment in the 1960's (Prevedouros et al., 2006). The industrial manufacturing of PFAS was performed via two procedures: firstly by the mentioned electrochemical fluorination (ECF), secondly by telomerisation of tet-rafluorethylene (TM) (Parsons et al., 2008). The ability to analyze and quantify PFAS in environmental compartments is a more recent achievement, whereby first data of organic fluorine in human blood sera were published in the 1990's (Hansen, Clemen, Ellefson, & Johnson, 2001; Sunderland et al., 2019). Thereby the majority of monitored PFAS in hu-man and environmental compartments was attributed to the ECF-procedure (Hoff et al., 2003, 2004; Martin, Smithwick, et al., 2004; Martin, Kannan, et al., 2004), which is why this way of production was banned in North America and Europe in 2002 (Parsons et al., 2008). Eventhough, this phase-out of PFAS production (especially PFOS and its parent precursors) induced a subsequential decrease of observed PFAS in serum concentrations (Sunderland et al., 2019), PFAS are observed globally in variuous environmental com-partments. Studied environmental compartments reach from surface water, groundwater, soil, air even in Artic systems, to biological matrices like occasionally exposed humans, higher animals, microorganisms, plants and food crops (Martin, Smithwick, et al., 2004; Martin, Kannan, et al., 2004; Higgins, Field, Criddle, & Luthy, 2005; Ahrens, Barber, Xie, & Ebinghaus, 2009; Dreyer, Matthias, Weinberg, & Ebinghaus, 2010; Blaine et al., 2014; Rotander, Toms, Aylward, Kay, & Mueller, 2015; Sunderland et al., 2019). Further

investigations regarding the exposure of people not predestined due to their profession pointed out, that indoor air, house dust, drinking water, seafood and breastmilk are potential causes of enhanced PFAS levels in human (Houde, Martin, Letcher, Solomon, & Muir, 2006; Skutlarek, Exner, & Färber, 2006; Barber et al., 2007; Kärrman et al., 2007; Lau et al., 2007; Teaf et al., 2019; Sunderland et al., 2019). The widespread occurence of the anthropogenic compounds - without natural analogues - is caused by their production and application (Giesy & Kannan, 2001; de Voogt & Sáez, 2006) in a diverse field of industry and commercial products - mainly due to their tensidic properties and high solubility in water, in combination with their high thermal, chemical and biological resistance. In the industry PFAS are used in the manufacturing procedure, e.g. for plastics, polytetrafluorethylene (Teflon) and fluorochemicals, as components in fire-fighting foams, or as surfactants in the mining and oil industry (Moody & Field, 2000; Olsen et al., 2005; Teaf et al., 2019; Mahinroosta & Senevirathna, 2020; Bolan et al., 2021). Whereas in consumer products PFAS occur as surfactants in polishes, insecticides and pesticides as well as additives in stain-resistant coatings, food-wrapping paper products, non-sticking coatings for cookware and medical applications (Key, Howell, & Criddle, 1997; Renner, 2001; Darrow, Stein, & Steenland, 2013; Cheremisinoff, 2016; Yeung & Mabury, 2016). These sources might not contain perfluorinated substances, but could emit precursor compounds, which would eventually transformed to persistent pollutants for the environment by physical, chemical or biological degradation processes (Prevedouros et al., 2006; Liu & Avendaño, 2013; Y. Zhang et al., 2013; Butt, Muir, & Mabury, 2014; Anderson, Long, Porter, & Anderson, 2016; Munoz et al., 2017). An overview of the wide range of PFAS sources presenting potential introduction into ecosystems, and eventually forming potential exposure to human, are illustrated in Figure 2.

Figure (2) Overview of potential PFAS sources from typical applications and occurences (from Bolan et al. 2021; after Ghisi et al. 2019).

3.1.3 Distribution

The anthropogenic production and introduction of precursor and terminal PFAS in the environment together with the thermodynamical stability and biogeochemical inertness of latter lead to a dynamic global distribution resulting in accumulation in various ecosystems (Dreyer, Weinberg, Temme, & Ebinghaus, 2009; Ahrens et al., 2016; Sunderland et al., 2019). In late research the distribution pathways and mechanisms of terminal compounds like PFOA and PFOS have been under investigation, while little is known for the environmental fate of other (short-chained) PFAS (Sima & Jaffé, 2020). It is assumed, that the usage of PFAS in aqueous fire fighting foams (AFFF) on fire-fighting training areas, airports and military establishments is one of the major point sources into proximate soil and groundwater systems (Cousins et al., 2019; Bolan et al., 2021; Shahsavari et al., 2021). Besides these point sources, the introduction by diffusive transport from deposited consumer products, wastewater treatment plants (WWTP), and leakage of landfills into natural compartments is proposed (Sinclair & Kannan, 2006; Bolan, 2019). After Kannan et al. (2004), differences in the geographical distribution of PFAS levels in media (e.g. human blood serum) result from the spatial variability of source levels and corresponding exposure patterns. Thus, in order to localise and evaluate contamination sites the description of distribution processes and mechanisms, especially in the soil and aquatic compartments, is crucial next to the identification of the corresponding sources. Besides the quantitative correlation of contamination sites, the relation of PFAS occuring in human blood samples to environmental samples is a concern to face. An established approach performed for other contaminant classes (e.g. PCBs, PAHs) is chemometrics, which correlates the ratio of two chemical homologues in a biological samples to the corresponding ratio in an environmental sample (Sunderland et al., 2019).

To describe the distribution behaviour of compounds between different phases (e.g. solid, aqueous, gaseous) their preferential partitioning behaviour is evaluated. This mainly depends on the molecular physico-chemical properties of a specific compound, which eventually determine macroscopic properties like volatility, solubility, sorption, coordinated complexation and persistence (Prevedouros et al., 2006). Preveduoros et al. (2006) describes the physical partitioning behaviour of PFOA as a representative compound of the group of perfluoralkylic acids, while it is differentiated between the dissociated (ionic) form and the non-dissociated (molecular) form of the compound. For example is the vapour pressure for the dissociated form neglectable but significant (eventhough small) for the molecular form (after Prevedouros et al., 2006). Regarding the solubility, it is assumed that the molecular form is less soluble than the ionic form, whereby the solubility of both forms is significantly affected by the ability to form micelles (Prevedouros et al., 2006). The formation of micelles results from the amphiphilic properties of the molecules. This causes, that if sufficient PFAS are present in an aqueous (polar) solution, the hydrophilic functionalities to orientate towards the surrounding solution, while the hydrophobic head groups orientate towards another and from spheric micelles. The micelle formation depends on concentration and temperature and is described by the Krafft point and the critical micelle concentration, which gives a critical concentration depending on the temperature, after which the formation of micelles occurs and the solubility increases significantly (Prevedouros et al., 2006; Hellsing, Josefsson, Hughes, & Ahrens, 2016; ITRC, 2021). For the ionic form of PFOA the critical micelle concentration

is reported with 3.7 $\frac{g}{L}$ with the Krafft point of 20 °C (Nakayama, 1967). Variations of this phenomena can also occure, if surfaces charged contrary to the ionic headgroup are present (Figure 3).
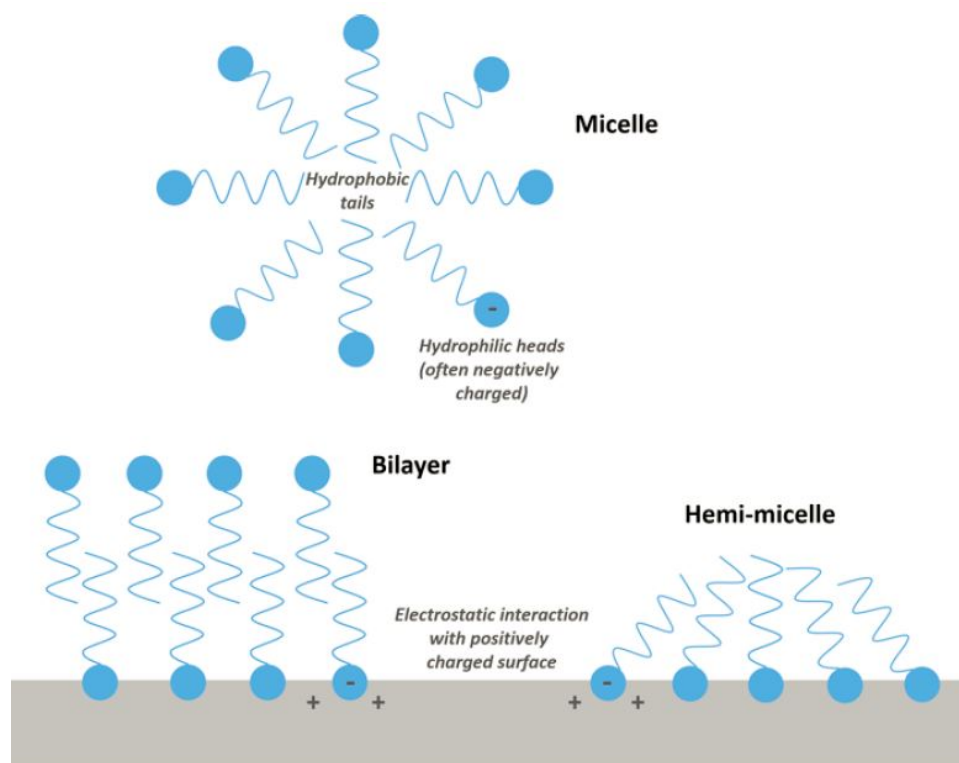
Figure (3) Micelle formation of amphiphilic PFAS molecules in polar solution or in polar solution and surface interaction (from ITRC report 2021, figure 5-2; after D. Adamson, GSI).

Due to the differences in physical properties of the ionic and molecular form, the pH plays an important role regarding the physical behaviour. But in environmental systems the pH is mostly higher than the acid dissociation constant pK_a (e.g. for PFOA, see Figure 4), which indicates the anionic form is dominant under environmental conditions. At a neutral pH of 7 it is estimated, that the abundance of the dissociated species is about 5 magnitudes higher than the molecular one, while at pH 4 the relative portion of the latter one is estimated to make around 6 % (Prevedouros et al., 2006). Due to the dominance of the dissociated form under environmental pH conditions, the volatility of PFOA itself can be neglected, whereas the transport via aerosols is possible.

The partitioning behaviour in a porous medium like soil are determined by the individual properties of PFAS, properties of the solid phase and environmental factors (Milinovic, Lacorte, Vidal, & Rigol, 2015). The totality of these cumulative factors define the dynamics of PFAS in the subsurface by affecting the retention in the soil occuring as sorption and complexation onto the solid phase (D. Zhang, Zhang, & Liang, 2019).
The compound specific characteristics are the chain length, the specific head group and the resulting solubility (Milinovic et al., 2015). Eventhough the wide variety of PFAS
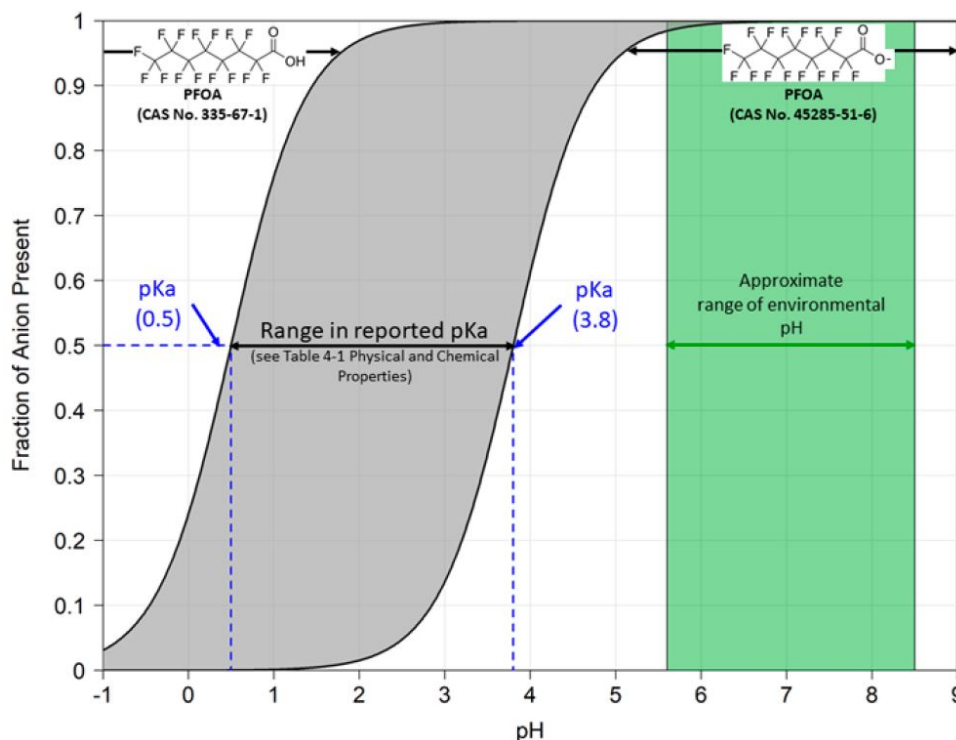
Figure (4) Speciation of aqueous PFOA as acid dissociation constant by titration curve depending on pH (from ITRC report 2021 figure 4-1; after E. DiFilippo, S.S. Papadopulos & Associates, Inc.).

compounds, some tendencies and mechanism resulting from the compound structure regarding the partitioning behaviour are derivable. As illustrated for PFOA as a representative PFCA, most PFAS occur as their ionic species under environmental pH conditions. This implies an affinity towards contrary charged mineral surfaces, like for clay minerals, oxides and hydroxides or alumina. Because the majority of produced PFAS form anions, especially oxidated grain surfaces (e.g. ironoxides and -hydroxides) and aluminia interact with the dissolved PFAS anions, while the clay minerals with a negative surface charge would repel these anions electrostatically (Hellsing et al., 2016; ITRC, 2021). Besides the polar interaction with solids, PFAS also show hydrophilic behaviour due to the nonpolar chain group (Darlington, Barth, & McKernan, 2018; Ross et al., 2018). This shows in the preferred sorption to organic matter in the soil, whereby this tendency increases with the length of the fluorinated chain and with the content of particulate organic matter (Milinovic et al., 2015; Brusseau, 2018; Bolan et al., 2021). Whether the polar or the nonpolar behaviour is dominant is mainly determined by the polarity of the (dissociated) headgroup relative to the lenght of the nonpolar chain. Furthermore, under low pH conditions, functional groups of present organic matter can electrostatically interact with the headgroup of PFAS compounds (e.g. protonated carboxy, amino, hydroxy or sulfidic functional groups). Eventually the partitioning onto the solid phase by complexation with divalent cations (e.g. Ca^{2+}) coordinated as ligands between negatively charged surfaces (clay minerals) is suggested by (Ross et al., 2018; Y. Li, Oliver, & Kookana, 2018). The

occurence of such complexes on negatively charged surfaces depends on the present pH and the ionic strength of the corresponding solution. The mechanisms are depicted in Figure 5 from Li et al. 2018b as the hydrophobic interaction of the chain group with organic matter, the complex coordination onto the soil surface with divalent cation serving as ligands, and the electrostatic interaction of the dissociated headgroup with positively charged mineral surfaces, protonated organic matter functionalities or oxides.
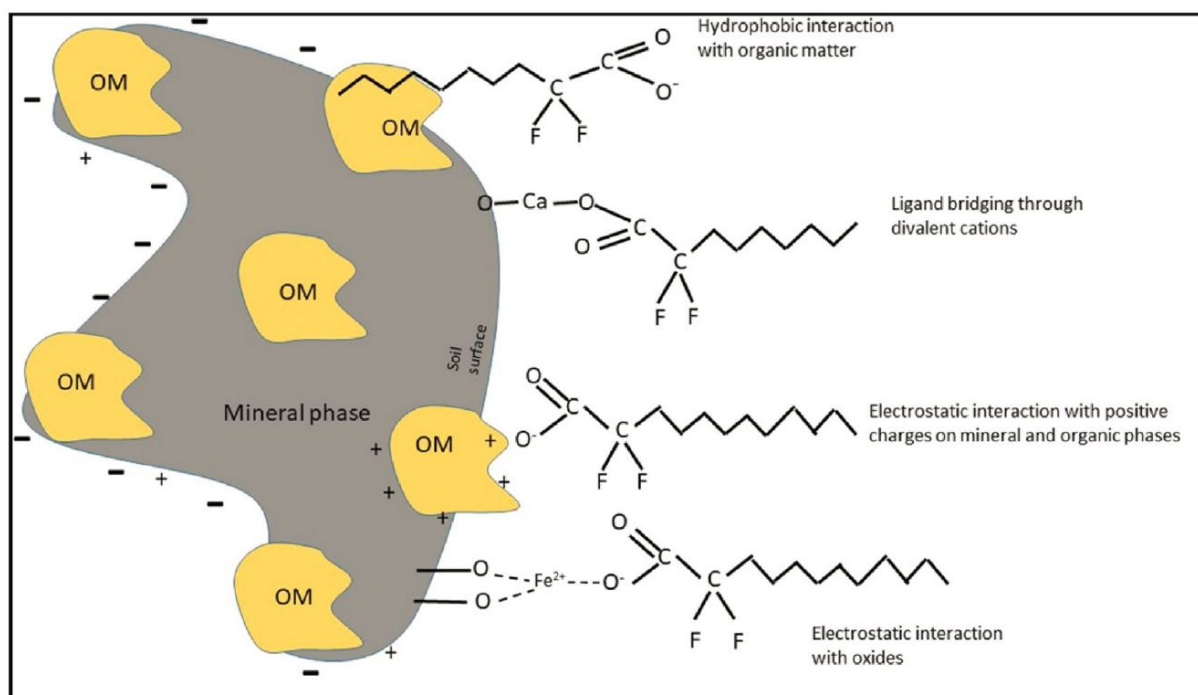
Figure (5) Suggested sorption mechanisms of PFAS onto sediments and soil surfaces from aqueous solution, shown for perfluorinated carboxylic acids (illustration from Li et al. 2018b).

Especially the adsorption onto organic matter can immobilize long-chained PFAS from pore- or groundwater, but due to the relative high solubility in water compared with other organic pollutants (e.g. PAH, PCB) the removal is mostly temporarily (Post, Gleason, & Cooper, 2017). Thus, temporal adsorption onto the solid phase in the subsurface just causes retention of PFAS transport, but does not serve as a longterm sink. Depending on the interplay of environmental conditions and soil composition, the retention can differ for long- and shortchained PFAS. This can be derived from the weaker hydrophobic properties of shorter chained PFAS, whereas the mechanisms resulting from the polar headgroup (e.g. higher solubility, physical sorption to charged surfaces, coordination in complexes) dominate the partitioning behaviour. This leads to less retention of short chained PFAS ($C < 7$), causing a higher mobility in the subsurface, and vice versa for long-chained PFAS. Thus, light PFAS tend to distribute faster in the environment, while the heavy PFAS threaten a longterm pollution on a contaminated sites due to slow desorption. Whereas the higher mobility increases the long-distance transport ability of the persistent contaminants, the longterm exposure of a polluted site encourages the potential of bioaccumulation (Vierke, Möller, & Klitzke, 2014; Milinovic et al., 2015; Shahsavari et

al., 2021).

Besides the longterm exposure the (bio-)tranformation of co-occuring precursor compounds as an indirect source increases the capacity of bioavailability. That is especially applicable for perfluorinated substances, whose precursors can mainly be classified as PFAS as well, while they do not have a fully fluorinated carbon chain or contain other functionalities (e.g. fluorinated side-chains, fluorotelomers, ether functional headgroups; see Figure 7) (Parsons et al., 2008; Liu & Avendaño, 2013; Shahsavari et al., 2021). Thereby, biotic and abiotic degradation processes transform precursor compounds into thermodynamically more stable secondary chemicals. Various aerobic, anoxic and anaerobic biodegradation mechanisms of various precursor compounds are described in the literature as well as abiotic processes (Ellis et al., 2004; Liu, Lee, Nies, Nakatsu, & Turco, 2007; Parsons et al., 2008; Liu et al., 2010; Liu & Avendaño, 2013; Zhao et al., 2017). The terminal degradation products are most often thermodynamically more stable perfluorinated compounds, which contribute as an indirect source to the totality of these anthropogenic pollutants.
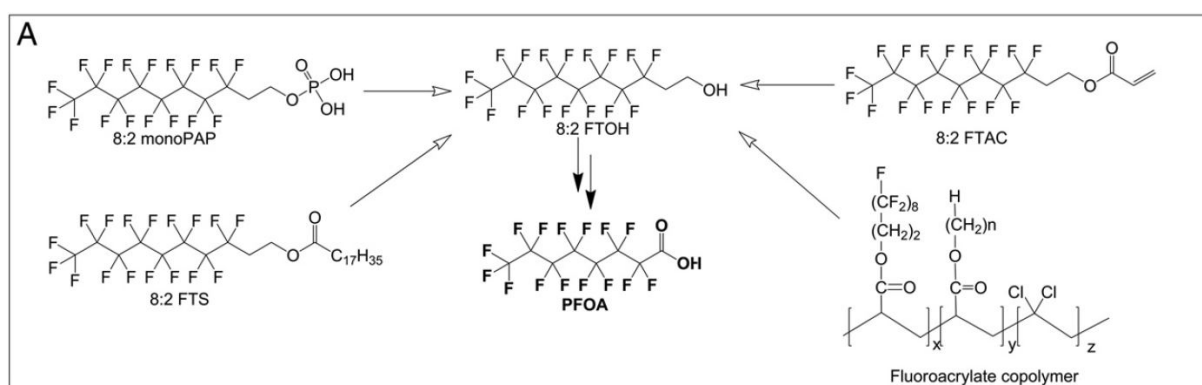
Figure (6) Illustration by Liu and Mejia Avendaño (2013) indicating 8:2 fluorotelomer and derivatives as precursors of PFOA (from Liu and Mejia Avendaño (2013), Fig. 1).

The global occurence of PFAS in most environmental compartments like surface water, soil, sediments, snow, ice and biota even in remote areas indicates the capability of long-range transport, which can mostly be attributed to their persistence under environmental conditions. It is suggested that the main long-range transport mechanisms from direct anthropogenic sources are atmospheric transport and carriage by ocean currents of PFAS and corresponding precursors (Ellis et al., 2004; Wania, 2007; Armitage et al., 2009; De Silva, Muir, & Mabury, 2009). The introduction of PFAS into the ocean can occur via direct discharge of rivers, surface waters, precipitation or deposition of atmospheric particles, after which the compounds are transported with the currents. The mechanisms of air transport are complex, but it can be distinguished between volatile precursor compounds and PFAS sorbed to airborne particles. In the atmosphere the PFAS can are transported with the wind over short or long ranges (ITRC, 2021).

3.1.4 Bioaccumulation and toxicity

The ubiquitous distribution of PFAS and therefore the bioavailability causes a global occurence of these compounds in animals, whereby the bioaccumuluation potential tends to increase with increasing chainlength (Shahsavari et al., 2021) and biomagnification along the foodchain is suggested (Kelly et al., 2009). Due to the high water solubility, especially aqueous animals are affected, which is why seafood is discussed as a main exposure for humans as well (Sunderland et al., 2019). While the global significance of seafood as a major exposure pathway is discussed, it's communicated that dietary pathways are the exposition cause for PFAS in humans (Sunderland et al., 2019; Teaf et al., 2019). Thereby, the exposure to contaminated drinking water often correlates to the proximity of a drinking water source to a PFAS related industry (Parsons et al., 2008; Sunderland et al., 2019). Furthermore, the exposure via contaminated food (especially seafood) and food packing materials is considered to be significant. Besides dietary pathways, the accumulation of PFAS in indoor air and dust is considered to be a significant source. The accumulation in food can be related to the usage of contaminated sewage sludge from wastewater treatment plants as fertilizer in agriculture (Sunderland et al., 2019). These contaminated biosolids allow the transfer of PFAS into plants along the intake of water via the roots. The accumulation in plants and crops depends on the PFAS chainlength determining, if the polar or non-polar character dominates (Bolan et al., 2021). Thereby, short-chained, polar PFAS are rather transported along the pathway of water in a plant from the roots to the leaves, where the accumulated due to low volatility, whereas long-chained PFAS rather accumulate in the rootsystem.

The contribution of these exposure pathways to the accumulation of PFAS in human is often related to the proximity to a industrial PFAS source, depends on the frequency of contact and the specific toxicological parameters (species-specific toxicokinetics) of the contaminants (Sunderland et al., 2019). In epidemiological studies of exposed human and animals, enhanced PFAS concentrations in the blood serum are related to diseases and health threats like cancer of the liver and testicles, chronic kidney disease, increased serum cholesterol, decreased birth weight, alteration of hormone-receptor (estrogen, androgen) and immune functions (Starling et al., 2017; Sunderland et al., 2019; Teaf et al., 2019; Shahsavari et al., 2021). The accumulation of PFAS in the serum protein albumin and the liver, no metabolism of perfluorinated compounds, and the potential of carcinerogenic effects on humans are results mostly agreed in relevant literature (Sunderland et al., 2019; Teaf et al., 2019; Shahsavari et al., 2021). The well studied PFAS representative PFOA is considered to be not genotoxic nor mutagenic, while its classified as "possibly carcinogenic to humans" (IARC; respectively "suggestive evidence of carcinogenic potential of PFOA in humans" by USEPA, 2016b) (Barry, Winquist, & Steenland, 2013; Agency, 2016; for Research on Cancer, 2016; ITRC, 2021).

3.1.5 Restrictions and remediation

Monitoring of the specific PFAS observed in serum concentrations over the last decades indicate a global decrease, which implies the effectiveness of implemented restrictions since the early 2000's like the phase-out of PFOS and its precursors in industrial usage (Sunderland et al., 2019). However, the industrial usage mainly shifted to other, often shorter-chained PFAS, which are less frequently monitored in human serum and the environment. Sunderland et al. (2019) proposes, that the restriction of PFOS and PFOA successfully decreases their occurence in human and environment, but the substitutional PFAS do not just replace them in industrial use, but also in the risk exposure for humans and environment. Further, the toxicological effects and the environmental fate of substitutional PFAS (e.g. PFHxS, PFHxA, and GenX) is less studied and understood (Sima & Jaffé, 2020).

TABLE 1: State and US Environmental Protection Agency guidelines for PFAS in drinking water[a]

	Long chain (ng/L)							Short chain (ng/L)			
	PFOA	PFOS	PFNA	PFHxS	PFHpA	PFDA	Total	PFBA	PFHxA	PFBS	GenX
No. of carbons	8	8	9	6	7	10		4	6	4	6
USEPA	70	70	—	—	—	—	Yes (2)[b]	—	—	—	—
CA	10	40	—	—	—	—	No[c]	—	—	—	—
CT	70	70	70	70	70	—	Yes (5)[b]	—	—	—	—
MA	20	20	20	20	20	20	Yes (6)[b]	—	—	2000	—
MI	8	16	6	51	—	—	No	—	400 000	420	370
MN	35	15	—	47	—	—	No	7000	—	2000	—
NH	12	15	11	18	—	—	No	—	—	—	—
NJ	14	13	13	—	—	—	No	—	—	—	—
NY	10	10	—	—	—	—	No	—	—	—	—
NC	—	—	—	—	—	—	—	—	—	—	140
OH	70	70	21	140	—	—	Yes (2)[d]	—	—	140 000	700
VT	20	20	20	20	20	—	Yes (5)[b]	—	—	—	—
WA	10	15	14	70	—	—	—	—	—	1300	—

[a]Proposed and final standards and guidelines as of May 2020. States not listed generally use US Environmental Protection Agency Health Advisories for perfluorooctanoic acid (PFOA) and perfluorooctane sulfonate (PFOS).
[b]Guideline applies to total concentration of long-chain per- and polyfluoroalkyl substances (PFAS) shown (number of PFAS included in total).
[c]Guidelines apply to each long-chain PFAS individually.
[d]Guideline of 70 ng/L applies to total concentration of PFOA and PFOS. Other guidelines apply to individual PFAS.
PFNA = perfluorononanoic acid; PFHxS = perfluorohexane sulfonate; PFHpA = perfluoroheptanoic acid; PFDA = perfluorodecanoic acid; PFBA = perfluorobutanoic acid; PFHxA = perfluorohexanoic acid; PFBS = perfluorobutane sulfonate; GenX = hexafluoropropylene oxide-dimer acid; CA = California; CT = Connecticut; MA = Massachusetts; MI = Michigan; MN = Minnesota; NH = New Hampshire; NJ = New Jersey; NY = New York; NC = North Carolina; OH = Ohio; VT = Vermont; WA = Washington.

Figure (7) Drinking water guidelines for PFAS by American States and by US Environmental Protection Agency, Table from G. B. Post (2021).

Even though, the more restrictions for PFAS are established with decreasing concentration limits, the persistence of the pollutants in the environment challenges the remediation of contaminated sites. While several conventional remediation methods like pump and treat or soil vapor extraction are not effective (Teaf et al., 2019), more cost intensive methods show some success like the adsorption to granular activated carbon, reverse osmosis (high pressure filtration), advanced chemical oxidation/reduction, washing of contaminated soil or thermal destruction (Shahsavari et al., 2021). Effective approaches often have a significant disadvantage, like just ex situ application for reverse osmosis, inconsistency for short-chained PFAS of GAC adsorption, intensive use of chemicals for advanced oxidation/reduction or significant expanses for soil washing (Bolan et al., 2021; Shahsavari et al., 2021). Furthermore, most approaches target the remediation of groundwater and do

not result in a mass reduction of the contaminant, but in an highly contaminated residual, which has to be deposited in a landfill site (Shahsavari et al., 2021).

3.1.6 Bioremediation

An alternative in-situ approach would be biodegradation, which was successfully applied in the past for other contaminants like BTEX, PAHs, and halogenated pollutants like PCBs and chlorinated ethenes (Wiedemeier, Rifai, Newell, & Wilson, 1999; Sabaté, Vinas, & Solanas, 2004; Weathers, Harding-Marjanovic, Higgins, Alvarez-Cohen, & Sharp, 2016; Horváthová, Lászlová, & Dercová, 2018; Ge, Huang, Han, & Jaffé, 2019; Murray et al., 2019). Thereby, the organic contaminants are degraded by microorganisms (MO) during metabolic reactions, where the carbon containing pollutants can be targeted as carbon source, as oxidizing agents of the metabolic reaction (electron acceptors) or degraded co-metabolically. Due to the strength of the covalent C-F bond in PFAS, the dissociation of the bond in a biological reaction requires to be catalyzed by enzymes to occur. These enzymes would induce a break of the C-F bond by addition of oxygen (oxidation) or the addition of electrons (reduction) (Shahsavari et al., 2021). Comparable processes have been observed for other halogenated pollutants of concern like chlorinated ethenes or PCBs, eventhough the thermodynamic stability of the C-F bond in PFAS exceeds the carbon-chlorine bond in chlorinated contaminants (dissociation energies: C-F bond 450 $kJ\,mol^{-1}$, C-Cl bond 330 $kJ\,mol^{-1}$ (Parsons et al., 2008)). The occurence of these processes can mostly be related to the involvement of certain enzymes, which catalyze the energy-gaining dehalogenation reaction, like reductive dehalogenase (metabolic reduction of chlorinated carbons), methane monooxygenase (co-metabolic degradation of PCE during aerobic methane oxidation), or aerobic and anaerobic oxidation (Wiedemeier et al., 1999; Grandel & Dahmke, 2008; Buttet, Willemin, Hamelin, Rupakula, & Maillard, 2018; Ge et al., 2019; Shahsavari et al., 2021). For the degradation of PFAS, especially perfluorinated compounds, the number of studies of a successful observation of biodegradation is small (see Shahsavari et al. 2021) and all examine experiments performed on a laboratory scale. Nevertheless, these laboratory experiments offer important insights regarding the substainable (mass reduction) in-situ remediation of PFAS in a simple and cost-efficient manner.

3.1.7 Analytical methods

The analysis of PFAS from different matrices is usually performed by high-performance liquid chromatography-tandem mass spectrometry (HPLC-MS/MS) resulting in highly sensitive and selective results (Dufková, Čabala, Maradová, & Štícha, 2009; Washington, Henderson, Ellington, Jenkins, & Evans, 2008; Z. Li & Sun, 2020). The high performance analysis is quite cost intensive and it's availability is limited, which limits the possibility for extensive PFAS studies, thus data acquisition opportunities. Alternatively an analytical approach using a gas chromatographic system, which are more available, less expensive to maintain and operate, is applied in several studies for the analysis of PFAS (Scott et al., 2006; Washington et al., 2008; Dufková et al., 2009; Z. Li & Sun, 2020). This

method requires a pre-analytical derivatization of the non-volatile target compounds in more volatile derivates, whereby different chemical transformation reactions are suggested (e.g. esterfication, amidification) (Scott et al., 2006; Z. Li & Sun, 2020).

3.2 Idea and Objective

The objective of this study is to investigate the co-metabolic degradability of PFOA (as a well studied representative of PFAA) during aerobic oxidation of methane in different soil samples in enclosed systems on a laboratory scale.

The idea originated from the studies of Huang and Jaffe (2019) and Ge et al. (2019), which investigated the cometabolic biodegradation potential of the Feammox reaction induced by Acidimicrobium sp. strain A6 regarding PFOA and PFOS (Huang & Jaffé, 2019), respectively PCE and TCE (Ge et al., 2019). Both studies state to observe a significant mass reduction of the corresponding pollutant of interest during the biologically induced oxidation of ammonium to nitrite while reducing ferric iron (Feammox) in form of a co-metabolic dehalogenation (defluorination, respectively dechlorination). These results imply the involvement of one or more specific enzymes, which are able to catalyze the Feammox reaction as well as the dehalogenation of the contaminants. Ge et al. (2019) describes the identification of two oxygenase related genes in the incubation experiments with 92-93% similarity to particulate methane monooxygenases (pMMO), which is also present in the genome of the autotroph Acidimicrobium sp. strain A6. Due to the complex isolation of the Acidimicrobium sp. A6 and the specific conditions to induce the Feammox reaction, the applicability of a biodegradation approach for halogenated pollutants is limited (Ge et al., 2019). But as stated in several biodegradation studies of chlorinated compounds, Ge et al. (2019) states the importance of various oxygenases enzymes in these co-metabolic, aerobic dehalogenation processes (examples Ge et al. 2019).

To test the cometabolic biodegradation of perfluorinated compounds under aerobic methane oxidizing conditions in soils, samples of agricultural topsoil, the topsoil and the B-horizon from a core sample of a forrested area were trained to consume methane under aerobic conditions in a closed system. Subsequentially the samples should be contaminated with PFOA and PCE for the incubation period with continued methane supply. Thereafter, the porewater, respectively the gas phase, is analyzed for the contaminants' concentrations and results of the biotic samples under methane treatment are compared to biotic control samples (without methane) and results of abiotic partitioning experiments. In combination with analyses of the soil properties, the partitioning experiments allow a correlation of the solid phase partitioning of PFOA with corresponding soil properties to derive corresponding dependencies.

Furthermore, the porewater analyses for PFOA were performed using a GC-MS system with pre-analytical derivatization to corresponding anilides (using Li and Sun, 2020; after Scott et al., 1998, 2002, 2006), which presents a cost-effective alternative to the conventional LC-MS/MS analysis of PFCA. Results are examined regarding their reliability and applicability.

24

3.3 Soil samples

Three different soil samples will be investigated in this study, which were choosen due to significant differences regarding expected soil properties of interest and relevance of implications from experimental results.

Agricultural soil The first sample originates from a topsoil of an agricultural test field of the Norwegian University of Life Sciences (NMBU) at Aas in southeast Norway. The soil originiates from the comparative study of Nadeem et al. 2020 investigating the effect of liming acidic soils with calcareous (conventional) and siliceous material regarding N_2O emission rates by ammonium oxidizing microorganisms. The sample used in this study originates from an agricultural soil, which was limed with calcite (Nadeem, Bakken, Frostegard, Gaby, & Dörsch, 2020). The soil is described as clay loam, which has been under rotational crop use since 1953 (Nadeem et al., 2020). Due to the agricultural usage, a high biological activity induced by the frequent application of fertilizers is expected. The results regarding the PFAS experiment are of interest, due to the potential dietary exposure pathway of humans from contaminated agricultural soils directly via crops or indirectly via farm animals. The soil characteristics of interest are the sedimentological clay loam composition, the expected high concentrations of nutrients and the content of organic matter resulting from annual usage in agriculture.

Forrest soil The second and third soil sample originate from a core sample taken by Lars-André Erstad from a forrested area in Nesbyen municipality (WGS 84: 32 W 0509508; 6709478 - elevation: 236 m) in Viken county, Norway at the 30th September 2019. The sampling area is a planted pine forrest, which is about 60 years old. The last time the underwood has been cut was around 20 years ago. On the ground a lot loose tree part are present.

The soil horizons occuring in the 30 cm core are described in the field with an occuring O-horizon from 0-10 cm, followed by an E-horizon 10-15 cm, and a B-horizon from 15-30 cm. Subsequential a C-horizon occurs, which was not sampled in the core (personal correspondence L.-A. Erstad). After the core was taken it has been stored in the freezer at $-21°C$ until it was further processed.

The sampled soil is characterized as a podzol soil, which is the most commonly occuring soil under the climatic conditions. The soil is characterized by a organic rich to-player, which can be followed by a leached E-horizon due to high biological acitivity inducing acidic condition by carbon dioxide emission and the presence of humic acids. The dissolved mineral constituents of the E-horizon precipitate in the subsequential oxic B-horizon, which is often characterized by iron-oxide/-hydroxide precipitates giving the horizon a characteristic brown-reddish colour. In a typical soil profile, the B-horizoon is followed by the bedrock, respectively C-horizon. As this forrest soil profile is highly abundant in Norway under cool humid climates (Lundström, van Breemen, & Bain, 2000), the abiotic and biotic behaviour of PFAS in the different horizons is of general interest. Furthermore, common sites of PFAS contamination are airports and military bases due to the frequent application of AFFF, which are commonly located in or proximate to forrest areas. The investigation of PFAS behaviour in the soil profile can give implications

regarding preferred accumulation, further fate and transport and resulting remediation approaches.

The properties of interest in the core sample are the high content of organic matter in the top and the presence of iron-oxide and -hydroxide coatings in the bottom of the core. Due to the limited amount of material from the core and the interest in properties of the top and the bottom of the core, two merged soil samples were prepared from the present horizons. One core soil sample represents the top soil and results from blending the forrest floor material, the O-horizon and some material of the E-horizon (hereafter soil sample 2). This sample contains very high content of organic material with a dominating sandy mineral fraction. The other core sample results from blending the E-horizon and the iron-coated B-horizon and is further referred to as the bottom core (hereafter soil sample 3). The leached E-horizon was split between the samples to ensure sufficient material of the top and bottom soil is available for following experiments, especially for the partitioning and incubation experiments.

The resulting three soil samples are firstly the agricultural clay loam soil expected to contain an enhanced amount of major nutrients (nitrate, phosphate), secondly the forrest top-core soil with high content of fresh organic material and a sandy mineral moeity, and thirdly the sandy, forrest bottom-core soil with visually low content of organic material, but coatings of ironoxide and -hydroxide. The expected soil properties are investigated by analyzing the grain size distribution, the content and composition of organic matter, and the mineralogical composition. Due to the high content of organic matter in the second soil, subsamples for the analysis of the mineralogical composition were taken from the E- and B-horizon, before the horizons were blended. Investigating the soil characteristics and relating them to results of the partitioning and incubation experiments will give insights regarding the accumulation potential, respectively mobility, and partitioning mechanisms of PFAS.

4 Method

4.1 Soil Characterization

4.1.1 Pretreatment and subsampling

The agricultural soil sample and the separated horizons from the core sample were spread out to dry partially to reduce the moisture content, while coarse organic material like small stick and roots were removed. Thereafter, all samples were sieved manually using a sieve of 2 mm meshsize to ensure no larger particles to be present and homogenize the samples. Subsamples for the mineralogical XRD-analysis were taken from the agricultural soil 1, from the E- and the B-horizon of the core sample. Subsequentially the individual core horizons were merged as described in the previous section to receive samples of sufficient material representing the organic rich core top and the iron-coated core bottom. From the resulting three soil samples, subsamples for the biotic incubation experiments were taken and stored in sealed bags in a fridge at $4\,^{\circ}C$ to ensure the biological activity of the samples will be minimal, while the microorganisms are preserved until the biodegradation experiments. The remaining soil sample material was dried in an oven for 24 h at $60\,^{\circ}C$ to prepare them for the soil property analyses and the abiotic partitioning experiments. Hereafter, the semi-quantitative analysis of the mineralogical phase using powder X-ray diffraction (pXRD), the determination of the grain size distribution by laser diffraction particle size analysis (LPS), and the quantitative and qualitative analysis of organic matter via loss of ignition (LOI) and organic element analysis (OEA) for the different soil samples are described before the experimental design of the partitioning and incubation experiment are illustrated.

4.1.2 Mineralogical Composition by XRD

Method The mineralogical composition of the anorganic moeity of a soil can affect its physico-chemical properties like the water retention or ion exchange capacity significantly. One of the most common methods for the qualitative and semi-quantitative analysis of mineral phases in solid samples is X-Ray Diffraction (XRD) (respectively Powder X-Ray Diffraction, hereafter used synonymously) besides conventional optical crystallographic methods like microscopy of thinsections. The XRD analysis is based on the scattering of X-rays on atoms of the crystal structures of the present minerals. The constructively interferring scattered X-rays contain information about the spacing between the crystallographic layers. By detection of these scattered X-rays and knowledge of the incident wavelength and the incident angle, the spacing between the atomic layer can be computed according to Bragg's law (Bragg & Bragg, 1913):

$$2d * \sin\theta = n * \lambda$$

Bragg's law describes the interaction of electromagnetic waves with periodically arranged atoms in a crystal lattice. Thereby, the spacing between two approximately parallel crystallographic layers corresponds to d (also d-spacing), while the incident radiation is described by its wavelength λ and the incident angle θ. The integer n described the

condition for constructive interference of the dispersed X-rays, after scattering on atoms of different crystallographic layers.
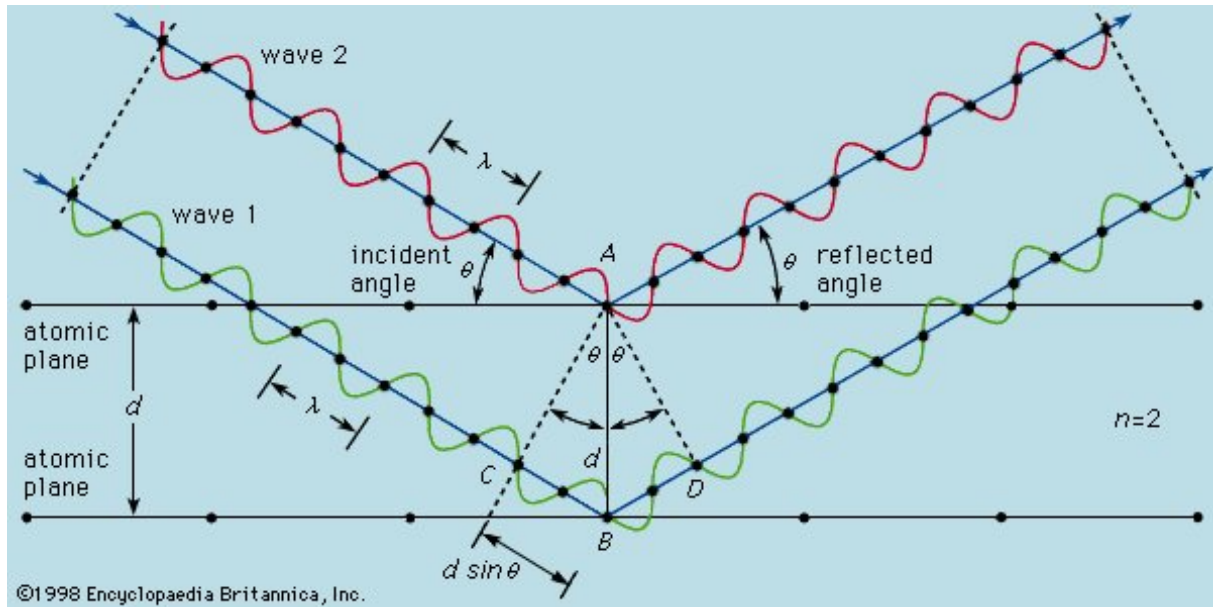
Figure (8) Schematic geometry of diffraction of X-rays on crystal lattice fulfilling condition for constructive interference after Bragg's law (from Encyclopedia Britannica, 2021).

The integer implies, that if the difference of travelpaths of rays of the sample incident angle scattered on different crystallographic planes is equal to a multiple of the rays wavelength, constructive interference occurs (Chauhan & Chauhan, 2014). It is important, that the wavelength of the incident X-rays is conserved during the scattering, which allows the geometrical derivation of Bragg's law illustrated in Figure 8.
The analysis of the bulk composition of the mineral phase of the abiotic subsamples from soil 1, the E-horizon and the B-horizon of the core samples, was performed on a X-ray diffractometer D8 Advanced of the company Bruker equipped with a LynxEye detector using nickel filtered $Cu - K_\alpha$ radiation in the Geological Department of the University of Oslo. Hereafter the sample preparation and analysis are described.

Preparation and Analysis To analyze the mineralogical bulk composition of the samples, the grain size of the samples is homogenized by two successive milling steps. The bulk subsamples were dried in an oven for 24 h at $60\,^\circ C$, before each sample was dry milled at 40 Hz for two minutes in a rock mill to get an average grain size of $\leq$ 0.5 mm. Subsequently the grain size of the samples is further decreased by wet-milling (micronizing) to approximately 10 μm. Therefore, the 3 g of the pre-milled sample is transferred into a milling beaker filled with agate milling stones with 9 ml ethanol. The sample is micronized for ten minutes in a McCrone Micronizing Mill, before the ethanol suspension is collected and the milling beaker rinsed with 3 ml ethanol. The collected suspension is dried in an oven overnight at 60 $^\circ C$. The dried sample is transferred onto

a hard plastic XRD-sample holder, whereby the sample is compacted and a homogenically flattend surface created without causing a prefered orientation of the minerals. Subsequently the samples are analyzed in the D8 Advanced X-ray diffractometer over a diffraction angle range up to $2\theta = 65\,^\circ$. The resulting diffractograms are analyzed using the XRD-analysis software Profex. The analysis software performs a Rietveld refinement based on the BGMN program to identify and quantify mineralogical phases present in the samples (Doebelin & Kleeberg, 2015). Mineral phases are identified using XRD-pattern literature (Pei & Chen, 1977) and a software internal "search/match"-function. By importing instrument specific setting the acquired results are compared to an internal library. Computed synthetic diffractograms are compared to the corresponding measured ones and evaluated based on the sample background and statistical parameters.

4.1.3 Grain Size Distribution by LPS

Method To determine the volumetric grain size distribution of the soil a Beckman Coulter LS13 320 Laser Diffraction Particle Size Analyzer at the Geological Department of the University of Oslo was used. The instrument measures the intensity of a diffraction pattern resulting from monochromatic light dispersing during the transmission through a suspended soil sample, allowing the quantification of the relative grain size distribution within a range from 0.4 to 2000 μm. The diffraction angle of the light on a particle in solution depends on it's size, which is why the measurement of the intensity of the diffraction pattern correlates to the relative abundance of corresponding grain sizes in the sample. Under the assumption of constant density, approximated sphericity, and homogeneity regarding optical properties of analyzed grains, the results are comparable to conventional mass-based analysis like sieving. As a textural property the grain size distribution affects geochemical and hydrological characteristics of a soil, like sorption potential, ion exchange capacity, surface reactivity as well as storage capacity and hydraulic conductivity.
To presume optical homogeneity, the soil samples have to be pretreated as described in the following paragraph. The samples analyzed are the agricultural soil 1, the merged top-core sample soil 2 and the merged bottom-core sample soil 3.

Preparation and Analysis Even though just a small amount of material is required for the analysis, a representative subsample of 10 g was taken from the soil samples. The dried and pre-sieved subsamples of the soil samples meet the instrumental particle size limits. But due to significant differences of optical properties of organic matter and minerals, the organic moeity of the samples has to be removed. Therefore a 30-% hydrogenperoxide solution was used to dissolve the organic material under formation of CO_2 without affecting the mineral constituents significantly. The absence of degassing CO_2 indicates the complete dissolution of organic matter, after which the solution was neutralized and subsequently dried at 60°C in an oven. Because the optical properties of salts also differ significantly of the ones of other minerals, their absence after the evaporation can be ensured by resuspending the dried sample in distilled water and dry it again.

From the dry sample a representative subsample is taken, whereby the required amount of subsample depends on the dominant grain size and can vary from 0.2 g to 2 g for diameter medians from 10 μm to 600 μm. To disintegrate all grains of a subsample (especially the fraction $< 50\ \mu m$) 5 to 10 ml of a 5-% sodium-hexametaphosphate solution $((NaPO_3)_6$ in $H_2O)$ are added to the sample and the suspension is placed in an ultrasonic shaker for 5 minutes. Subsequently, the sample suspension is directly poured in the sample vessel of the instrument, the beaker is rinsed with distilled water to ensure the transfer of the whole sample. If the relative obscuration between the incident beam and the detected light amounts 10-12 %, sufficient sample material for the analysis is in suspension. Before an analysis run the instrument has to be internally auto-aligned and inbetween each sample the background should be measured. To validate the results two replica of each sample are analysed and the grain size distribution of a sample is computed as a mean of these replica as well as corresponding statistical values based on the momentum-method (after Blott and Pye, 2001).

4.1.4 Organic Element Analysis by OEA & LOI

The partitioning behaviour of organic contaminants in the subsurface is significantly determined by the content of organic matter (OM) present. The term organic matter is vaguely defined, but generally describes all mattter in the subsurface that is or has been alive. Due to large variance in molecular mass and structural complexity of OM, most analysis are limited to the total quantification or the quantification of the integrated chemical composition of OM. Common methods for these measurements are based on dry combustion, whereby the total amount of OM can be derived from the Loss of Ignition (LOI), while the integrated chemical composition can be measured by an Organic Element Analysis (OEA) (Chatterjee, Lal, Wielopolski, Martin, & Ebinger, 2009). Both analytical methods were performed for all soil samples to be compared and are described hereafter.

Loss of Ignition (LOI) The determination of the content of organic matter by the loss of ignition is based on the thermal decomposition of the organic moeity (Rather, 1918; Mitchell, 1932). For the analysis a representative subsamples of the soils are taken and pre-dried at $105\,^{\circ}C$ overnight, before the thermal decomposition of the organic matter takes place in a ventilated muffle furnace at $550\,^{\circ}C$ for 3h. After each temperature treatment the samples are immediately placed in a desiccator filled with hygroscopic, granular silica to avoid re-moisturing of the sample from the atmosphere. After the samples cooled down, their exact weight was determined using a microscale. The mass loss during the high temperature treatment indicates the oxidation and volatilization of the organic moeity in the sample and is used to compute the relative content of OM. Thereby, it is assumed that the mass loss solely results from the complete decomposition of organic material, with constant carbon content in the sample (no internal sinks/sources). These presumption already imply insecurities resulting from additional mass loss due to further volatilization reactions. Especially the presence of carbonates, hydrated salts and (clay-)minerals containing structural water can cause an overestimation of the OM-content. Therefore, the LOI results will be compared with the results of the organic element analysis, described subsequently.

Organic Element Analysis (OEA)   The Organic Element Analysis (OEA) is an integrated quantitative method to distinguish the contribution of the main constituents of the OM composition, namely carbon, nitrogen, hydrogen, sulfur and oxygen. The method is based on dry combustion of the sample in an oxygen-supplied atmosphere under high temperatures with subsequent detection of the gaseous oxidated products. A precisely weighed sample wrapped in a tin crucible is combusted at 950°C under a constant flow of carrier and supply gas (helium and oxygen). Because of the high temperature and the oxic environment, the tin crucible reacts heavily exothermic with the oxygen to tin dioxide, which increases the effective combustion temperature of the sample to approximately 1800°C. The high temperature ensure the complete transfer of all organic components into the gaseous phase as their corresponding oxides. Susequently the combustion products are transferred to a packed reactor containing copper oxide and electrolytic copper to unify various oxide species present by reduction and to trap the excess oxygen. The reduced combustion products are carried on by the helium gas flow towards a chromatographic column, which separates the analytes according to the retention in the column. Then, the separated gases elute from the gas chromatograph after characteristic retention times to a thermal conductivity detector. The detector converts the amount of combustion products into an electric signal. By measuring standards and blanks, the detected signal of the samples can be converted to a corresponding mass of analyte. Normalizing the mass to the exact mass of the sample, the relative portion of the corresponding organic element in the sample can be computed. The analytical principles are depicted in Figure 9.
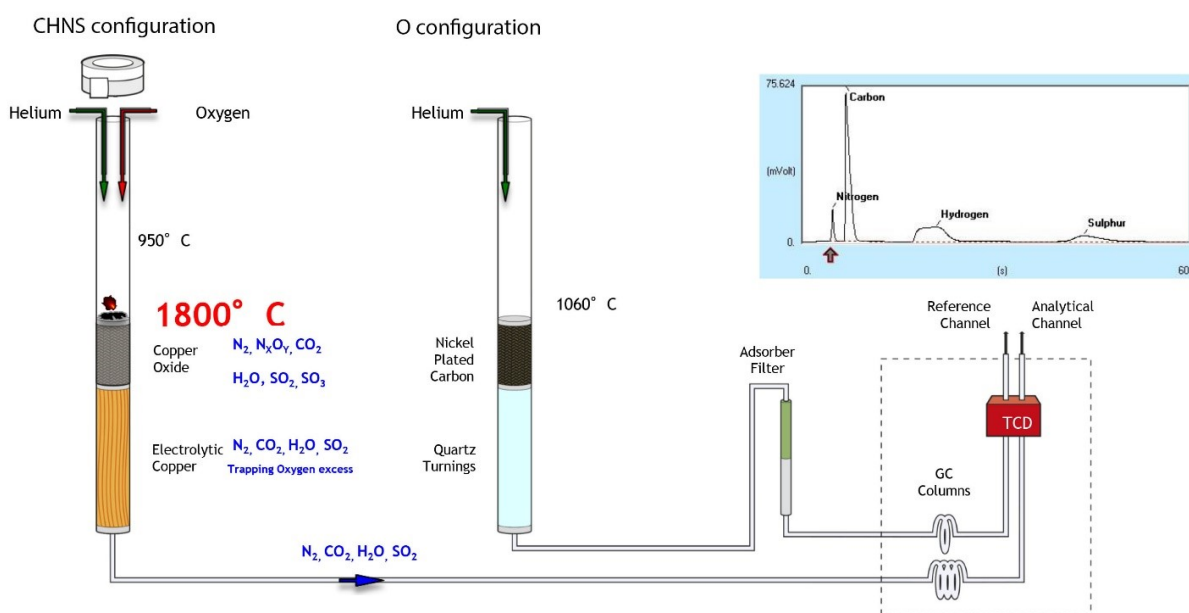
Figure (9)   Scheme of organic element analyzer ThermoScientific FlashSmart CHNS/O Analyzer (Figure provided by M. S. Naoroz (2021).

To distinguish the contribution of total organic carbon (TOC) and total inorganic carbon (TIC) to the total carbon (TC) measured, sample replica pretreated with hydrochloric acid are measured. The difference of measured carbon (as CO_2) between the replica allows to compute the inorganic and organic moeity of carbon (TC = TOC + TIC). Because the purpose of the method is to determine the OM-content and relate the results to the LOI measurement, the OEA focused on measuring carbon, nitrogen and hydrogen, while sulfur and oxygen were neglected.

4.2   Experimental Design

To examine biodegradation of PFAS in soils (in closed systems), the abiotic mass distribution between the different phases has to be quantified as well. PFOA is used in this study as a representative long-chained PFCA, the partitioning into gaseous phase can be neglected due to the very low vapour pressure (Parsons et al., 2008; Teaf et al., 2019). In order to investigate the physico-chemical partitioning between the aqueous and the solid phase of PFOA in the different soil samples, two abiotic partitioning experiments are performed additionally to the biotic incubation experiment. Furthermore, PFOA will be co-contaminated with perchloroethylene (PCE) in the experiments to validate the occurence of biodegradation in the incubation experiment. PCE was choosen as a co-contaminant, because it is well known to be biodegraded during the aerobic methane oxidation as well as other metabolic processes (see Ge and Jaffe 2019, lecture from Kiel). The initial aqueous concentration ratio of PFOA and PCE is constant in the incubation and partitioning experiments (see Table 2, Table 3).

The first partitioning experiment (B) aims to investigate the adsorption behaviour of PFOA onto the solid phase of agricultural soil 1 in dependence of the initial aqueous contamination level. From the results sorption isotherms can be derived and compared with corresponding literature suggestions. The second partitioning experiment compares the sorption behaviour of PFOA onto the different soils with equal initial aqueous concentrations, which were chosen based on the results of the prior experiment. The concentrations shouldn't exceed inhibitory levels for biological activity, but should still be high enough to ensure sufficient bioavailability of the contaminants in the aqueous phase and subsequent analytical detectability. The chosen concentrations are used in the second partitioning experiment and in the subsequential incubation experiment to allow a comparability under abiotic and biotic conditions. It is expected, to relate differences in the soil properties to potential differences in the observed phase distribution. Similar observations can be made for the co-contaminant PCE to validate the methodological approach.

Results and implications from the partitioning experiments are used for the incubation experiments, especially regarding the choice of initial aqueous concentrations to avoid an inhibition of the biological activity due to toxicity of PFOA and PCE (Weathers et al., 2016; Ge et al., 2019; Huang & Jaffé, 2019). Replicated samples of each soil are distinguished respectively a control treatment and a methane supplied treatment. The methane supplied samples will be trained for aerobic methane oxidation before the contamination with PFOA and PCE, while the control treatment does not receive any external supply.

Table (2)   Sampling scheme partitioning experiment B (PE-B) and partitioning experiment C (PE-C), including sample blanks. Concentrations describe injection solutions used, target concentrations achieved by dilution of same stock solution. Variance in porewater volume according to desired saturation. All samples prepared with 20 g in 120 ml headspace vials.

Experiment	Soil	Sample	PFOA [ppm]	PCE [ppm]	Inj. Vol [ml]
B	Soil 1	PE-B 1	0	0	8
		PE-B 2	0	0	8
		PE-B 3	2.5	0.5	8
		PE-B 4	2.5	0.5	8
		PE-B 5	7.5	1.5	8
		PE-B 6	7.5	1.5	8
		PE-B 7	12.5	2.5	8
		PE-B 8	12.5	2.5	8
		PE-B 9	25	5	8
		PE-B 10	25	5	8
		PE-B 11	50	10	8
		PE-B 12	50	10	8
C	Soil 1	PE-C 1.1	0	0	8
		PE-C 1.2	12.5	2.5	8
		PE-C 1.3	12.5	2.5	8
		PE-C 1.4	12.5	2.5	8
	Soil 2	PE-C 2.1	0	0	6
		PE-C 2.2	12.5	2.5	6
		PE-C 2.3	12.5	2.5	6
		PE-C 2.4	12.5	2.5	6
	Soil 3	PE-C 3.1	0	0	6
		PE-C 3.2	12.5	2.5	6
		PE-C 3.3	12.5	2.5	6
		PE-C 3.4	12.5	2.5	6

Afterwards both contaminants are added simultaneously to both treatments, while the methane supply for the methane treatment is continued. Also the samples of the methane treatment are monitored respectively the methane and CO_2 content in the gaseous phase. After the incubation period all samples are further analyzed for the contaminants and the chemical porewater composition. Potential differences of PFOA and PCE concentrations in the different treatments will be compared to each other and with the results of the second partitioning experiment.

For the partitioning experiments 20 g of the abiotic soil samples are weighed into 120 ml headspace vials, before the solutions of PFOA and PCE concentrations following the experimental design are added (Table 2). Then the vials are gas tightly enclosed using aluminium crimp caps and butyl rubber septa and placed in a closet under room temperature for 7 days to equilibrate. After the equilibration, the gas phase of each sample is analyzed for PCE concentrations by SHSI-GC-MS, before the porewater of the soils is sampled. The porewater is analyzed for major anions and cations by ion chromatography (IC), for major and minor cations by inductively coupled plasma - mass spectrometry

Table (3) Sampling scheme incuabtion experiment (IE-A) with samples of control and methane treatment including sample blanks. Concentrations describe injection solutions used, target concentrations achieved by dilution of same stock solution.

Treatment	Control			Methane		
Soil	Sample	PFOA	PCE	Sample	PFOA	PCE
Soil 1a)	IE-1	0	0	IE-5	0	0
	IE-2	12.5	2.5	IE-6	12.5	2.5
	IE-3	12.5	2.5	IE-7	12.5	2.5
	IE-4	12.5	2.5	IE-8	12.5	2.5
Soil 1b)	IE-9	0	0	IE-13	0	0
	IE-10	12.5	2.5	IE-14	12.5	2.5
	IE-11	12.5	2.5	IE-15	12.5	2.5
	IE-12	12.5	2.5	IE-16	12.5	2.5
Soil 2	IE-17	0	0	IE-21	0	0
	IE-18	0	0	IE-22	0	0
	IE-19	12.5	2.5	IE-23	12.5	2.5
	IE-20	12.5	2.5	IE-24	12.5	2.5
Soil 3	IE-25	0	0	IE-29	0	0
	IE-26	0	0	IE-30	0	0
	IE-27	12.5	2.5	IE-31	12.5	2.5
	IE-28	12.5	2.5	IE-32	12.5	2.5

(ICP-MS), and PFOA by gas chromatography - mass spectrometry (GC-MS).

For the subsequent incubation experiments 20 g of each biotic soil was weighed in according to the sample scheme (Table 3), before purified MilliQ water was added to each sample tpo saturate the porespace partially (approximately 80 %). After all vials have been enclosed with crimp caps and butyl rubber septa, the samples of the methane treatment were placed in an automized gas chromatographic analyzer at the Biotechnological Institute of the NMBU in Aas to monitore gas phase concentration of methane and carbon dioxide. The samples of the control treatment were placed in dark boxes, while both treatments were exposed to room temperature. The methane treatment samples were trained for methane consumption by manually adding methane in the headspace of each vial. After consistent methane consumption of all soils was indicated by the automized monitoring, both treatments were contaminated with a PFOA and PCE solution resulting in equal intial contaminant concentrations as in the second partitioning experiment. After the incubation period, the samples analysis proceeded as described for the partitioning experiments prior to examine the gaseous phase for PCE and the porewater for major anions, major and minor cations, and PFOA. The exact procedures of the analyses are described in the following chapters.
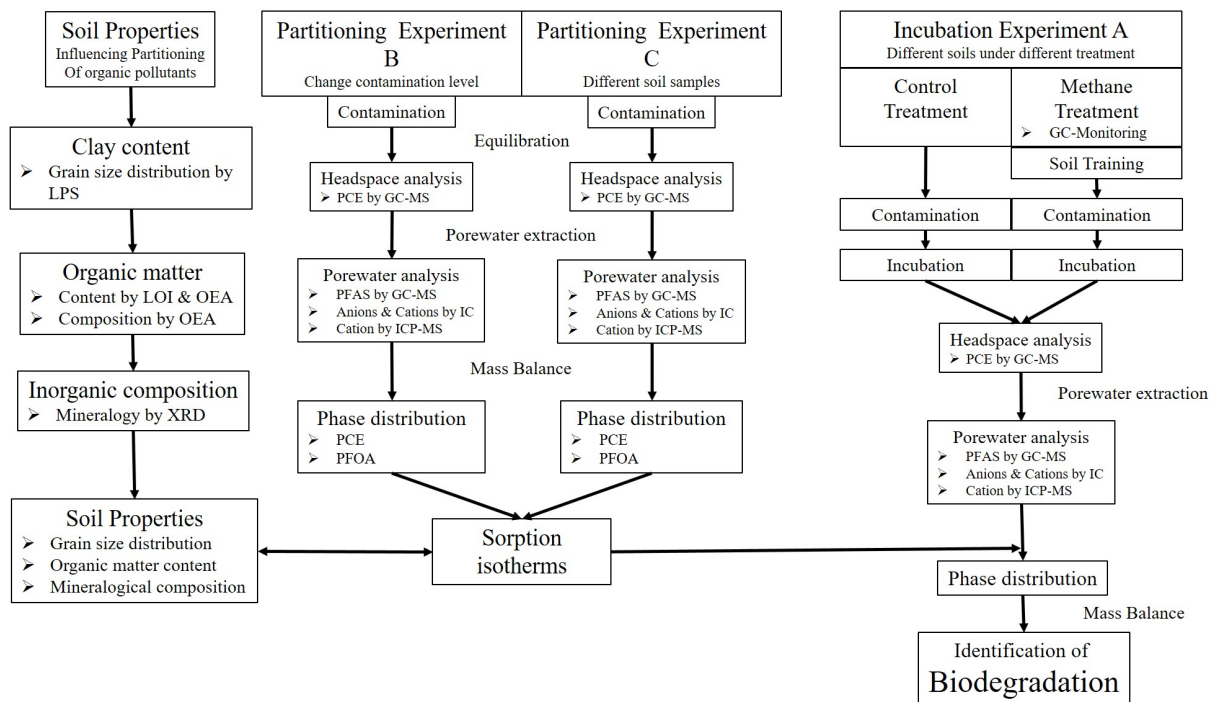
Figure (10) Scheme of experimental design to investigate partitioning behaviour and biode-gradatbility.

4.3 Porewater Extraction

To analyze the porewater of the partitioning and incubation experiments, the soil samples are removed from the headspace vials by irreversibly disrupting the closed system. Therefore, the crimp caps are removed and the majority of the soil sample is manually transferred to a 50 ml polypropylene centrifuge vial using a spatula. Small residuals are washed out from the headspace flask in the centrifuge vial by rinsing with a controlled volume of purified water (MilliQ) and adding the suspension to the centrifuge vial. The rinsing causes a dilution of the porewater concentrations, but also ensures the extraction of sufficient porewater for further analytical methods. After the whole sample is transferred to the centrifuge vial, the vial is closed, occasionally manually shaken and left to equilibrate for 30 minutes. Susequently the aqueous and the solid phase are distinguished by density separation using a Hettich Rotofix 32 centrifuge for two minutes at 1500 rpm and for 15 minutes at 4000 rpm. The supernatant is isolated using a one-way polypropylene syring, in which the volume of the extract is quantified. Susequently the extract is filtered through a 0.45 μm filter into a 15 ml centrifuge vial (polypropylene, PP), which is enclosed and stored in the fridge at 4 °C. Subsamples for further porewater analyses are taken from the filtered extract of diluted porewater. The results of the these analysis can be correlated to the original porewater by considering the dilution factors of the extraction (Table 4).

Table (4) Dilution of porewater samples during extraction procedure for used soils in different experiments and resulting dilution factors. Dilution factors applied for correction of porewater analyses.

		Volume	Original	Extract	Total	**Dilution**
Experiment	**Soil**	[ml]	[ml]	[ml]	Factor
PE B	Soil 1	8	8	16	2.00
PE C	Soil 1	8	8	16	2.00
	Soil 2	6	16	22	3.67
	Soil 3	6	8	14	2.33
IE A	Soil 1	8	8	16	2.00
	Soil 2	6	16	22	3.67
	Soil 3	6	8	14	2.33

4.4   Incubation Robot NMBU

To investigate the co-metabolic biodegradation of PFOA during the aerobic methane oxidation, the soil samples are trained to consume methane, before the contaminants PFOA and PCE are added to the incubations with continued methane supply. An automized GC-monitoring system at the Biotechnological Institute of the NMBU in Aas is used to monitore the gaseous amount of methane and carbon dioxide in the samples of the methane treatment. The headspace composition was monitored during the soil training period and the incubation period. The instrumental funcionality is described in detail in Molstad et al. (2007), and is briefly described hereafter.

After the samples of the methane treatement of the incubation experiment are enclosed with crimp caps and butyl rubber septa, the samples are placed at designated positions at room temperature. To monitore the gas phase composition of each sample, a Varian CP-4900 Micro-GC equipped with two columns (10 m poraPlot U and 20 m 5 A Molsieve) and connected to thermal conductivity detectors (TCD). The sample injection takes place externally via a robotized autosampler coupled to a peristaltic pump. For an analysis, the autosampler injects a gaseous headspace sample from a sample of designated position to the GC instrument, where the injected sample is split between both columns. Subsequently the taken sample volume of the headspace sample is replaced with inert helium, which also serves as carrier gas in the GC, by reversing the peristaltic pump. Inbetween measurements the helium flow is reversed through the injection system to avoid contamination via inflow of the surrounding laboratory atmosphere. In the GC-columns the chromatographic separation of the analytes takes place as described earlier (Method 4.5), while the coloumns differ regarding the ability to separate certain analytes of interest. From the coloumns the analytes are forwarded to TCDs, which register the change in thermal conductivity induced by gas component different from the background gas and convert the change to a correlating electrical signal. The signal is forwarded to a computer acquiring the data, where the measured retention time after sample injection can be related to certain atmospheric compounds. The corresponding integrated signal area can be converted to gaseous concentrations by measuring analytical standards. The Plot U GC coloumn is operated at 200 kPa helium pressure and 36 $°C$, while for the Molsieve

coloumn the pressure amounts 250 kPa at 50 °C. The time intervals between the monitoring are controllable and were choosen for 12 h during the training period and decreased to continous monitoring of the samples during the incubation period. During the experimental period the quantification of oxygen by the instrument was inconsistent, thus unreliable, which is why all samples were just monitored regarding methane and carbon dioxide. To convert the measured concentrations of the injected samples to concentrations in the gas phase of the headspace vials and derive resulting kinetics, the evaluation spreadsheet KINCALC is used (Bakken, 2020).
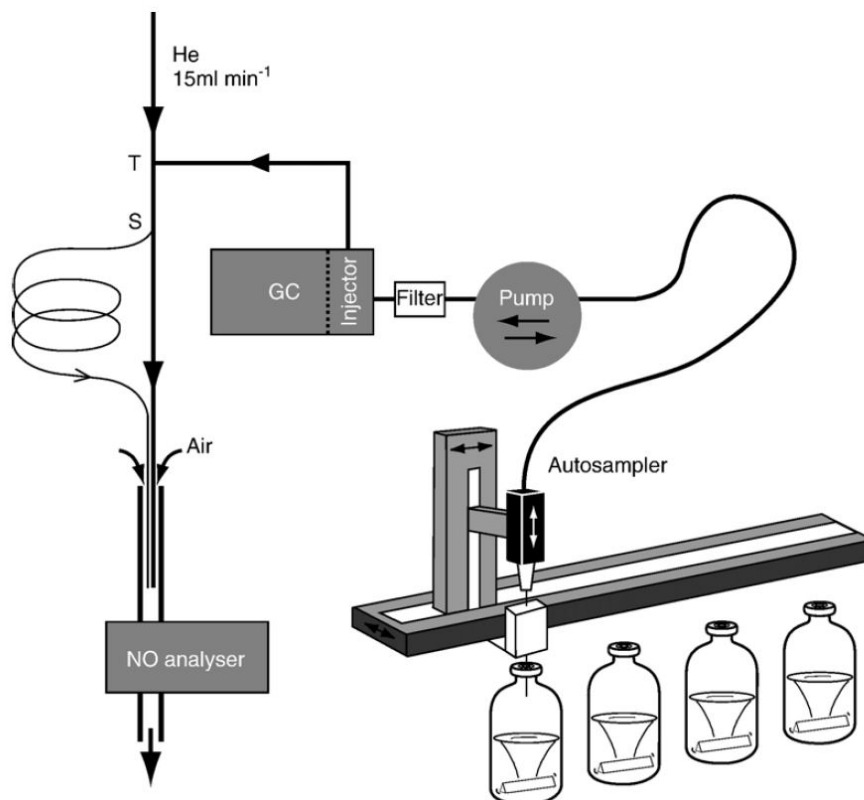
Figure (11) Schematic illustration of automized sampling and GC-analysis system for monitoring of gas phase composition of methane treated incubation experiments, figure from Molstad et al. 2007.

4.5 Measuring Contaminants

To analyze the contaminants used in the partitioning and incubation experiments a coupled gas chromatography - mass spectrometry system (GC-MS) at the Chemistry Department of the University of Oslo was used. The GC-MS allows the chromatographic separation of volatile analytes with a subsequent selective quantification of analyte ions according to charactistic mass-charge ratios (m/z). The GC system used was a 6890N Network Gas Chromatograph from Agilent (check company country, like other papers) equipped with a Zebron Phenomenex ZB5 column of 30 m length, an 0.25 mm inner diameter, and 0.25 μm film thickness of a low-polarity stationary phase with 5-% phenyl-methyl-polysiloxane. The GC was coupled over a GC-MS-interface to a 5973Network Mass Selective Detector from Agilent with an EI-ion source (electron ionization), hyperbolic single quadrupole mass filter and a high-energy dynode (HED) electron-multiplier detector. Most instrumental compartments are independently heatable and the whole system is linked over a local network controlled via the ChemStation software from Agilent. The assembled instrument was shutdown due to low frequent usage in the recent past and has not been used for the analysis of the contaminants used in this study. The setup of the instrument and methodological adjustments are described in Appendix 8.2. The combined GC-MS allows a chromatographical separation of analytes before the m/z selective analysis of ionized target compounds by mass spectrometry. The general principle is explained hereafter, while analytical details for the analyses of PCE and PFAS are described in the corresponding sections.

Because there was no autosampler available, all samples were injected manually using a gas-tight microsyrringe for gaseous samples of the PCE analysis and a microsyrringe for liquid samples of the PFOA analysis. The samples are injected through a septum in the temperature controlled injector, where the sample is pre-heated before the injection onto the chromatographic column. The temperature control of the injector is especially important for liquid samples to transfer them into the gaseous phase, which is required for the GC-separation. From the injector the sample is transferred into the continous carrier gas flow, whereby the sample can be artifically diluted using the split mode. For the analysis in this study a splitless injection was choosen and purified helium was used as inert carrier gas (mobile phase). With the carrier gas flow the sample is transported onto the chromatographic column, which is placed in an oven, that can be programmed to follow a specific temperature ramp program. While the sample runs through the column with the programmed carrier gas flow, the molecular constituents of the sample are in contact with the inner surface of the column, respectively stationary phase. Due to the specific chemical composition of the inner surface, gaseous molecules of comparable polar properties as the stationary phase adsorb from the mobile phase (gas flow) to the stationary phase and are retained until they are substituted by molecules of the carrier gas. This ad- and desorption occurs repetetively over the whole column, which statistically causes a similiar integrated retention of analyte molecules of similiar affinitiy to the stationary phase. The statistical occurence depends on the affinity to the column film, the column length, the carrier gas flow and the temperature of the GC-oven. In general non-polar columns (stationary phases) retain non-polar molecules more effectively, while polar molecules are less retained, and vice versa for polar columns. Therefore, the (non-)polarity of the chemical of interest determines the preferred choice of column in use. Furthermore,

different analytes can be separated using the temperature program for the GC, which allows separation of molecules corresponding to their volatility. Less volatile compounds tend to remain longer on the stationary phase, than volatile compounds of comparable polarity at the same temperature. Additionally the quality of separation is affected by the flow rate of the carrier gas, which influences the general resolution of the chromatographic separation, because it determines the flow velocity of through the column. The GC serves as the pre-separation of analytes in the sample to to allow a resolved analysis of analytes in the mass spectrometer.

From the GC-column the separated molecular constituents are forwarded with the carrier gas flow in a heated transfer line to the mass spectrometer, before it is injected in the ion source. In the electron ionization (EI) ion source, the injected molecules are transformed to corresponding ions of specific m/z. The ionization results from the collision of accelerated electrons with the injected molecules (removal of free electrons or heterogenous cleavage of molecule). The accelerated electrones originate from heated filament (thermoionic emission) and are accelerated by a potential difference of 70 V, causing a statistical electron energy of 70 eV, which induce the ionization of the injected sample molecules. While electrons and generated ions of negative charge are discharge using a repeller, the generated cations are focussed by extraction lenses towards the hyperbolic quadrupole mass analyzer. The quadrupole consists of four linear rods of hyperbolic shape arranged parallel to each other along a negative electrical potential gradient from the ion source towards the detector. The electrical gradient causes the positively charged analyte ion to move along the quadrupole. Simultaneously an alternating current is applied to the rods, whereby opposite rods have the same polarization.

This induces an alternating electrical and magnetical field, causing the alternating attraction and repulsion of the passing cations towards/from the rods. Depending on the amplitude and frequency of the alternating current on the quadrupole, ions of a specific m/z can be stabilized or destabilized on the way through the mass filter. Controlling the AC allows the selective stabilization of certain ions (certain m/z) and destabilize others, which will be discharged on the quadrupole rods. To improve the ion mean free path, the pressure in the mass analyzer is reduced to approximately 10^{-6} mbar by an external pump. After the selectively stabilized ions pass the mass filter, they are tranferred towards a HED electron multiplier detector, which transforms each ion impact to a correlated electron cascade. The integrated electrical signal is forwarded to a computer with a data acquisition program resulting in m/z specific signals correlating to the abundance of specifically filtered ions.

The chromatographic signal contains m/z-specific signal amplitudes, which allows the ion specific signal integration. By using calibration standards the integrated signals of analyte ions can be converted to corresponding concentrations in the sample. By using internal standards in repetitively measured blank samples, the instrumental signal drift over a measurement session and the analyte background signal can be corrected. For the choice of characteristic m/z for an analyte the potential interference with ions resulting from other molecules can be avoided by measuring several characteristic m/z ratios.

The pre-analytical setup of the GC-MS instrument and the instrumental setting for the analyses of PCE and PFOA are described in the subsequent sections and in Appendix 8.2.

4.5.1 Perchloroethylene by GC-MS

The vapour pressure of PCE causes the contaminants to partition significantly in the gaseous phase of the headspace vials, whereby an equilibrium with the aqueous phase is established according the Henry's Law (McMurry, Fay, & Robinson, 2008). Henry's law described the distribution of a compound between a gaseous and liquid phase in an equilibrated closed system according to solubility and vapour pressure of the compound in the corresponding phases depending on temperature and pressure. The dimensionless form of the Henry's law constant (K_H) of a specific compound can be described by the ratio of the concentration in the gaseous phase (C_{gas}) to the aqueous concentration (C_{aq}):

$$K_H = \frac{C_{gas}}{C_{aq}}$$

Under the absence of other organic pollutants (neglection of Raoult's law) the concentration of PCE in the aqueous phase can be computed with Henry's constant and by known concentration in the gaseous phase and vice versa. This allows the computation of a mass distribution of PCE in the partitioning and incubation experiments can be determined by measuring the PCE concentration in the gaseous phase. Therefore, Henry's law is rearranged for the aqueous concentration.

$$C_{aq} = \frac{C_{gas}}{K_H}$$

With the compound specific Henry constant and the measured gaseous concentration, the aqueous concentration can be computed. With the known vial volume, the bulk density and weight of the solid phase, and the volume of the aqueous phase, the mass of PCE in the aqueous and gaseous phase can be computed from the concentrations. The dimensionless Henry's law constant K_H for PCE was taken as an average value of a given range from a DTSC report (1994) with $K_H = 0.5987$ (Currie, Chiao, & McKone, 1994).

$$Vol_{gas} = Vol_{total} - V_{aq} - \frac{m_s}{\rho_s}$$

$$m_i = Vol_i * C_i$$

Under the presumption of mass conservation in the closed system, the computed mass distribution and the known initially added mass a mass balance can be formulated to derive the mass of PCE adsorbed to the solid phase in the abiotic partitioning experiments.

$$\sum m_i = constant$$

$$m_{t=0} = m_{gas} + m_{aq} + m_s$$

$$m_s = m_{t=0} - m_{gas} - m_{aq}$$

For these computations it is assumed, that the partitioning from the gaseous to the solid phase just occurs via transfer through the aqueous phase, respectively no direct

interface of the solid and gaseous phase occurs (neglection of vapourization).

The PCE concentration in the gas phase was determined using the GC-MS at the Chemistry Department at the University of Oslo, while the samples are injected by static headspace injection (SHSI-GC-MS). The samples were taken manually using a gastight microsyringe, piercing through the butyl rubber septum in the headspace of the sample. A sample of 50 μl of the gaseous headspace is injected through the injector septum of the instrument, whereby two replica of contaminated samples are measured, while sample blanks are just measured once. To convert measured signals of the target ions to corresponding gaseous concentration of PCE, calibration standards were measured in the beginning of every measuring session. Furthermore, instrumental blanks (purified MilliQ water) containing a certified internal standard (EPA 524 Internal Standard Mix, by Supelco$^{©}$) were measured repeatedly during the measurement to determine an instrumental drift and the instrumental background.

The calibration standards and blanks are prepared in 20 ml headspace vials with 10 ml aqueous solution and are sealed with crimp-caps and butyl rubber septa. The instrumental blanks are prepared from purified MilliQ water and are sealed before the internal standard was added. The solutions of the calibration standards were prepared from the same PCE stock solutions (10 ppm, 100 ppm) used for the partitioning and incubation experiments (prepared from a pure PCE solution), diluted with MilliQ water to the desired concentration. The calibration standards are stored in a fridge before 24 h of usage, when they were removed to acclimate and induce equilibrium conditions under room temperature as the samples. The gas phase concentration in the calibration standards is computed via Henry's law, with a dimensionless $K_H = 0.5987$ (Currie et al., 1994). The subsequential sample measurements represent the gaseous concentration in the headspace of the samples in the 120 ml vials.

The integrated signal area of the GC-MS measurements are corrected for an instrumental drift of the signal for each measurement session. The drift was derived from the internal standards in the blanks measured over the corresponding measurement day. Under the presumption, that the instrumental drift trend is equal for the internal standard ion and the analyte ion of PCE, the drift is approximated as a linear trend of the form:

$$S_{IS}(N) = m * N + b$$

The integrated signal area of the characteristic ion of the internal standard (S_{IS} depends on the number of the number of the measurement (N) under the assumption the time interval between each measurement is equal. From the linear approximation a correction factor (δ) depending on the measurement number of the corresponding session is computed for each measurement, normalizing the measured analyte signal S_i^{meas} to the initial conditions with $N_0 = 0$:

$$\delta(N) = \frac{m * N_0 + b}{m * N + b} = \frac{b}{m * N + b}$$

$$S_i^{Drift}(N) = \delta(N) * S_i^{meas}(N)$$

Thereafter, the measured signal of the analyte ion of the calibration standards and the samples (S_i) is corrected for the mean of the corresponding signal from the instrumental

blank measurements $\overline{S}_i^{blk}$.

$$S_i^{correct} = S_i - \overline{S}_i^{blk}$$

With the corrected signal $S_i^{correct}$ of the calibration standards, the calibration curve is determined by linear correlation of the measured integrated signal with the known gaseous concentration, which computed by the known aqueous concentrations and Henry's law.

$$S_i = m * C_{gas} + b$$

Determing the slope m and the y-axis intersection b allows to rearrange the equation for the gaseous concentration and subsequently compute the gaseous concentrations of the samples via the corrected signals for the analyte ion.

$$C_{gas} = \frac{S_i - b}{m}$$

These instrumental corrections are applied for the samples and the calibration standards. After computing the concentration from the lineary approximated calibration curves, the contaminated samples were corrected for the sample blanks. Therefore, the maximum concentration measured in a sample blank is substracted from the computed concentration of the corresponding samples.

$$C_{gas}^{correct} = C_{gas}(sample) - C_{gas}^{max}(blk)$$

The corrected gaseous concentration of each sample can be converted to the corresponding aqueous concentration by Henry's law and the corresponding masses of PCE in the gaseous and aqueous phase can be computed with the corresponding volumes.
Computing the masses of PCE distributed between the gaseous and the aqueous phases in the abiotic partitioning experiments allows to set up the mass balance with the initially added mass of PCE. Under the assumption the initial mass is constant in the closed system, without any sinks or sources, the mass adsorbed to the solid phase can be calculated. With the known soil weight, the adsorbed concentration is calculated. The sorption behaviour for the different soils is estimated by correlating the results of the aqueous concentrations with the concentration of contaminant adsorbed to the solid phase. The relation of the aqueous and the solid concentration is approximated lineary and nonlineary, resulting in the derivation of a linear isotherm and a Freundlich isotherm of the form.

$$C_s = K_d * C_{aq}$$

$$C_s = K_F * C_{aq}^n$$

The linear isotherm describes the relation between the aqueous and the adsorbed concentration with the distribution coefficient K_d as a factor. The factor can experimentally be determined by measuring the ratio of the solid to the aqueous concentration. A resulting sorption isotherm intersects the origin, which implies that no mass is adsorbed, if no mass is present in the aqueous phase. This relation is comparable to Henry's law.
The nonlinear Freundlich isotherm assumes the presence of adsorption sites on the solid phase onto which a compound can adsorb from the aqueous phase via different adsorption

mechanisms (e.g. see Figure 5). The nonlinear isotherm describes the consideration that the adsorption onto the solid phase becomes gradually less with more mass adsorbed to the solid phase (Van Loon & Duffy, 2005). The sorption sites present on the solid phase are not limited, which implies the occurence of multilayer adsorption. Compared to the more empirical Freundlich isotherm the nonlinear Langmuir isotherm presumes a limited number of equal sorption sites, which implies a specific limit for the solid phase concentration (Van Loon & Duffy, 2005). The empirical Freundlich equation tends to describe the observed adsorption behaviour more precisely than the more theoretical Langmuir isotherm, which is why the Freundlich equation is used to approximate the relation between the aqueous and the solid concentration nonlineary.

To derive the linear coefficient K_d measured concentrations of the aqueous and the solid phase are lineary approximated. To derive the Freundlich coefficient K_F and the Freundlich exponent n of the Freundlich isotherm the logarithm of aqueous and the solid phase concentrations are approximated lineary.

$$ln(C_s) = ln(K_F) + n * ln(C_{aq})$$

To evaluate which isotherm describes the adsorption to the solid phase better, the statistical fit described by the coefficient of determination R^2 is used.

The sorption isotherms for PCE derived from the partitioning experiments are further used for the evaluation of the respective soils of the incubation experiments. The computation of the aqueous concentration from the measured gaseous concentration follows as in the partitioning experiments. But the derived partitioning from the prior experiments is used to compute the solid phase concentration according to the computed aqueous concentration. Deriving a mass balance including the mass present in all three phases of the closed system with the initially added mass, allows to compute the biodegraded mass as a sink term.

$$m_{t=0} = m_{gas} + m_{aq} + m_s + m_{sink}$$

$$m_{sink} = m_{t=0} - m_{gas} - m_{aq} - m_s$$

4.5.2 Perfluorooctanoic acid by GC-MS

Unlike PCE, the partitioning of PFOA from the aqueous solution to the gas phase is neglectably small, which is why the analysis via SHSI-GC-MS is not possible for the analysis of PFOA (Prevedouros et al., 2006; Jahnke, Ahrens, Ebinghaus, Berger, et al., 2007; Jahnke, Ahrens, Ebinghaus, & Temme, 2007; Z. Li & Sun, 2020). Furthermore, the low volatitility of PFOA and presence in the anionic form in the aqueous sample restricts the direct analysis from porewater sample, which is why a pre-analytical derivatization of PFOA from the extracted porewater samples is performed. The intention of the pre-analytical derivatization is the complete conversion of present PFOA in the porewater sample to a thermodynamically more stable derivate with a lower boiling point, which is analyzable by GC-MS analysis (Belisle & Hagen, 1980; Langlois, Berger, Zencak, & Oehme, 2007; F. Li et al., 2019). This analytical approach is suggested in early studies from Belisle et al. (1980), Scott et al (1998), and has been described in further studies (Scott, Spencer, Marvin, MacTavish, & Muir, 2002; Scott et al., 2006; Langlois et al.,

2007) and extensively described by Li and Sun (2019). The analytical approach performed in this study follows the derivatization method by Li and Sun (2019), while slight adaptions to the available laboratory equipment and the instrumental analysis were made. The pre-analytical derivatization is described hereafter, followed by the instrumental analysis and the processing.

For each batch of samples derivatized and subsequently analyzed, the corresponding calibration standards and a processing blank are processed simultaneously and treated like a sample. While the processing blank consists of 5 ml purified MilliQ water, the calibration standards are prepared from the same stock solution, that was used to prepare the contaminantion solutions used for the experiments. The number of samples processed per derivatization varies between 8 to 12 samples, excluding the blank and standards. Limitations were given by the used laboratory equipment and the consequential time of the GC-MS analysis.

For the PFOA GC-MS analysis, a 1 ml subsample of the extracted porewater samples is added to 4 ml purified MilliQ water in a 30 ml Erlenmeyer glass flask. Subsequently the pH of the aqueous phase is decreased to 1 by addition of 0.5 ml 1N HCl,to ensure the presence of PFOA in the sample in the molecular, protonated form (Figure 4). Afterwards 0.2 g NaCl are added to increase the density of the aqueous phase and favour the density separability with the co-solvent ethylene acetete (EAc), of which 5ml are added thereafter. Then 0.2 ml of 0.1 M 2,4-difluoroaniline (DFA) and 0.4 ml of 0.1 M N,N'-dicyclohexylcarbodiimide (DCC) solution in dichloromethane (DCM) are added and the Erlenmeyer flasks are covered with parafilm foil. The covered glass flasks are placed on a horizontal shaker at 200 rpm for 30 minutes under ambient temperature. While on the shaker the DFA and the protonated PFOA react in the presence of DCC in the emulsion of water and EAc to PFOA-anilide and water. DCC serves as a dehydration agent, while DFA reacts with PFOA to PFOA-anilide in an amidification reaction as illustrated in Table 5.

After 30 minutes the samples are removed from the horizontal shaker, 1 g NaCl is added and dissolved under occasional manual swirling of the vial. After the salt is dissolved, the ethylene acetate and the aqueous phase separate due to density differences and immiscibility. The 5 ml EAc phase of lower density is extracted and tranferred to a 15 ml polypropylene centrifuge vials by pipetting. Successively, 3 ml new EAc are added to the residual aqueous phase in the Erlenmeyer flask and swirled manually to ensure a complete transfer of the analyte (re-extraction). After isolating and transferring the EAc of the re-extraction, the total 8 ml of isolated EAc phase are washed in the centrifuge vial with 1 ml 1 N HCl, 1 ml saturated $NaHCO_3$ solution, and 1 ml saturated NaCl solution by shaking the enclosed vials. Afterwards, the sample is tranferred in separatory funnel to separated the EAc phase from the aqueous washing solution. While the washing solution is discarded, the EAc phase is transferred into a 30 ml Erlenmeyer vial. To ensure complete dehydration of the isolated EAc phase containing the PFOA-anilides, anhydrous Na_2SO_4 is added, which binds residual water and forms hydrated Na_2SO_4. Addition of Na_2SO_4 and swirling are repeated, until no more floccation of the $Na_2SO_4 \cdot nH_2O$ occurs. After the dehydrating solid settled, the liquid phase is carefully decanted into 15 ml polypropylene centrifuge vials without transferring the settled solid phase. Subsequently, the centrifuge vials are placed under an air-flow evaporator under moderate air-flow and

ambient temperature, until the volume decrease to 0.5 ml. Because no evaporator was accessible, an air-flow distributing device was constructed using a stand, clamps, tubes, pipette tips and two 300 ml polyethylene bottles of square base shape. This air-flow evaporator was connected to the air tab in the fume hood, which allows adjustment of the air-flow with progressing evaporation. The evaporation causes higher concentrations of PFOA-anilides in the final volume, which is transferred into a 1.5 ml polypropylene sample vial. The 0.5 ml analyte solution is diluted with 0.5 ml n-hexane to 1 ml, which is used as the analysis solution for the GC-MS. The sample vial is closed, wrapped with parafilm foil and placed upright in a fridge at 4 $°C$ until the GC-MS analysis.

Table (5) Amidification reaction without DCC as dehydrating agent not shown.

PFAA + DFA $\Rightarrow$ PFA-anilide + Water
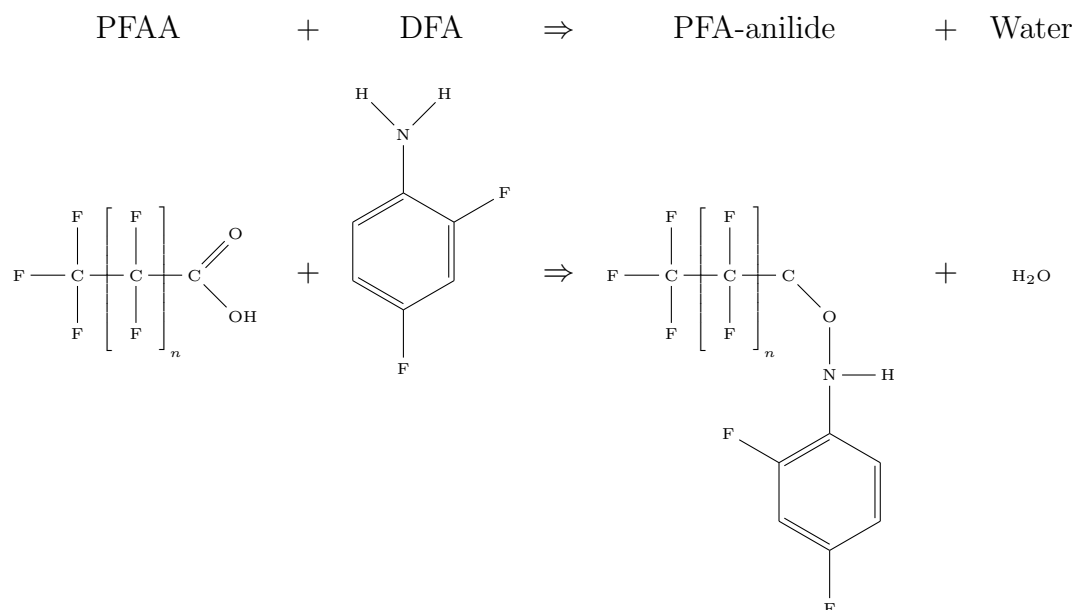
Before the GC analysis 5 μl of 1 ppm pentachloronitrobenzene (PCNB) solution in n-hexane (original solution: 10 ppm PCNB in cyclo-hexane by Dr. Ehrenstorfer, diluted in n-hexane) was added to the blank, standards and sample, before 1 μl of the analysis solution was manually injected in the instrument. Each standard and sample was measured twice; in the beginning, after the calibration standards and after 10 measurements the processing blank was measured. The instrumental setting for the analysis are shown in Figure 30 (Appendix 8.2).

The measured signal for the samples can be converted to the corresponding concentration in the 1 ml analysis solution. Under the presumption of a complete derivatization reaction, a complete analyte transfer, and neglection of analyte loss onto laboratory equipment used, the measured concentration can be converted to the concentration in the extracted porewater solution, respectively the porewater in the sample. Due to the mixing ration and final sample volume after the derivatization, the PFOA-anilide concentration in the n-hexane equals the PFOA concentration of the extracted porewater. By multiplication with the correction factor resulting from the porewater extraction (see Table 4), the original porewater concentration can be calculated.

Like for the PCE measurement, the acquired signals are corrected for the instrumental

drift approximating a linear trend from the signal of the internal standard in the blank over the measurement session. Also the mean of the analyte signal measured in the processing blank is substracted from the signals of the calibration standards and the samples. The resulting signals of the calibration standards are used to derive a calibration curve for the theoretical concentration of PFOA-anilide in the 1 ml analysis solution (n-hexane).

The maximum concentration measured in a sample blank is substracted from the measured concentration in the analysis solution of the corresponding samples. The resulting corrected concentrations in n-hexane is converted to the concentrations in the extract solution and eventually to the porewater concentrations.

For the partitioning experiments the adsorbed concentration on the solid phase can be determined by a mass balance of the initial mass, the aqueous concentration and the injected volume of contaminant solution. The partitioning in the gaseous phase is neglected due to the low vapour pressure of PFOA, which simplifies the mass balance.

$$m_{t=0} = m_{aq} + m_s$$

The concentration in the solid and aqueous phase are computed analogue as described for PCE. From the correlation of the aqueous and the solid concentration, the sorption behaviour is approximated using a linear and a Freundlich isotherm.

The determined distribution coefficients from the partitioning experiments can further be used in the incubation experiments to estimate the mass on the solid phase for each soil based on the aqueous concentrations measured. A subsequent mass balance with the initially injected mass in the contaminated incubations allows an estimation of potentially biodegraded PFOA as a sink.

$$m_{t=0} = m_{aq} + m_s + m_{sink}$$

These computations presume a complete derivatization of the analyte, no loss during the pre-analytical treatment or on the incubation vials and the applicability of the abiotic phase distribution derived from the partitioning experiments to the biotic incubation samples.

4.6 Porewater Composition

Additionially to the analysis of PFOA, the porewater is analyzed regarding the inorganic chemical composition. The chemical aqueous composition can give implications for the ionic strength of the porewater solution, the presence of micronutrients (e.g. iron, cupper) and potential ligands for the formation of complexes. Comparing the porewater composition of the different experiments can give insights in changes of the reducing/oxidizing conditions in the closed systems, occurence of biological and mineral reactions and presence of anorganic inhibitors/pollutants.

4.6.1 Major Anions and Cations by IC

To analyze the extracted porewater from the partitioning and incubation experiments chemically regarding the major anions and cations, subsamples of the extracted porewater are analyzed by ion chromatography using an ICS-2000 Ion Chromatography System (ICS-2000) equipped with an AS-40 autosampler, a AERS500 self-regenerating suppressor and conductivity detector cell DS6 from Dionex at the Geological Department of the University of Oslo. This method allows the quantification of the major porewater anions fluoride, chloride, bromide, sulfate, nitrate and phosphate, and the cations sodium, potassium, magnesium and calcium. The principle of the analysis is described hereafter.

Like the gas chromatography the ion chromatography analysis is based on the separation of analytes by ad- and desorption from a mobile phase to/from a stationary phase inducing retention of the analytes depending on the specific affinity to the stationary phase. Practically the set-up differs from a GC instrument, because aqueous samples are used and the analytes are effectively charged (in GC selective retention by polarity). The aqueous samples are injected into a continous flow of potassiumhydroxide solution (KOH, 30 mM), which serves as eluent (= mobile phase). With the eluent flow, the sample is transported towards two ion exchange columns, where the first column serves as a guard column protecting the instrument from contaminations (e.g. large organic molecules). In the following analytical column the selective retention of the analytes due to sorption processes to the stationary phase on the inner surface of the column occurs. Thereafter, the separated analytes pass a suppressor cell, in which dissociated eluent ions are suppressed by a suppressor current corresponding to the used eluent concentration (75 mA). The suppressor current compensates the background signal for the eluent and thus enhances the induced signal of the target anions in the following conductivity detector. In the conductivity detector the charged analytes induce changes in the continous detection signal, which correlated to the amount of passing analytes. Due to the chromatographic separation, the measured signals can be related to certain ions by their specific retention time (and order of occurence). The analytes concentration is derived from comparing integrated signal areas of analogues blanks and calibration standards of known concentration. Because one coloumn-system is specific for anions or cations, the injected sample is equally split after the injection, while one part of the sample is directed to a column system for anion separation and the other part to an equivalent for cation separation. Both column systems are operated under 30 $^\circ C$ with a constant eluent flow rate of 1 $\frac{ml}{min}$.

4.6.2 Major and minor Cations by ICP-MS

To validate the results of the major cation concentrations from the ion chromatography and further analyze the porewater regarding minor elements like iron, manganese and cupper, subsamples of the extracted porewater were analyzed by inductively coupled plasma - mass spectrometry (ICP-MS). The analysis was performed with a Bruker Aurora Elite ICP-MS equipped with a Cetac ASX-250 autosampler and an ESI oneFAST sample introduction system at the Geological Department of the University of Oslo. Hereafter the analytical principle is described briefly.
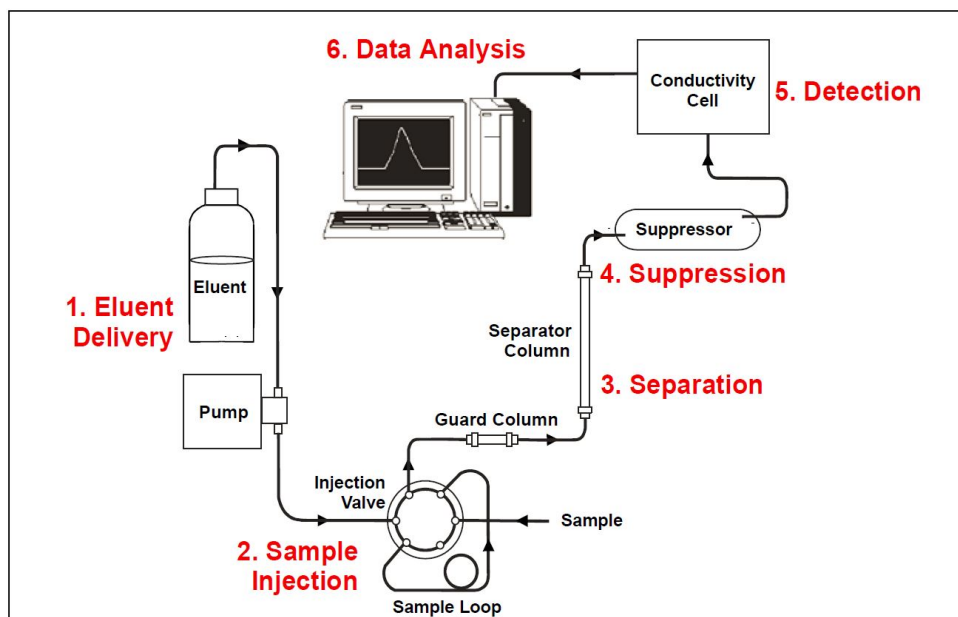
Figure (12) Schematic functionality of ion chromatography (figure 1.1 from ICS-2000 IC system opertator's manual, Dionex Corp, Thermo Scientific, 2005).

Orientated on the results of the previously performed IC, the extracted porewater samples were diluted 1:40 with 1-% nitric acid to match the concentration limits of the more sensitive ICP-MS instrument. The sample injection is performed by the automized introduction system, which guides the aqueous sample to a vapourizer. The vapourizer transforms the sample to an aerosol, which is sprayed in an inductively coupled argon plasma torch. The vapourization ensures a more homogeneous thermal ionization of the sample in the plasma torch of approximately 6000 $°C$. The high temperature causes a complete dissociation and ionization of all analytes present. Consequently the positively charged ions are forwarded towards the single quadrupole mass analyzer along gradually decreasing pressure sections while be focussed by instrumental optics. The quadrupole selectively stabilizes the ions according to their specific m/z-ratios by adjusting the alternating current inbetween the quadrupole rods (see subsection 4.5). The stabilized ions pass the mass analyzer and fly towards the detector, where each appearing ion causes the release of a correlated electron cascade forming an electrical signal. The signal is forwarded to a computer collecting the acquired data. By measuring standards of known concentration and instrumental blanks, the m/z-specific sample signals can be converted to corresponding concentrations.

The used calibration standard was ICP-MS Tuning Standard solution for 6020 CLP-M, Specpure© by Alfa Aesar in the concentrations 10 ppb, 100 ppb, 500 ppb, and 1000 ppb (diluted in purified MilliQ water), as internal standards scandium (^{45}Sc), yttrium (^{89}Y), and indium (^{115}In) were used. As an unknown the certified high-purity standard CRM-TMDW-A was analyzed parallel to the samples to ensure the analysis quality. The resulting errors are element specific for each sample, which are computed as relative standard deviation in percentage (RSD [%]).

48

5 Results

In this chapter the major results of the soil characterizing experiments, the corrected results of the partitioning and incubation experiments and relevant correlation are presented. Results not presented hereafter are graphically or tabulary shown in Appendix 8.1 .

5.1 Soil Characterization

Hereafter the results of the soil characterization regarding the grain size distribution by the LPS-analysis, the organic matter content and composition by LOI and OEA and the mineralogical composition by XRD-analysis are presented.

5.1.1 Grain Size Distribution

The results of the grain size distribution for the soil samples are averaged for two replica measured for by LPS analysis with automized statistical analysis. Additionally the relative grain size distribution was analyzed using the Grain Size Program GRADISTAT v9.1 by Simon Blott (2020) to derive descriptive characterizations and the graphical classification in a ternary diagram. The samples analyzed are the agricultural soil 1, the topcore sample soil 2 and the bottom core sample soil 3.

Table 6 shows the relative volumetric portion of particle size ranges in each sample from 0 μm to 2000 μm, which is exemplary illustrated as the differential and cumulative volumetric grain size distribution for soil 1 in Figure 14.

Table (6)   Differential grain size distribution of sampled soils.

Particle Range [μm]	Soil 1 Vol.-%	Soil 2 Vol.-%	Soil 3 Vol.-%
0 - 2	20.25	3.51	5.31
2 - 4	15.23	2.96	3.68
4 - 8	20.37	4.82	5.33
8 - 10	6.46	1.90	1.98
10 - 16	11.63	4.38	4.49
16 - 20	4.60	2.33	2.40
20 - 32	6.89	5.72	5.70
32 - 50	3.93	6.68	6.05
50 -63	1.25	3.68	3.13
63 - 90	2.38	6.31	5.30
90 - 100	0.74	2.04	1.69
100 - 125	1.09	4.41	3.58
125 - 250	5.08	18.10	15.19
250 - 500	0.10	17.80	15.61
500 - 1000	0.00	14.29	15.00
1000 - 2000	0.00	1.08	5.57

For soil 1 the relative distribution shows that the majority (ca. 75 %) of the grains range from 2 to 63 μm, while 20.25 vol-% of the sample have a grain size smaller than 2 μm. The mean grain size for sample 1 is 21.73 $\pm$ 2.08 μm and the geometric median is 6.60 $\pm$ 0.19 μm (Table 16, Appendix 8.1.1). According to the Grain Size Program GRADISTAT, these values with the resulting standard deviation, skewness and kurtosis of the distribution classify soil sample 1 as a fine silt (mud), which is poorly sorted with a bimodal distribution. The bimodality results from the grain size fraction (5 %) between 125 to 250 μm, which corresponds to the fine sandy fraction. After the Folk and Ward method, the sample would be classified as a poorly sorted, coarse silt, whose distribution is coarse skewed and mesokurtic (Table 18, Appendix 8.1.1).
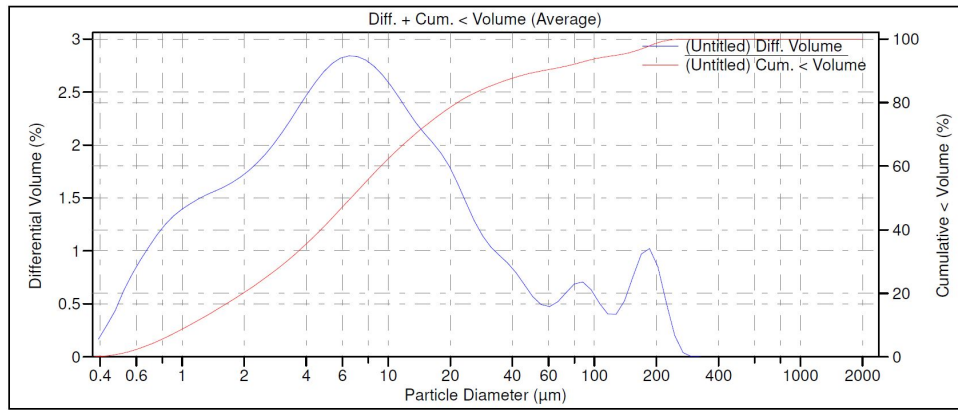
Figure (13) Soil 1

Figure (14) Differential (blue line) and cumulative (red line) volumetric grain size distribution from LPS analysis of soil 1.

The grain size distribution of soil 2 and soil 3 are comparable, but differ slightly regarding the relative clay and silt fraction, whereby the relative abundance of the fine fraction is slightly higher in soil 3. In both samples the mean fraction ranges around 250 μm, with 225.39 $\pm$ 5.96 μm for soil 2 and 281.54 $\pm$ 56.49 μm for soil 3. While the means of soil 2 and soil 3 are around ten time higher as the mean of for soil 1, the meadians are about 20 times larger as for soil 1, with 132.87 $\pm$ 3.59 μm for soil 2 and 136.01 $\pm$ 19.50 μm for soil 3. The similarity of the grain size distribution of all soil samples is graphically compared in Figure 29 in Appendix 8.1.1. According to the GRADISTAT analysis the two core samples are both very poorly sorted, polymodal distributed and fall in the textural group of muddy sand (Table 17, Appendix 8.1). While soil 2 is classified as a medium silty fine sand, soil 3 is slightly coarser and is described as a silty medium sand. After the Folk and Ward method both soil 2 and 3 are very fine sand, which are very poorly sorted with a platykurtic kurtosis and a (very) fine skewed distribution pattern (Table 18, Appendix 8.1.1).

Plotting the grain size distribution of all soil samples in a ternary sand-silt-clay diagram (using GRADISTAT), results in the classification of soil 1 as a silt, while soil 2 and soil 3 fall in the category of a silty sand (Figure 30, in Appendix 8.1.1).

5.1.2 Organic matter

Loss of Ignition (LOI)   To determine the LOI just one replica of each sample was measured due to the limited amount of sample material available for soil sample 2 and 3. The LOI is described as relative mass difference after the 105 °C and after the 550 °C temperature treatment and the results are presented in Table 7. As expected from the visual characterization, the LOI of soil 2 is the highest with 19.13 %, which is more than double of the mass loss of soil 1 with 7.57 %. Soil 3 showed the lowest relative mass difference with 3.04 %. The measured LOI was converted to estimates of the total organic carbon (TOC) for each sample presuming that 58 % of the weight loss result from organic carbon (after Chatterjee et al.,2009). The computed TOC values are shown in Table 7 soil 1 (4.39 %), soil 2 (11.10 %) and soil 3 (1.76 %) and are subsequently compared to the results of the Organic Element Analysis.

Table (7)   Weights of samples after temperature treatments to determine Loss of Ignition (LOI) with conversion to total organic carbon (TOC) after Chatterjee et al. (2009) assuming soil organic matter consists to 58% of organic carbon ($TOC = 0.58 * LOI$).

Temperature	Time	Soil 1 $[g]$	Soil 2 $[g]$	Soil 3 $[g]$
After 60°C	48h	3.45	3.49	3.59
After 105°C	16h	3.39	3.40	3.56
After 550°C	3h	3.13	2.75	3.46
LOI [%]		7.57	19.13	3.04
TOC [%]		4.39	11.10	1.76

Organic Element Analysis (OEA)   The results of the quantitative Organic Element Analysis regarding the main constituents are presented in Table 8 with the results of individual measurements for each soil sample and the results of the standards as means with standard deviation (SD). The measurement for total carbon (TC) were replicated twice for each sample, whereas the total organic carbon (TOC) was just measured once. As implied by the LOI results, soil 2 shows the highest total carbon and total organic carbon content with a relative TC content of 10.08 % and 9.53 % for TOC. For all results of the carbon measurements a standard deviation of 0.31 %, derived from the variation of the repeatively measured Peaty standard is assumed (see Table 19, Appendix 8.1.2). The relative difference of the total carbon and the total organic carbon for soil 1 and 2 is minimal, whereby the TC- and the TOC-fraction of soil 2 is around 3.5 times higher than for soil 1 with a TC of 2.92 % and a TOC of 2.85 %. The lowest carbon content was measured in soil 3 with a TC of 1.27 % and a TOC of 0.82 %.

The difference between TC and TOC for all soils fall within the assumed standard deviation, whereby the TC and TOC of soil 1 are the most similiar. The TC and TOC difference of soil 2 and soil 3 are comparable, while the TC and TOC of soil 3 are approximately 10 times lower than for soil 2.

Compared to the carbon content estimations from the LOI analysis, the carbon moiety

Table (8) Conclusion of OEA analysis for soil samples with averaged results of the standards Peaty and BBOT with standard deviation (SD) treated like samples (unknown composition).

Sample ID	Analysis	Weight [mg]	Nitrogen [%]	Carbon [%]	Hydrogen [%]
Soil 1	TC	15.568	0.18	2.98	0.77
	TC	15.367	0.17	2.86	0.78
	TOC	15.482	0.18	2.85	0.72
Soil 2	TC	15.168	0.38	10.24	1.05
	TC	15.358	0.36	9.92	1.00
	TOC	15.48	0.33	9.53	0.96
Soil 3	TC	15.885	-0.02	1.24	0.25
	TC	15.453	-0.02	1.30	0.26
	TOC	15.525	-0.03	0.82	0.17
Peaty	Standard	13.250	1.26	15.71	0.00
	SD	0.435	0.04	0.31	0.00
BBOT	Standard	2.486	6.40	72.75	6.04
	SD	0.036	0.08	0.03	0.06

measured by OEA in all samples is lower. The relative difference between the OEA results and the LOI estimations is bigger for soil 3 with the lowest carbon content and biggest for soil 2 of the highest carbon content. A correlation of the LOI with the OEA results (TOC) gives a correlation factor of 1.055 with an offset of 1.106 and a coefficient of determination R^2 of 0.997 (Figure 31, Appendix 8.1.2).

5.1.3 X-Ray Diffraction

From the measured diffractograms by the XRD-analysis synthetic diffractograms are derived for each sample (agricultural soil one, E-horizon of core sample, B-horizon of core sample) using the XRD analysis software Profex. The comparison of the measured and the computed diffractogram is exemplary shown in Figure 15 for soil 1. The identified, significant peaks are marked in each diffractogram (for E- and B-horizon sample see Figure 32 and 33, Appendix 8.1.3). The derived mineralogical compositions for each soil are shown in Table 9, while the resulting chemical composition is shown in Table 20, Appendix 8.1.3.

The semi-quantitively determined composition of the core horizons E and B are comparable regarding their relative composition of main constituents quartz (57.09 % and 50.59 %) and the feldspars plagioclase (21.70 % and 21.91 %) and microcline (19.04 % and 20.75 %) (Table 9). Whereas both horizons also show the presence of hornblende (E-horizon 1.66 %, B-horizon 3.89 %), the B-horizon contains 2.86 % muscovite, while the E-horizon consists to 0.51 % of actinolite. The similarity of the synthetic and the measured diffractogram is quantified by the χ^2 value, with 1.68 for the E-horizon and
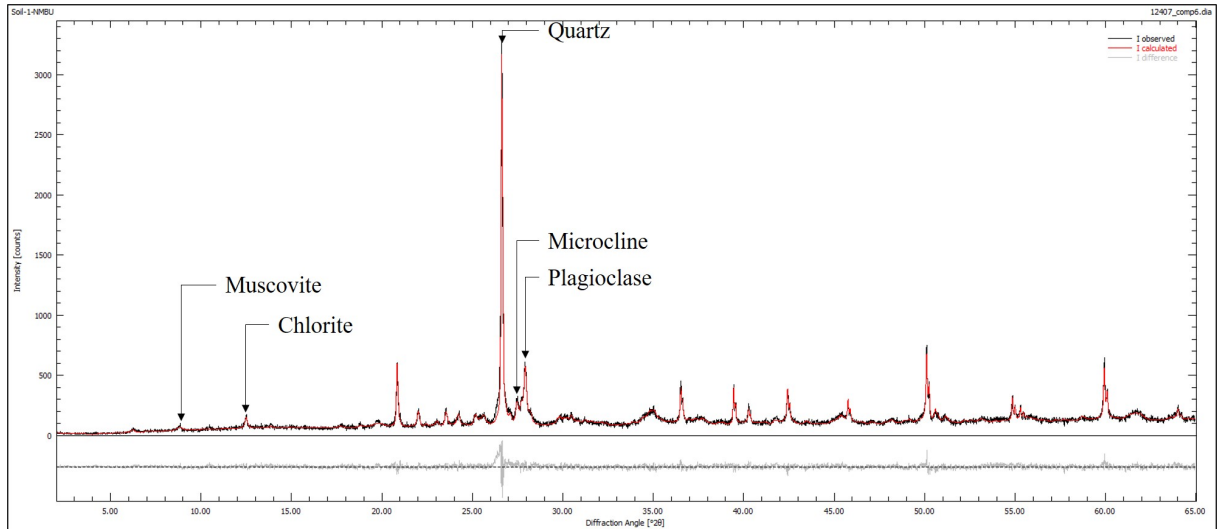
Figure (15) Measured diffractogram by XRD analysis (black line) and synthetic diffractogram simulated with XRD-analysis software Profex with identified peaks to main minerals for agricultural soil sample 1.

1.51 for the B-horizon. A value of χ^2 around 1.5 or smaller is considered to indicate a good determination.

Both core sample horizons differ from the agricultural soil sample 1, which shows a lower

Table (9) Relative mineralogical composition of synthetic diffractograms simulated for bulk samples of soil 1, E-horizon and B-horizon of core sample. Computed diffractograms derived from measured ones by XRD analysis using analysis software Profex with χ^2 as statistical parameter describing goodness of determination.

Minerals	Soil 1	E-horizon	B-horizon
Quartz [%]	33.35	57.09	50.59
Plagioclase [%]	20.50	21.70	21.91
Microcline [%]	10.13	19.04	20.75
Muscovite [%]	27.43	0.00	2.86
Chlorite [%]	8.59	0.00	0.00
Hornblende [%]	0.00	1.66	3.89
Actinolite [%]	0.00	0.51	0.00
Sum [%]	100.00	100.00	100.00
χ^2	1.38	1.68	1.51

relative quartz content (33.35 %), a lower relative amount of microcline (10.13 %), but comparable content of plagioclase (20.50 %). But the agricultural soil contains 27.43 % of muscovite and also another layer silica with 8.59 % chlorite, which are absent in the core samples. The minor minerals hornblende and actinolite quantified in the core samples, were not identified in soil 1. The χ^2 for soil one is the lowest with 1.38, which implies

the best synthetic reconstruction of the measured diffractogram was achieved for this soil. However, the identification of chlorite was not unambiguous due to similarity to other clay minerals.

While the organic matter analysis and the grain size distribution were performed for the samples later used in the partitioning and incubation experiments, just the XRD analysis of soil one directly corresponds to the soil used in the following experiments. The E- and B-horizons were merged to for a bottom-core sample (soil 3), while the O-horizon (not analyzed by XRD) was merged with the E-horizon to form a top-core sample (soil 2).

5.2 Partitioning Experiment B

The results of partitioning experiment B with differing initial concentrations of PCE and PFOA in the contaminating solution (see Table 2) were processed to compute the mass adsorbed to the solid phase and derive an isotherm describing the partitioning behaviour of the corresponding pollutant on the agricultural soil sample 1. Hereafter, the mass balance and isotherm for PCE are presented before the analogue for PFOA are described. Subsequently the results of the IC and the ICP-MS regarding the chemical porewater composition are shown.

5.2.1 Perchloroethylene

After the SHSI-GC-MS results were corrected for the instrumental drift trend, the instrumental and the sample blanks, the measured gaseous concentrations were converted to corresponding aqueous concentrations by Henry's law. A mean mass balance for the replicated samples was derived describing the distribution between the gaseous, the aqueous and the solid phase (Figure 16). From the mass balance the solid phase concentrations were computed. By a scatter plot of the aqueous and the solid concentrations the sorption behaviour was approximated by linear isotherms. The instrumental drift trends and the corrected calibration curves of the PCE measurements are shown in Figure 36 and Figure 37 in Appendix 8.1.4.

The relative mean mass distribution of PCE between the three present phases depending on the initial PCE concentration is illustrated in Figure 16. The figure illustrates, that the majority of PCE is present adsorbed to the solid phase. Thereby, the relative portion sorbed to the solid phase increases slightly with the initial concentration, respectively total mass of PCE. For a total mass of 4 μg ($C_{t0} = 0.5$ ppm) the mass partitioned onto the solid phase is 2.39 $\pm$ 0.54 μg (59.9 %), while for total mass of 80 μg ($C_{t0} = 10$ ppm) 59.25 $\pm$ 1.91 μg (74.1 %) are present on the solid phase of soil 1. Regarding the samples with the lowest initial concentration an average of 1.42 $\pm$ 0.48 μg (35.56 %) of the initial 4 μg partition in the gaseous phase and 0.181 $\pm$ 0.06 μg (4.55 %) are present in the aqueous phase. For the samples with the highest total amount of PCE (80 μg) 18.39 $\pm$ 1.70 μg (22.99 %) are in the gaseous and 2.35 $\pm$ 0.22 μg (2.94 %) in the aqueous phase. As an average of the relative partitioning of PCE 28.61 $\pm$ 5.15 % occur in the gaseous phase, 3.66 $\pm$ 0.66 % in the aqueous phase and 67.72 $\pm$ 5.81 % in the solid phase.

The solid phase concentration of PCE in the equilibrated partitioning experiments was
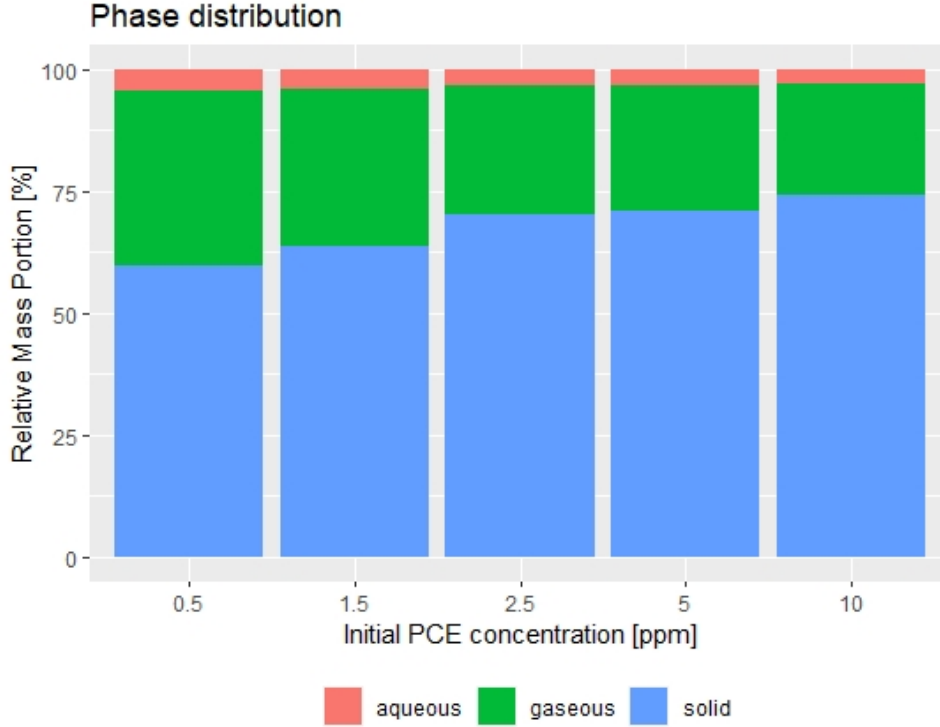
Figure (16) Relative mean mass distribution of PCE between gaseous, aqueous and solid phase of partitioning experiment B using soil one with different initial PCE concentrations. Means computed from replicated measurements for replica of same initial concentration.

computed by the masses derived from the mass balance equation. To characterize the partitioning behaviour, the solid phase concentrations are plotted with the corresponding aqueous concentrations as covariants. The resulting scatter plot is illustrated in Figure 17.

The correlation between the adsorbed and the aqueous PCE concentration is lineary approximated by two isotherms. The linear fit isotherm approximates the distribution with an intercept of the y-axis different from zero, while the linear fit forced-through-origin isotherm intersects the origin. The isotherm cutting the origin describes the theoretical assumption, that the adsorbed PCE concentration is zero, if no aqueous PCE is present. The other isotherm represent a simple linear approximation of the data, without correcting for a intersection through the origin. Due to the shape of the scattered data an approximation for a Freundlich isotherm was dispensed. The mathematical isotherm describes a linear relation of the solid and the aqueous concentration of $C_s = 10.269 * C_{aq} - 0.183$ with an R^2 of 0.960. The theoretical isotherm descibes the relation with the equation $C_s = 9.337 * C_{aq}$ with an R^2 of 0.978. Hereafter, if referred to the linear sorption isotherm for PCE to soil 1 in partitioning experiment B, the theoretically approximated isotherm is meant due to the better fit and the theoretical implication.
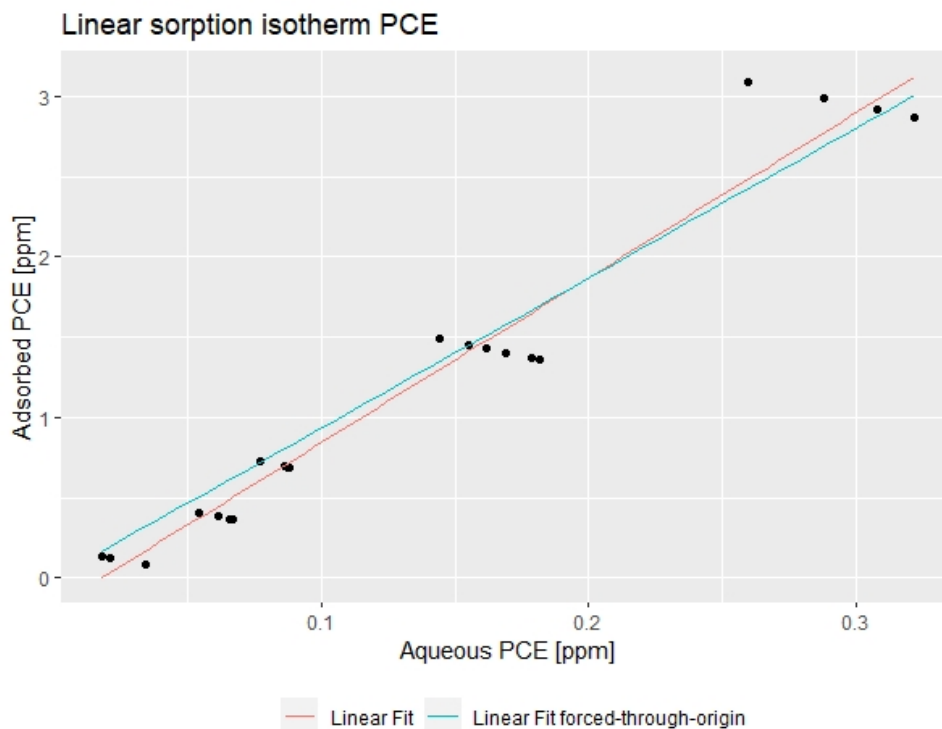
Figure (17) Partitioning of PCE in partitioning experiment B for soil 1 between aqueous and solid phase, derived from PCE measurements by GC-MS, Henry's law and mass conservation. Isotherms linear approximated, with linear fit and linear fit forced through origin by theoretical assumption.

5.2.2 Perfluorooctanoic acid

The measurements of PFOA by GC-MS after the pre-analytical derivatization were corrected for the processing, the sample blanks and the dilution during the porewater extraction. The aqueous PFOA concentrations in the porewater were used to formulate a mass balance under the neglection of partitioning into the gas phase to compute the mass adsorbed onto the solid phase. The instrumental drift trends and calibration curves for the PFOA measurements by GC-MS are illustrated in Figure 38, Figure 39 and Figure 40 in Appendix 8.1.4.

The relative mass distribution of PFOA between the aqueous and the solid phase in dependence on the initial PFOA concentration, respectively total mass, is illustrated in Figure 18.

The plot shows, that for initial PFOA concentrations of 2.5 ppm to 12.5 ppm (total mass of 20 μg to 100 μg), the majority of PFOA is adsorbed to the solid phase. For higher initial concentrations, this relative phase distribution shifts towards an equilibrated distribution of PFOA between the aqueous and the solid phase. The lowest relative portion of PFOA in the aqueous phase is measured for the samples of 12.5 ppm initial concentration, whereby 30.175 $\pm$ 6.87 μg (30.17 %) PFOA occurred in the aqueous phase and 69.83 $\pm$ 6.87 μg (69.83 %) of the total 100 μg PFOA in the solid phase. In contrast for the initial concentration of 50 ppm PFOA (400 μg), 226.86 $\pm$ 61.33 μg (56.71 %) PFOA are present
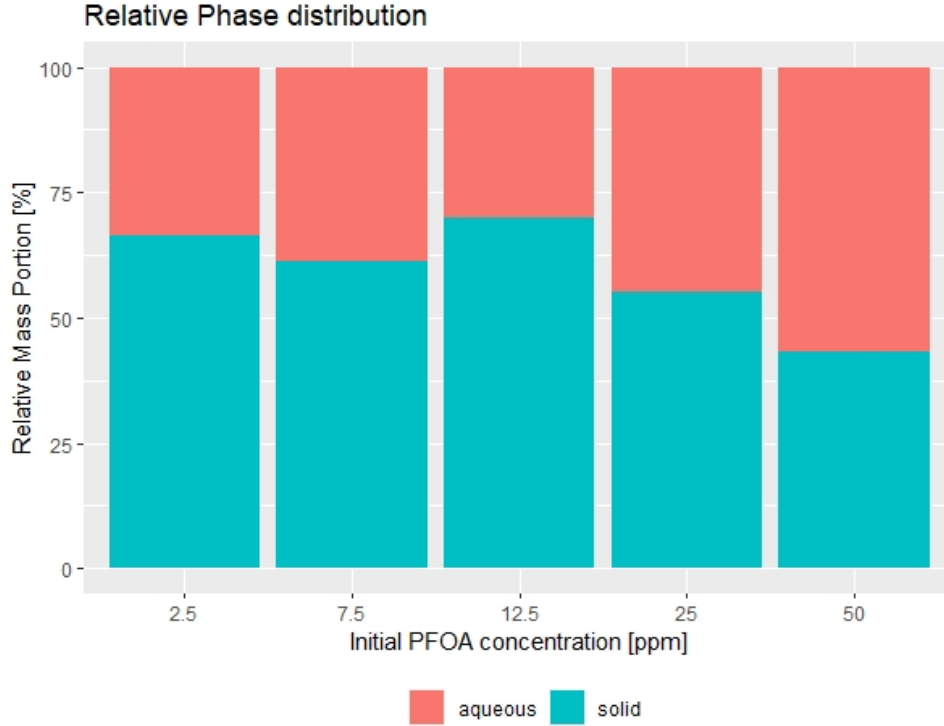
Figure (18) Relative mean mass distribution of PFOA between the aqueous and the solid phase of partitioning experiment B using soil one with different initial PFOA concentrations. Means computed from replicated measurements for replica of same initial concentration.

in the porewater, while 173.14 ± 61.33 μg (43.29 %) are adsorbed to the solid phase. The averaged relative phase distribution over the observed initial concentration range is 40.81 ± 10.45 % of PFOA are present in the aqueous phase, while the remaining 59.19 ± 10.45 % are adsorbed onto the solid phase.

As for PCE, the solid phase PFOA concentration is plotted as a scatter plot depending on the aqueous PFOA concentration. The relation of the concentrations is lineary approximated by a function with an intercept different from zero and an intercept forced through the origin as described for PCE. Due to the distribution of the data, the relation is also approximated by an Freundlich isotherm, which was derived from linear approximation of the data in a ln-ln-plot (Figure 41, Appendix 8.1.4).

Compared to the linear approximation for PCE, the both linear isotherms deviate further in this plot regarding their slope. While the "Linear Fit" isotherm is described by $C_s = 0.236 * C_{aq} + 1.510$ with a R^2 of 0.575, the theoretical approximated isotherm through the origin quantifies the relation of the concentrations with $C_s = 0.307 * C_{aq}$. The R^2 of the theoretical fit is 0.731, which is better than the linear fit, but worse than the one for the Freundlich isotherm with a R^2 of 0.834. In the logarithmic form the relation of the concentrations is described by $ln(C_s) = 0.681 * ln(C_{aq}) - 0.028$, which translates to a Freundlich coefficient K_F of 0.973 and a Freundlich-n of 0.681.
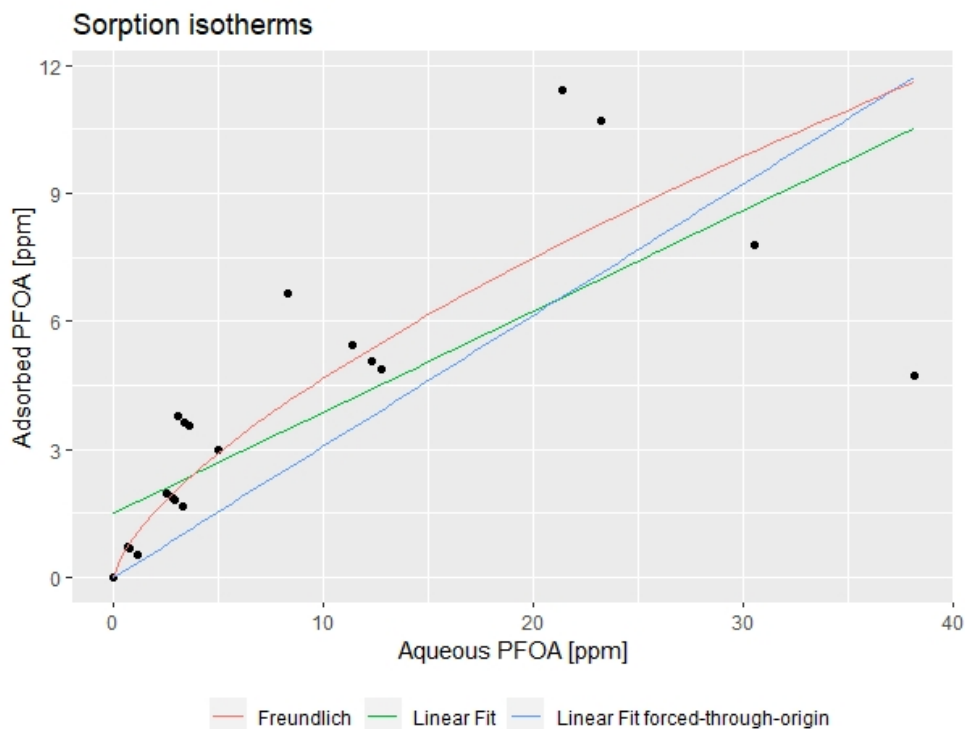
Figure (19) Comparison of sorption isotherms of PFOA from partitioning experiment C, derived with assumption of theoretical intersection of origin. Aqueous concentrations from GC-MS measurements and adsorbed concentration computed via mass balance. Data corrected for instrumental drift, processing and sample blanks.

5.2.3 Porewater Composition

Inductively Couple Plamsa - Mass Spectrometry (ICP-MS)   For the ICP-MS analysis the extracted porewater samples were diluted 1:40 in 1-% HNO_3 solution. The results presented in Table 10 show the porewater concentrations, which were computed from the analytical dilution factor and the extraction dilution factor (Table 4). The presented values are means computed from the replicated samples of the same initial concentration.

In all porewater solution calcium is the dominant cation with the lowest mean concentration of 181.541 ppm in the samples without added PFOA and the highest concentration of 330.197 ppm in the samples with 12.5 ppm initial PFOA. With higher initial PFOA concentration, the measured calcium concentration decreased again to 223.849 ppm measured for the samples with 50 ppm initial PFOA. The mean calcium concentration is 257.198 $\pm$ 52.032 ppm. A comparable trend occurs for magnesium with a mean concentration over all experiments of 4.869 $\pm$ 1.617 ppm. For sodium the highest concentration is measured for the samples with an initial PFOA concentration of 25 ppm with 11.367 ppm, while the total mean is 8.785 $\pm$ 1.425 ppm. For potassium the least variation of the total mean of 7.330 $\pm$ 0.875 ppm occurs. Regarding the minor cations iron shows the highest mean concentration of 0.272 $\pm$ 0.116 ppm. The mean concentrations of manganese with 0.063 $\pm$ 0.069 ppm and of copper with 0.038 $\pm$ 0.012 ppm were comparably low.

Table (10) Porewater concentration of major and minor cations with different initial PFOA concentrations in soil one by ICP-MS analysis.

PFOA [ppm]	Na [ppm]	Mg [ppm]	K [ppm]	Ca [ppm]	Mn [ppm]	Fe [ppm]	Cu [ppm]
0	7.345	2.466	7.809	181.541	0.193	0.472	0.053
2.5	7.883	4.859	5.806	264.608	0.056	0.271	0.052
7.5	9.296	5.845	8.345	292.804	0.016	0.173	0.027
12.5	8.577	7.144	7.361	330.197	0.008	0.200	0.028
25	11.367	5.088	7.680	250.190	0.027	0.178	0.029
50	8.241	3.811	6.980	223.849	0.081	0.337	0.042

Ion Chromatography (IC)   The chemical composition of the porewater samples are also analyzed by IC for the major anions and cations. The analyzed samples were not diluted, which is why the results are just corrected for the dilution factor due to the porewater extraction. Because the results of the ICP-MS analysis already illustrate the chemical composition of the major and minor cations, the IC results for the cation analysis are shown in Table 21 in Appendix 8.1.4. In the following Table 11 the mean porewater concentrations of the major anions (except bicarbonate) computed from the replica of samples with equal initial PFOA concentrations are presented.

Table (11) Porewater concentration of major anions with different initial concentrations of PFOA in soil one from partitioning experiment B analyzed by IC.

PFOA [ppm]	F [ppm]	Cl [ppm]	SO4 [ppm]	Br [ppm]	NO3 [ppm]
0	2.558	22.643	92.439	1.522	41.224
2.5	1.997	16.459	62.186	1.109	576.664
7.5	1.795	16.387	45.399	0.759	723.941
12.5	1.643	18.303	39.376	0.726	856.026
25	1.960	15.952	44.028	0.661	574.416
50	2.250	14.231	69.093	0.980	345.360

Except for the porewater solution without initial PFOA, nitrate is the anion of highest mean concentration with a maximum concentration of 856.026 ppm measured in the samples of 12.5 ppm initial aqueous PFOA. In the samples without initial PFOA, the mean nitrate concentration is 41.224 ppm, while the mean over all samples is 519.605 ± 289.966 ppm. The second most abundant anion measured is sulfate with the highest mean concentration in the samples without initial PFOA of 92.439 ppm. The lowest concentration occurs for the samples of 12.5 ppm initial PFOA concentration with 39.376 ppm, while the mean concentration over all samples is 58.754 ± 20.120 ppm. Chloride occurs with a mean concentration of 17.329 ± 2.910 ppm as the third most abundant anion in all samples. The other halogen anions fluoride and bromide show the lowest overall

mean concentrations of 2.034 ± 0.328 ppm for fluoride and 0.959 ± 0.324 ppm for bromide.

5.3 Partitioning Experiment C

The analysis and processing of the samples of partitioning experiment C is similar to the previous regarding the derivation of the mass balance, but is performed for three different soil samples (see Table 2). Because the soils were only contaminanted with one initial concentration, the derivation of the sorption isotherms depends on the theoretical assumption that the solid concentration is zero, if the aqueous concentration is zero. Besides the mass balances and sorption isotherms for PCE and PFOA, the results of the chemical porewater analysis are presented hereafter.

5.3.1 Perchloroethylene

The measured data was corrected for the instrumental drift, the instrumental and the sample blanks. The instrumental trend and the corrected calibration curves are shown in Figure 42 and Figure 43 in Appendix 8.1.5.

Figure (20) Relative mean mass distribution of PCE between the gaseous, aqueous and solid phase for the three different soil samples of partitioning experiment C. Means were computed from replicated measurements of replica of same initial concentration.

The mean relative phase distribution of PCE in the replicated samples of the partitioning experiments in different soils is illustrated in Figure 20. It illustrates the major

differences in the phase distribution of PCE in the different soil samples. For the agricultural soil one the majority of PCE is present in the gaseous phase with 13.19 ± 1.16 μg (65.94 %) of the total 20 μg. Adsorbed to the solid phase are 5.12 ± 1.31 μg (25.62 %), while 1.69 ± 0.15 μg (8.44 %) are present in the aqueous porewater phase. For the second soil (top-core soil 2), the majority of PCE is present in the solid phase with 13.38 ± 0.47 μg (89.21 %), whilst 1.48 ± 0.43 μg (9.85 %) are in the gase phase and 0.14 ± 0.04 μg (0.93 %) in the aqueous phase. Also in the bottom core soil sample 3, the majority of PCE is present in the solid phase with 8.57 ± 1.18 μg, but the relative portion is less with 57.16 % than for soil 2. The mean of the mass of PCE in the gaseous phase is 5.87 ± 1.08 μg (39.16 %), and in the aqueous phase 0.55 ± 0.10 μg (3.69 %) PCE are present. As for the partitioning experiment B the mass balance of PCE allows the derivation of the adsorbed PCE concentrations for the different soils due to the known soil mass. The concentration of adsorbed PCE is plotted against the aqueous concentrations in a scatter plot to approximate the sorption behaviour lineary in Figure 21. Thereby, the assumption of an intersection through the origin had to be made. This assumption complies with the prior theoretical assumption described in the corresponding results of partitioning experiment B.
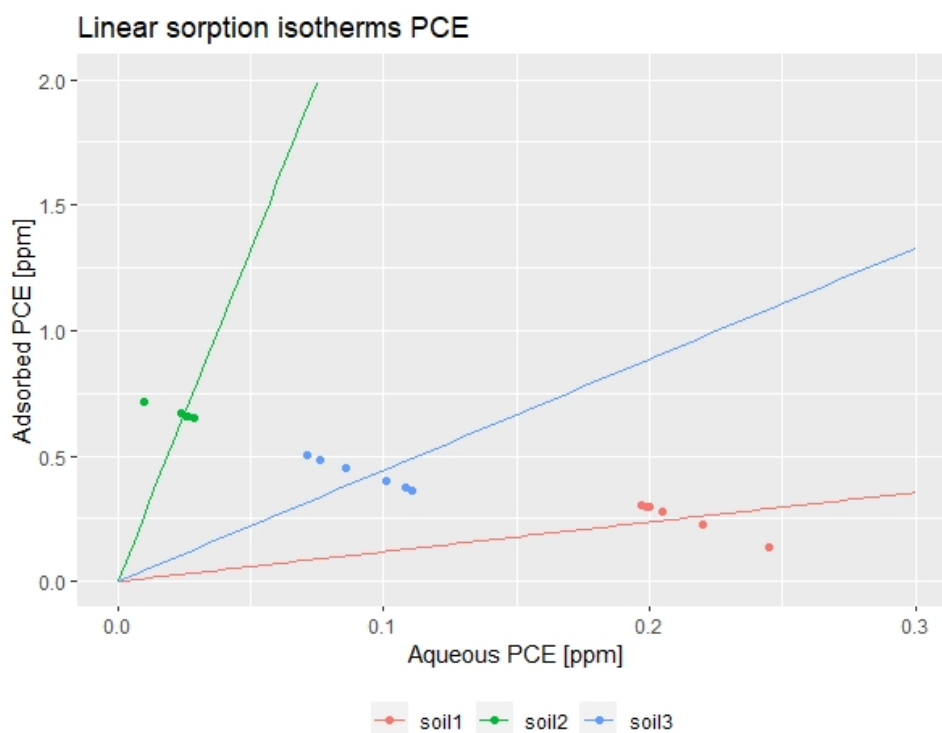
Figure (21) Partitioning of PCE in partitioning experiment C for soil 1, soil 2 and soil 3 between aqueous and solid phase, derived from corresponding PCE measurements by GC-MS, Henry's law and mass conservation. Linear isotherms forced through origin due to theoretical intersection.

From this linear approximation approach, three linear isotherms for the three soil samples result with significant differences regarding the slope, respectively partitioning

coefficient. The linear isotherm approximated for soil 1 implies the least partitioning towards the solid phase with $C_s = 1.184 * C_{aq}$ with a R^2 of 0.907, while the isotherm for soil sample 2 shows the highest sorption onto the solid phase described by $C_s = 26.482 * C_{aq}$ with a R^2 of 0.916. The partitioning of PCE onto the solid phase of soil sample 3 is intermediate compared to the other two soils with an approximated linear partitioning of $C_s = 4.430 * C_{aq}$ (R^2 of 0.918). The linear sortpion coefficient derived for soil 1 from this experiment ($K_d = 1.184 L/kg$) is approximately ten times smaller than the coefficient quantified in partitioning experiment B ($K_d = 10.269 L/kg$).

5.3.2 Perfluorooctanoic acid

The means of the relative phase distribution of PFOA between the aqueous and the solid phase of the different soils with an initial PFOA concentration of 12.5 ppm for all soils is shown in Figure 22. The volume of injected porewater for soil 1 differs from soil 2 and 3 due to expected porespace saturation. While for soil one 8 ml of the contaminating solution were injected (total PFOA of 100 μg), 6 ml were injected for soil two and three (total PFOA 75 μg) (see Table 2). The results are corrected for the linear instrumental drift, the processing and sample blanks. The measured concentrations are corrected for the dilution factor resulting from the porewater extraction. The instrumental drift and the calibration curves for the measurements performend on the 21.07.2021 and 23.07.2021 are illustrated in Figure 44, Figure 45 and Figure 46 in Appendix 8.1.5.

The mean relative mass distribution presented in Figure 22 implies a comparable distribution of PFOA between the solid and the aqueous phase for soil 1 and soil 3. For soil 1 44.48 $\pm$ 8.02 μg (44.48 %) of the total 100 μg occur in the aqueous phase and the remaining 55.52 $\pm$ 8.02 μg (55.52 %) are attributed to the solid phase. Regarding the relative distribution this is comparable to the distribution observed for soil 3 with 27.69 $\pm$ 5.88 μg (36.92 %) in the aqueous and 47.31 $\pm$ 5.88 μg (63.08 %) on the solid phase. The relative mass distribution for soil 2 differs from the one of the other two soils, where with 66.79 $\pm$ 5.96 μg (89.06 %) nearly all PFOA is present on the solid phase and 8.21 $\pm$ 5.96 μg (10.94 %) occur in the aqueous phase.

The solid concentrations were derived and plotted against the measured aqueous concentrations to estimate the partitioning behaviour of PFOA in the different soils. As for partitioning experiment B the adsorption was approximated for a linear isotherm and for a Freundlich isotherm with the assumption of an intersection through the origin. The Freundlich isotherm parameters are derived from a double logarithmic plot (natural logarithm) of the concentrations, which is illustrated in Figure 47 in Appendix 8.1.5. An assumed intersection of the origin in the ln-ln-plot used for the estimation of the Freundlich coefficients K_F and n corresponds to setting $K_F = 1$. Although this assumption was made, the approximation of the Freundlich isotherm for soil 2 is inadequate (see Figure 23, which is why it was neglected neglected hereafter.
As implied by the mass distribution, the relative partitioning of PFOA onto the solid phase is comparable for soil 1 and soil 3, which is also implied by the derived linear and Freundlich isotherms (Figure 23). The linear isotherm for soil 1 describes the solid-aqueous phase
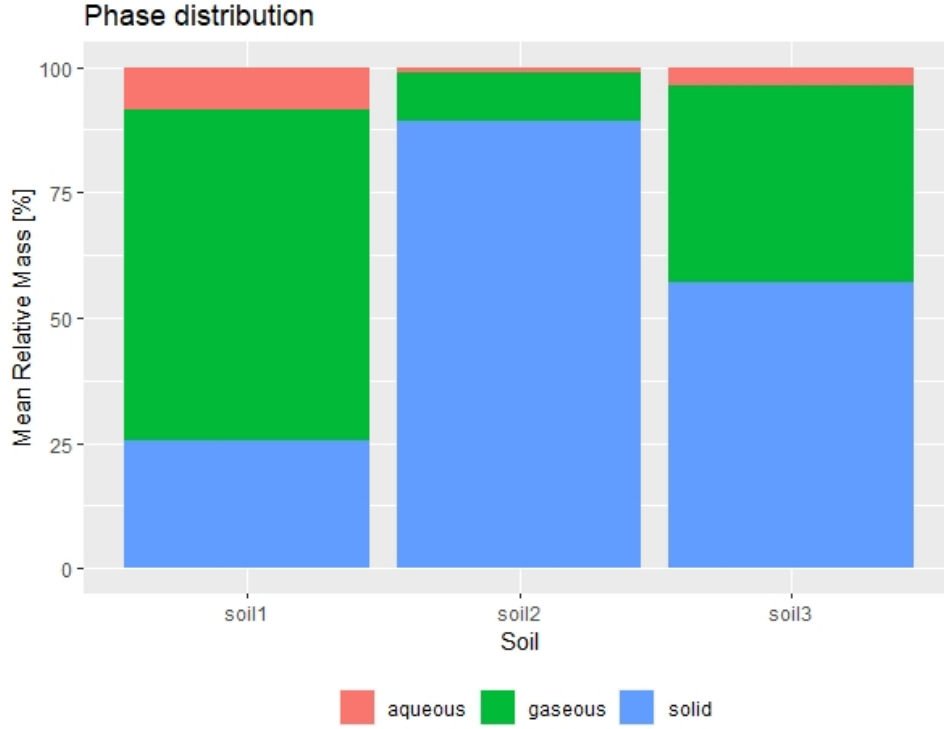
Figure (22) Relative mean mass distribution of PFOA between the aqueous and the solid phase for the three soil samples of partitioning experiment C with the sample initial PFOA concentrations, but different aqueous phase volumes. Means computed from replicated measurements for replica of same initial concentration.

concentration with $C_s = 0.476 * C_{aq}$ ($R^2 = 0.916$), which is very comparable to the one for soil 3 with $C_s = 0.483 * C_{aq}$ ($R^2 = 0.910$). Also the Freundlich isotherms of these two soil samples result in comparable equations with $C_s = 1 * C_{aq}^{0.582}$ with $R^2 = 0.949$ for soil 1 and $C_s = 1 * C_{aq}^{0.547}$ with $R^2 = 0.932$ for soil 3. Comparing the theoretically concentration distributions of the linear and the Freundlich isotherms of soil 1 and three, the predicted partitioning onto the solid phase for aqueous concentrations between 0.25 and 4 ppm is higher for the Freundlich isotherms. After the linear and Freundlich isotherms intersect at the means of the phase distribution of the corresponding soils, the adsorption predicted by the linear isotherm exceeds the estimations of the Freundlich isotherms. In an aqueous concentration range of 4 to 6.5 ppm the estimations the different type of isotherms are comparable for the corresponding soils.

While the Freundlich isotherm for soil 2 is neglected, the linear isotherm describes the phase distribution with $C_s = 1.6046 * C_{aq}$ with an R^2 of 0.618. The coefficient of determination (R^2) already implies, that this linear approximation is not as reliable as the ones for soil 1 and soil 3. The variation in the small sample set is too significant to allow a more robust estimation of a linear sorption behaviour.

Compared to the derived linear and Freundlich isotherms for soil one in the partitioning experiment B, the linear partitioning coefficient from this experiment is higher with $K_d = 0.476$ compared to the $K_d = 0.307$ of the previous experiment. Regarding the Freundlich isotherm, the Freundlich coefficient had to be slightly increased in this exper-

63
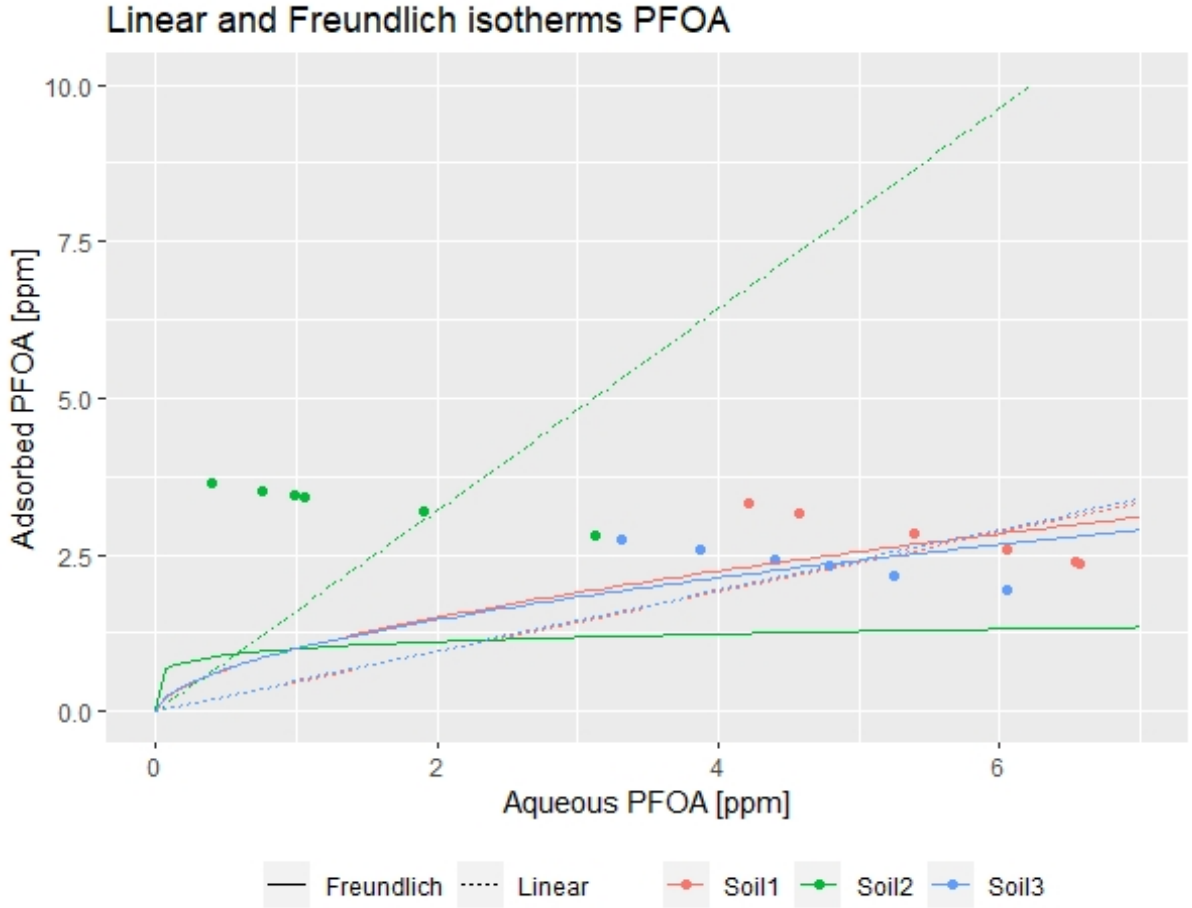
Figure (23) Comparison of sorption isotherms of PFOA from partitioning experiment C. Isotherms forced through origin with assumption of theoretical intersection of origin. Aqueous concentrations from GC-MS measurements and adsorbed concentration computed via mass balance. Data corrected for instrumental drift, processing and sample blanks.

iment to $K_F = 1$ - from $K_F = 0.973$ in partitioning experiment B - to allow a derivation of the exponent n. This value decreased from partitioning experiment B with $n = 0.681$ to $n = 0.582$ for partitioning experiment C.

5.3.3 Porewater Composition

Inductively Couple Plamsa - Mass Spectrometry (ICP-MS) The ICP-MS analysis for the major and minor cations in the porewater samples of partitioning experiment C were treated like the previous samples of partitioning experiment B. The results were corrected for the analytical dilution and the dilution factor from the porewater extraction (Table 4). For each soil one blank sample was measured, while the results of the triplicated samples of each soil are averaged.

The difference in the cation concentrations between the blank and the samples mean is the apparent for soil 1. The concentrations of all cations are higher in the contaminanted samples than in the blank, whereby the highest concentrated cation is calcium with a

concentration of 267.742 ppm in the blank and 367.797 ppm as a mean concentration in the contaminated experiments. The mean concentration in the contaminated samples equals 137 % of the measured blank concentration. A comparable relative difference occurs for magnesium and potassium, with a mean 7.854 ppm of magnesium in the samples compared to 5.898 ppm in the blank, which corresponds to 133 % and 4.365 ppm to 3.319 ppm (131 %) for potassium. The ratio is slightly lower with 122 % for sodium and the minor cation cupper with 126 %. For manganese and iron the concetration ratio is higher between the samples and the blank with 432 % for manganese and 320 % for iron.

Table (12) Porewater concentrations of major and minor cations for blanks and contaminanted sample for different soil samples in partitionig experiment C.

	Element	Na	Mg	K	Ca	Mn	Fe	Cu
Soil	**Type**	[ppm]	[ppm]	[ppm]	[ppm]	[ppm]	[ppm]	[ppm]
Soil 1	Blank	8.490	5.898	3.319	267.742	0.027	0.211	0.028
	Sample	10.345	7.854	4.365	367.797	0.116	0.675	0.036
Soil 2	Blank	18.561	26.402	98.067	71.375	1.484	4.715	0.058
	Sample	17.367	21.327	90.838	57.925	1.175	4.499	0.058
Soil 3	Blank	8.590	2.067	6.278	0.000	0.037	8.889	0.036
	Sample	9.778	2.445	6.118	2.478	0.053	13.787	0.100

For the samples of soil 2 the cation concentration ratios are reversed compared to soil 1, with lower concentrations observed in the contaminated samples. For the most abundant cation potassium the ratio is close to 1 with 98.067 ppm in the blank and 90.838 ppm in the averaged samples (92 %), which also occurs for sodium (94 %), iron (95 %) and cupper (99 %). For manganese, calcium and cupper the ratios range around 80 %. Except for calcium and cupper, all measured concentrations are higher in the second soil than in the first soil. For the third soil the trend is similiar as to soil 1, that all concentration are higher in the contaminated samples than in the blank, except for potassium which is slightly lower. For sodium, magnesium, manganese and iron the concentration increase in the contaminated samples ranges from 113 % for sodium to 155 % for iron. It is to emphasise, that iron is the highest concentrated cation in all samples of soil 3, while it occurs as a minor cation in soil 1. Compared to soil 2, the iron concentrations in soil 3 are about a factor of 2 to 2.5 higher. While the manganese concentration is soil 2 were enhanced, it occurs as a minor cation in soil 3.

Ion Chromatography (IC)   As for partitioning experiment B, the extracted porewater samples for the IC-analysis were not further diluted, which is why the results are just corrected for the dilution factor resulting from the porewater extraction (Table 4). As the cation concentrations have already been discussed for the ICP-MS analysis, the results for the major cation concentrations by IC are attached in Table 22 in Appendix 8.1.5.

A difference in concentrations of the major anions between the blank and the averged samples seems just to occur for nitrate in soil 1 and soil 2, whereby the concentrations

Table (13) Porewater concentration of major anions for blanks and contaminated of different soil samples from partitioning experiment C analyzed by IC.

Soil	Element Type	F [ppm]	Cl [ppm]	SO4 [ppm]	Br [ppm]	NO3 [ppm]
Soil 1	Blank	1.709	14.829	43.437	0.607	526.514
	Sample	1.470	15.514	42.240	0.592	861.958
Soil 2	Blank	6.768	59.528	1.084	5.177	0.879
	Sample	5.584	62.514	0.810	3.476	2.796
Soil 3	Blank	0.283	21.205	7.395	5.555	0.758
	Sample	0.588	22.663	9.126	13.993	0.848

are higher for the contaminated samples, and for bromide in soil 3 and soil 2. The nitrate concentration in the blank of soil 1 amounts 526.514 ppm compared to an averaged concentration 861.958 ppm in the contaminated samples. This relative increase of 163 % also occurs in soil 2 with a concentration of 0.879 ppm in the blank and 2.796 ppm in the samples (318 %). Regarding the change of the bromide concentrations a drop occurs in soil 2 from the blank to the averaged samples from 5.177 ppm to 3.476 ppm, while for soil 3 the concentration increases from 5.555 ppm to 13.993 ppm. In soil 2 and soil 3 the major anion present (excluding bicarbonate) is chloride, while for soil 1 nitrate is the most abundant one.

5.4   Incubation Experiment A

Before the results of the headspace analysis for PCE and the results of the porewater analysis are presented, the results of the monitored headspace content for methane and carbon dioxide for the samples of the methane treatments are described. Thereafter, the potential mass reduction in the contaminated samples is estimated using the results for the linear and Freundlich isotherms from partitioning experiment C. They allow the computation of the solid phase concentration from the measured aqueous phase concentrations of the contaminants, while for PFOA the partitioning in the gaseous phase is neglected. A mass balance according to mass conservation allows to compute potential sink terms. The control and the methane treatments of the different soils are compared regarding these sinks and the measured aqueous concentrations of the contaminants. Subsequently the results of the chemical porewater analyses by ICP-MS and IC are presented.

5.4.1   Monitoring Biological Activity

For the samples of the methane treatment the content of methane (CH_4) and carbon dioxide (CO_2) in the headspace is monitored by an automized GC system. The monitored results for soil 1 b) are exemplary illustrated in Figure 24 and described hereafter. Corresponding plots for the methane treatments of soil 1 a), soil 2 and soil 3 are presented in

Figure 48, Figure 49 and Figure 50 in Appendix 8.1.6. The training of the soils for oxic methane consumption started on the 12.07.2021 with an initially added methane content of approximated 30000 ppmv in the headspace volume. For the samples the contaminats were injected on 28.07.2021, which started the incubation period. For soil 1 a) the incubation period was terminated at the 30.07.2021, while the other soils were resupplied with methane and further monitored until the 02.08.2021.

During the training period the methane content decreased gradually in all samples until the 18.07.2021, when the monitoring was interrupted due to the breaking of the sampling needle. While methane depleted the CO_2 content in all samples increased, whereby the content in soil 1 a), soil 1 b) and soil 3 rose approximately 12000 ppmv. In the same period the CO_2 content in soil 2 rose up to 90000 ppmv. Because no contaminants were added yet, there were no differences between the blanks and samples. The broken sampling needle was replaced on the 23.07.2021, after which methane was added occasionally for soil 1 a) and soil 1 b), which depleted rapidly after methane injections. The CO_2 content rose up to approximately 40000 ppmv until the 25.07.2021, after which it stagnated until the contamination on 28.07.2021. For soil 2 the CO_2 content stagnated at around 70000 ppmv after the sampling needle was replaced until the injection of the contaminants, while the content of added methane decreased slowly from the 23.07.2021 until the 27.07.2021 from ca. 30000 ppmv to 17000 ppmv. For soil 3 the CO_2 content was approximately constant around 18000 ppmv in the end of the training period until the contamination. The methane content decreased slowly from 22000 ppmv to 10000 ppmv, but at a faster rate than in soil 2, before all samples were resupplied at the 27.07.2021.

The contaminant solution containing PCE and PFOA was added at the 28.07.2021 and the samples were resupplied with methane to approximately 20000 ppmv. After the injection of the contaminants a drop of CO_2 was observed for all samples as well as a decrease of the methane content. Soil 1 a), soil 1 b) were depleted in methane at the 30.07.2021, when the incubation for soil 1 a) was terminated and more methane was added to the other samples. In the samples of soil 1 b) the methane content stagnated at around 12000 ppmv until the 01.08.2021, before it dropped to 9000 ppmv at the 02.08.2021. From the 30.07.2021 to the 02.08.2021 the CO_2 content increased from 8000 ppmv to 17500 ppmv.

After the contamination the CO_2 level in the samples of soil 2 decreased until the 30.07.2021 from 50000 ppmv to 8000 ppmv, before it started to increase to 22000 ppmv until the end of the incubation at the 02.08.2021. After contaminants and methane were added at the 28.07.2021, the methane decreased slowly from 25000 ppmv to 15000 ppmv until the resupply at the 30.07.2021. Thereafter the methane level stagnated at 20000 ppmv until the 01.08.2021, before it increased nearly 40000 ppmv without additional supply. A comparable pattern of the methane content is observed for soil 3, which decreased from 28000 ppmv after the contamination to 10000 ppmv at the 30.07.2021. After the resupply with methane the methane content stagnated at 14000 ppmv until the 01.08.2021, when it increased to approxiatedly 22000 ppmv before subsequent stagnation.

The CO_2 content between samples and blanks was similiar for all soils and the methane content just differed for soil 2 and soil 3 in the end of the incubation period. Thereby, the methane in the blanks of soil 2 was slightly lower, while the content was significantly higher in the blanks of soil 3 than in the contaminated samples. During the incubation
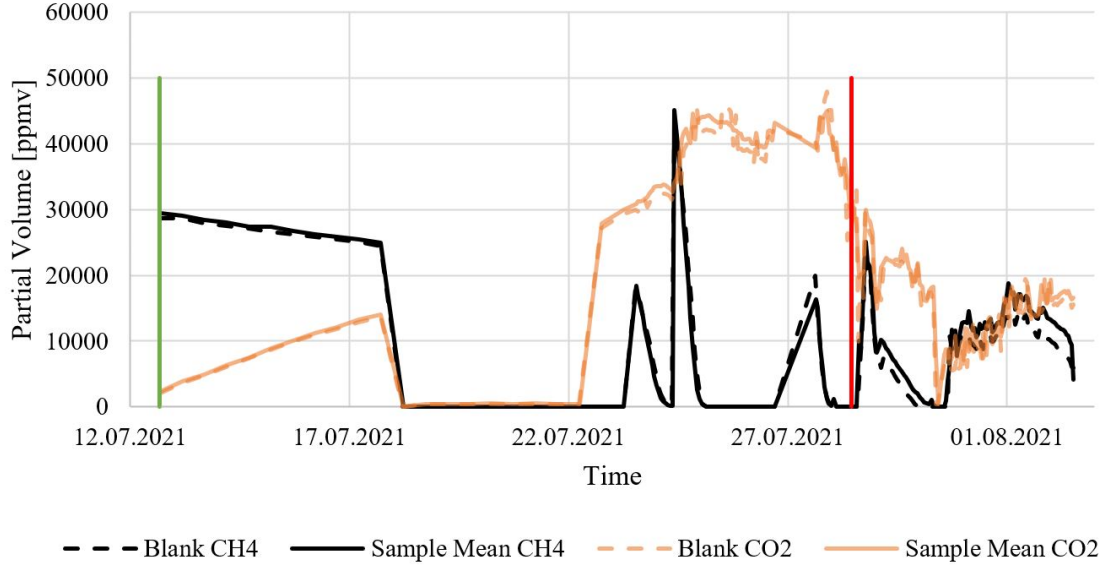
Figure (24) GC-monitored headspace content of methane and carbon dioxide for training period (12.07.2021 to 28.07.2021) and incubation period (28.07.2021 to 02.08.2021) for soil 1 b) for blank and mean of triplicated samples. The green line indicates the start of the methane consumption training, while the red line indicates the the addition of the contaminants.

period, the sampling intervals were shortened from 12 h during the training period to 1.5 h during the incubation period. During the incubation period the results for methane and CO_2 varied significantly, where consecutive measurements of methane fluctuated with up to 10000 ppmv (samples and blanks). The fluctuations were corrected for zero-measurements by interpolation of preceding and consecutive results.

5.4.2 Perchloroethylene

As for the partitioning experiments, the presented PCE results are corrected for the instrumental drift trend, for the instrumental and the sample blanks. The instrumental drift trend and the corrected calibration curves for the measurements on the 03.08.2021, 04.08.2021 and 05.08.2021 are shown in Figure 51 and Figure 52 in Appendix 8.1.6. The aqueous concentrations were computed for the added porewater volume.

To compare the effect of the methane treatment on the PCE the aqueous concentrations of the control and the methane treatment for each soil are compared in Figure 25. The used boxplots indicate the individual results (points), the resulting mean (thick horizontal line) and the 25th and 75th percentile for the different treatments of each soil. The statistical indications of the boxplots for the aqueous PCE concentrations imply that there is no significant difference between the treatments of the different soils with the exception of soil 1 b). In soil 1 b) the aqueous concentration of PCE in the control treatment is approxmately half of the mean concentration measured in the corresponding methane treatment, with a mass of PCE of 0.088 ± 0.035 ppm in the control and 0.165 ± 0.015 ppm in the methane treatment.
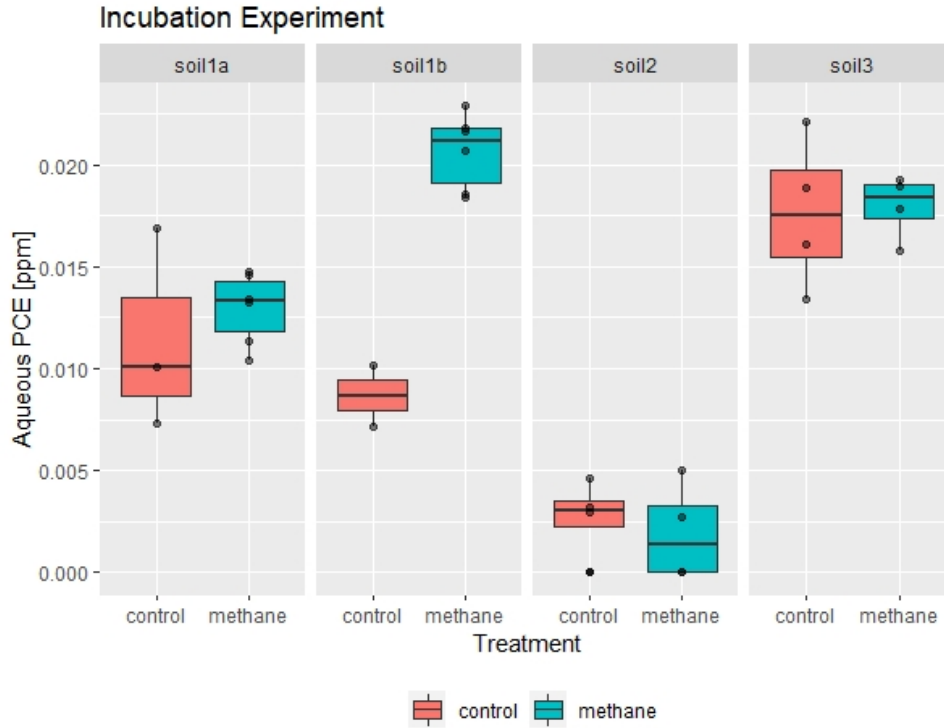
Figure (25) Comparison of aqueous PCE concentrations in incubation experiment A by GC-MS analysis between methane treatment and control treatment. Aqueous concentrations computed by Henry's law. Samples and corresponding calibration standards corrected for instrumental drift, processing and sample blanks.

To derive a mass balance from the measured gaseous PCE concentrations, the aqueous concentrations were computed by Henry's law, before the linear isotherms determined in partitioning experiment C are used to compute the corresponding solid concentrations for each soil. With the volume, respectively mass, of each phase the corresponding masses can be computed. The formulation of a mass balance with the initially added total mass allows to compute a sink term. The relative mass distribution between the phases and the sink term is depicted in Figure 26 for the different treatments of each soil.

Comparing the relative mean mass distribution of PCE between the phases and the computed sink term respectively the control and the methane treatments implies, that there are differences in the relative mass distribution and mass losses (sink) between the control and the methane treatment for soil one b) and soil two. In the control treatment of soil 1 b) 2.09 ± 0.82 μg are sorbed to the solid phase (10.44 %), 0.689 ± 0.273 μg are present in the gas phase (3.44 %) and 0.088 ± 0.035 μg are dissolved in porewater (0.44 %). With an initial mass of 20 μg a loss of 17.135 ± 1.134 μg results as the sink term (85.68 %). In the methane treatment of soil 1 b) the sink term equals 14.629 ± 0.480 μg (73.15 %), while 6.46 % of PCE are present in the gaseous, 0.83 % in the aqueous and 19.57 % on the solid phase.
In the control of soil 2 the sink term equals 3.42 ± 2.934 μg (22.80 %) while in the methane treatment it is computed with 8.766 ± 7.810 μg (58.44 %). The high standard
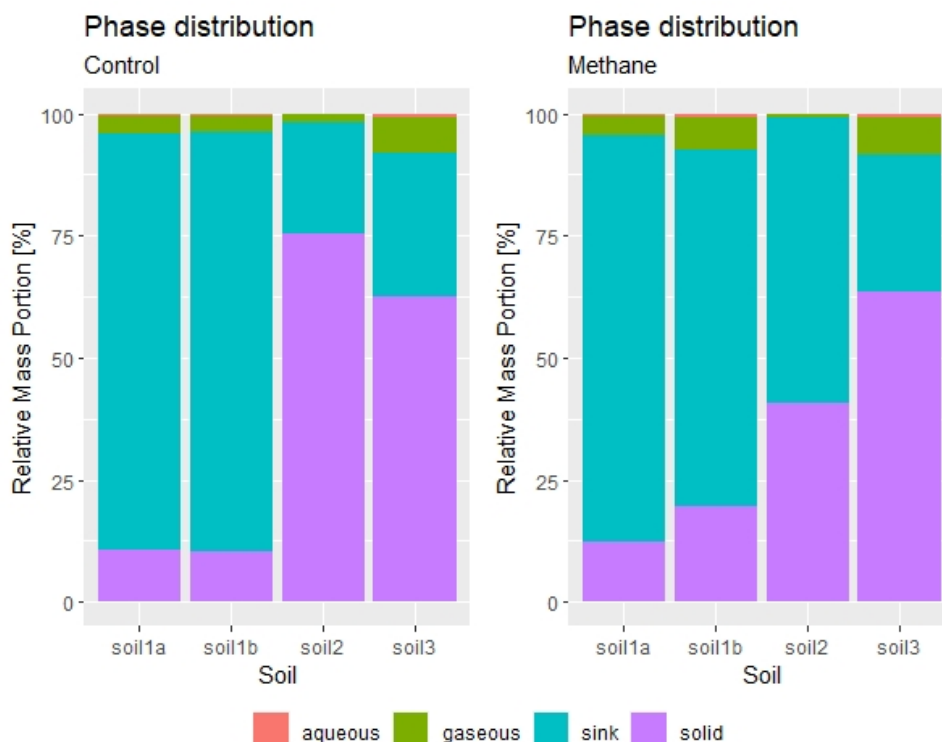
Figure (26) Relative mean mass distribution of PCE between the gaseous, aqueous and solid phase and the sink for the three different soil samples in the two different treatments of incubation experiment A. Means were computed from replicated measurements of replica of same initial concentration.

deviations for the computed results of soil 2 imply a poor reliability of these values and consequential implications.

The comparison of the treatments of soil 1 a) of shorter incubation time and soil 3 imply no significant difference between treatments. The relative mass of PCE accounting to the sink term in in the control treatment of soil 1 a) was 85.15 % ($17.029 \pm 1.287 \ \mu g$) and 83.17 % ($16.633 \pm 0.456 \ \mu g$) in the methane treatment. In the control treatment of soil 3 the sink term amounts 29.35 % ($4.403 \pm 2.260 \ \mu g$) of the mean relative mass distribution of PCE, while it is computed to be 28.04 % ($4.207 \pm 0.948 \ \mu g$) in the methane treatment.

5.4.3 Perfluorooctanoic acid

Like for the contaminant PCE, the aqueous concentrations of PFOA in the different treatments of the soils are compared by boxplots before the relative mean mass distribution including a sink term is presented. As for the prior partitioning experiments, the partitioning of PFOA into the gaseous phase is neglected. The presented results are corrected for the instrumental drift, processing and sample blanks and the dilution factor resulting from the porewater extraction. The instrumental drift and the corrected calibration curves are showed in Figure 53 and Figure 54 in Appendix 8.1.6.

In contrast to the boxplots of the aqueous concentrations for PCE, the analogue plots

for PFOA in Figure 27 suggest differences regarding the observed aqueous concentrations between the treatments for soil 2 and soil 3.
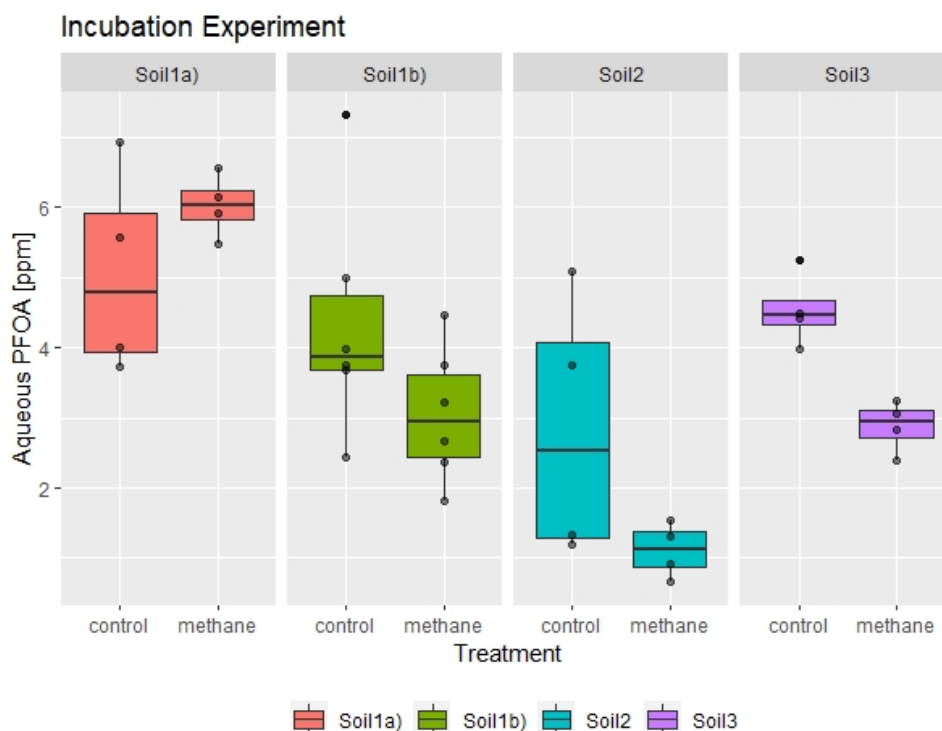
Figure (27) Comparison of measured aqueous PFOA concentrations in incubation experiment A by GC-MS analysis between methane treatment and control treatment. Samples and corresponding calibration standards corrected for instrumental drift, processing and sample blanks.

For soil 1 a) the mean aqueous concentration in the methane treatment appears higher than in the control treatments, but the variations of the observations are significant and the number of observations to small to neglect outliers (number of samples n=2 per treatment). The computed mean concentration in the aqueous phase of the methane treatment of soil 1 is 6.02 ± 0.44 ppm (48.16 ± 3.56 μg) and 5.05 ± 1.49 ppm (40.41 ± 11.91 μg) for the control treatment.

Also in the other batch of soil 1, which experience more methane supply, the variation of the small data set (n=3) prohibits a discrimination between the results of the different treatments. But in contrast to the experiment of soil 1 a), the mean aqueous concentration in the methane treatment is lower with 3.04 ± 0.97 ppm (24.344 ± 7.732 μg) than in the control treatment of soil one b) with 4.35 ± 1.66 ppm (34.817 ± 13.295 μg).

For the experiments of soil 2 and 3 the mean aqueous concentrations of the methane treatments are also lower than in the corresponding controls, whereby the sample set for these experiments are also n=2 per treatment. But the variation in the observations are lower than the ones observed for soil 1, except for the control treatment of soil 2. In the control treatment of soil 2 the mean aqueous concentration of PFOA is 2.83 ± 1.90 ppm (17.00 ± 11.40 μg) and 1.11 ± 0.39 ppm (6.68 ± 2.37 μg) in the methane treatment. The most significant difference in observed aqueous concentrations between treatments

occured for soil 3 with a mean concentration of 4.53 ± 0.52 ppm (27.21 ± 3.14 μg) in the control and of 2.88 ± 0.37 ppm (17.29 ± 2.21 μg) in the methane treatment.

To compute the mass of PFOA accouting to the sink term in the mass balance, the solid phase concentration is computed from the measured aqueous concentrations. Therefore, the linear isotherms derived in partitioning experiment C are used, even though the Freundlich isotherms of soil 1 and 3 approximated a better fit. But because the derivation of a Freundlich sorption isotherm for soil 2 was inadequate, the following computations were performed with the linear isotherms. Furthermore, are the observed aqueous concentrations in the range of acceptable accordance of the linear and the Freundlich isotherms (see Figure 23). The results derived from the Freundlich isotherms are presented in Figure 55 in Appendix 8.1.6.
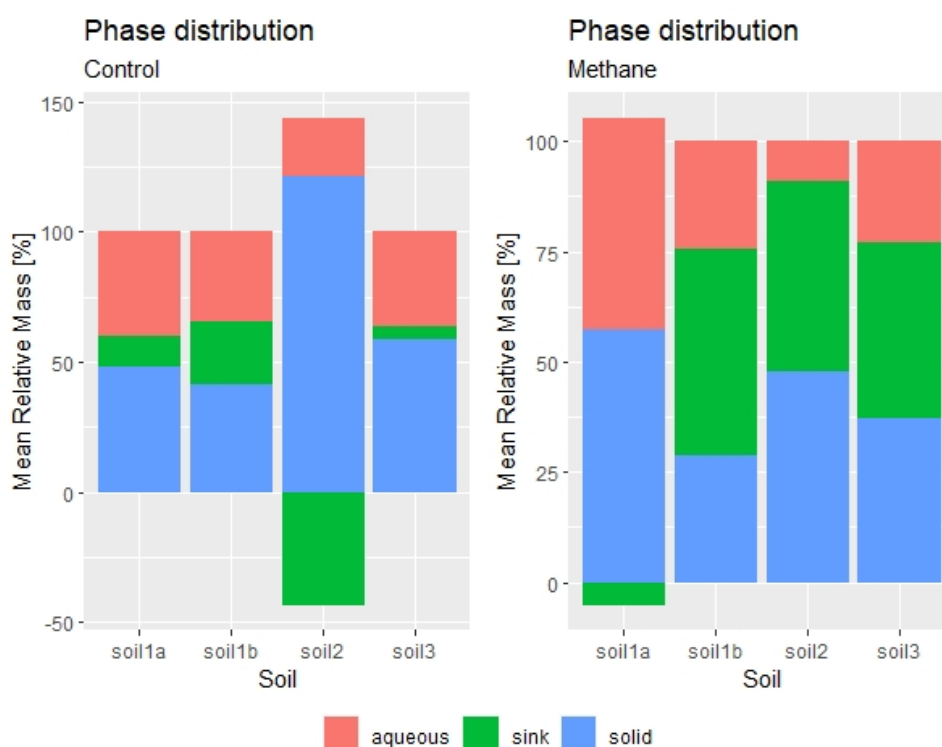
Figure (28) Relative mean mass distribution of PFOA between the aqueous and solid phase and the sink for the three different soil samples in the two different treatments of incubation experiment A. Solid phase concentrations computed from linear isotherms derived in partitioning experiment C. Means were computed from replicated measurements of replica of same initial concentration.

The mean relative mass distribution of PFOA between the aqueous and the solid phase and the sink is illustrated in Figure 28. The presented results of the mass balance imply insecurities in the computation for soil 1 a) and soil 2, because the sum of relative portions exceeds 100 %. Using the Freundlich sorption isotherm instead leads to the same result for soil 1 a) (see Figure 55, Appendix 8.1.6). Thus, the mass balances of soil 1 a) and soil 2 are not further evaluated.

For the control treatments of soil 1 b) the mean relative mass of the sink term is 23.80

$\pm$ 29.10 μg (23.80 %), whilst it is around two times higher in the methane treatment with 46.72 $\pm$ 16.92 μg (46.72 %). In the control treatment the mean relative mass in the aqueous phase amounts 34.82 $\pm$ 13.30 μg (34.82 %) and 41.38 $\pm$ 15.80 μg (41.38 %) on the solid phase of the total 100 μg PFOA in the incubations. In the methane treatment 24.34 $\pm$ 7.73 μg (24.34 %) PFOA are present in the aqueous phase and 28.94 $\pm$ 9.19 μg (28.94 %) are sorbed to the solid phase of soil 1 b). The mean aqueous PFOA mass in the control treatment of soil 3 is 27.21 $\pm$ 3.14 μg (36.28 %), the mean adsorbed mass is 43.82 $\pm$ 5.05 μg (58.43 %) and 3.97 $\pm$ 8.19 μg (5.30 %) contribute to the sink. In the methane treatment of soil 3 a mean mass of PFOA in the aqueous phase is 17.29 $\pm$ 2.21 μg (23.05 %), 27.84 $\pm$ 3.56 μg on the solid phase (37.13 %) and 29.87 $\pm$ 5.768 μg are contributed to the sink (39.82 %).

The computed standard deviations of the treatments of soil 1 b) are higher than the ones computed for soil 3, even though the sample number was n=3 for soil 1 b) and n=2 for soil 3 (all sample measurements replicated twice).

If the standard deviations are neglected, the computed sink terms in the methane treatment of soil 1 b) and soil 3 are bigger than in the corresponding control treatments. This implies an increase of the PFOA removal from the closed systems with the methane treatment compared to the controls. The relative mean mass distributions computed by usage of the Freundlich isotherms for soil 1 b) and soil 3 support this implication (see Figure 55, Appendix 8.1.6).

5.4.4 Porewater Composition

Inductively Couple Plamsa - Mass Spectrometry (ICP-MS)   Like the porewater samples of the partitioning experiments, the extracted porewater solutions were diluted 1:40 in 1-% nitric acid for the ICP-MS analysis for major and minor cations. The results are corrected for the analytical dilution and the dilution from the porewater extraction procedure (see Table 4). The results for the blanks of soil 1 a) and b) result from one replica, while for the triplicated samples an average was computed. For soil 2 and soil 3 all samples and blanks were replicated twice and results presented in Table 14 show the averages of these.

For soil 1 a) and b) the most abundant cation is calcium, whereby the concentrations in both control treatments are approximately two times higher than in the methane treatments. Between the blanks and the samples in the treatments of soil 1 a) and b) no significant differences are obvious.

For soil 1 a) the concentrations of the major cations (sodium, magnesium, potassium, calcium) were in general higher in the control treatment than in the methane treatment, except for the sodium concentration in the blank of the methane treatment with 72.231 ppm and the mean potassium concentration of the samples of the methane treatment with 3.718 ppm. This trend is inversed for the minor cations manganese and iron, which show a higher concentration in the methane treated samples than in the control samples. In the methane treatments the corresponding concentrations are higher for the blanks than for the averaged samples. For copper the concentrations are lower in the methane treatment than in the control treatment, whilst the mean sample concentration is lower than the blank concentration in the control treatment. For the methane treatment it is

the opposite.

Table (14) Porewater concentrations of major and minor cations in different treatments of soil samples used in incubation experiment A for blanks and contaminated samples. For replicated samples the means were computed.

		Element	Na	Mg	K	Ca	Mn	Fe	Cu
Soil	**Treat.**	**Type**	[ppm]	[ppm]	[ppm]	[ppm]	[ppm]	[ppm]	[ppm]
Soil 1a	Control	Blank	28.562	11.752	3.862	326.754	0.062	0.604	0.221
		Sample	28.373	10.889	3.270	293.054	0.044	0.635	0.122
	Methane	Blank	72.231	7.178	2.816	153.799	0.181	3.417	0.037
		Sample	23.915	7.518	3.718	167.589	0.127	2.432	0.086
Soil 1b	Control	Blank	26.399	11.526	3.176	331.759	0.031	0.577	0.035
		Sample	23.019	10.917	3.154	319.550	0.029	0.625	0.035
	Methane	Blank	5.418	4.216	2.018	164.782	0.082	0.167	0.027
		Sample	5.425	4.233	1.787	164.887	0.222	0.156	0.019
Soil 2	Control	Blank	43.647	15.622	80.289	51.657	0.526	12.600	0.630
		Sample	44.559	16.733	86.548	50.134	0.581	14.201	0.165
	Methane	Blank	9.030	5.833	68.089	15.966	0.332	3.929	0.039
		Sample	8.867	6.713	72.204	17.162	0.382	6.710	0.059
Soil 3	Control	Blank	35.922	3.637	8.225	7.536	0.024	6.950	0.066
		Sample	46.657	4.223	8.023	9.374	0.024	8.598	0.034
	Methane	Blank	7.331	0.839	7.623	-2.758	0.023	2.458	0.008
		Sample	6.714	0.880	8.111	-3.478	0.022	2.705	0.013

The concentrations of the control treatment of soil 1 b) are lower or comparable to the concentrations of the control treatment of soil 1 a). For the methane treatment all cation concentrations are lower than the corresponding controls. But they are also lower than the observed concentrations for the methane treatment of soil 1 a), except for calcium and manganese of the contaminated samples. The most abundant major cation present in the treatments of soil 2 is potassium, followed by calcium. In the control treatment the sodium concentrations are high for blanks and samples. For the methane treatments the concentrations were low for all cation except potassium compared to the control treatment. Between the blank and averaged samples of the control treatment no significant concentration gradient is obvious. Also in the methane treatment the concentrations of all cations are comparable except iron, which is higher in the samples than in the blank. Regarding soil 3 the dominant cation in the control treatment is sodium, while the sodium concentration in the methane treatment is significantly lower. Nevertheless it is the most abundant cation with potassium and iron. The iron concentration of the methane treatment is around four times lower than in the control treatment. The potassium concentration of the methane and the control treatment are comparable, but all other cation concentrations in the methane treatment are lower than in the control treatment. The

concentrations of the sample and the blanks in the control treatment differ for potassium, magnesium, calcium and iron, whilst the concentrations are slightly higher for the averaged samples. In the methane treatment no difference between the blank and the samples appear. The negative concentrations measured for the methane treatment result from an instrumental processing artefact due to the insignificant amount of calcium present in the samples.

Ion Chromatography (IC) In contrast to the IC analysis of the partitioning experiment, the porewater samples from the incubation experiments were diluted for the analysis additionally to the dilution during the porewater extraction (see Figure 4). The results of the analysis were corrected for the dilution factors. Hereafter the results for the anion analysis are presented as the cation concentration in the porewater samples have been described from the results of the ICP-MS analysis. The results of the cation concentrations of the porewater sample measured by IC are shown in Figure 29 in Appendix 8.1.6. The presented blank and sample results are derived as explained for the ICP-MS analysis.

Table (15) Porewater concentration of major cations for blanks and samples of incubation experiment A measured by IC.

Soil	Treat.	Element Type	F [ppm]	Cl [ppm]	SO4 [ppm]	Br [ppm]	NO3 [ppm]	PO4 [ppm]
Soil 1a	Control	Blank	1.545	19.441	30.610	2.660	709.400	0.000
		Sample	1.557	19.124	28.510	2.098	612.746	0.000
	Methane	Blank	2.222	18.242	18.135	1.883	2.589	0.000
		Sample	2.119	18.146	18.814	1.678	13.886	0.000
Soil 1b	Control	Blank	1.420	18.341	30.516	1.531	704.127	0.000
		Sample	1.441	16.390	29.119	1.344	673.659	0.000
	Methane	Blank	2.064	6.488	16.012	0.000	1.256	0.000
		Sample	2.002	5.247	12.917	0.706	0.821	0.000
Soil 2	Control	Blank	0.000	61.289	34.790	3.538	2.530	231.477
		Sample	0.000	63.588	30.759	3.691	2.268	240.147
	Methane	Blank	0.000	44.911	29.012	2.384	1.482	180.024
		Sample	0.000	43.282	34.241	2.424	1.368	191.960
Soil 3	Control	Blank	0.000	37.488	10.093	0.875	2.666	0.000
		Sample	0.000	45.965	12.386	0.865	2.824	0.000
	Methane	Blank	0.000	17.326	6.910	1.470	1.604	0.000
		Sample	0.000	17.791	6.917	1.510	1.543	0.000

In the controls of soil 1 a) and 1 b) the nitrate concentrations are comparable and more than one magnitude higher than the next most abundant anion sulfate. The concentrations of all anions in the blanks of both control treatments are slightly higher or

comparable to the averaged samples. In the methane treatment of soil 1 a) and 1 b) the nitrate concentrations are significantly lower compared to the control treatments. For the methane treatment of soil 1 a) the concentrations of the other anions are comparable to the control treatment except for sulfate, which is also decreased. In the blank of the methane treatment the nitrate concentration is lower than in the averaged samples, but similiar for the other anions. In the methane treatment of soil 1 b) the concentrations of chloride, sulfate and bromide are lower than in the control treatment additionally to the nitrate concentrations. The flouride concentrations are slightly higher for the blank and the averaged samples. The anion concentrations are slightly lower in the averaged samples than in the blank of the methane treatment, except for bromide.

For soil 2 and soil 3 no fluoride was measured due to the chromatographic interference with acetate present in the porewater. The anion concentrations in the methane treatment of soil 2 are lower for chloride, bromide, nitrate and phosphate compared to the corresponding control treatment. There seem to be no differences between the samples and the blanks of both treatments, except comparable variations of sulfate in both treatments with opposing trend.

For soil 3 the chloide, sulfate and nitrate concentration are higher in the control treatment, whereas the difference to the methane treatment is the largest for chloride. The bromide concentrations in the methane treatment are higher than in the control treatment. The anion concentrations of the averaged blanks and samples in the methane treatments are similiar, whereas the all anion concentrations are slightly higher in the samples than in the blanks of the control treatment except for bromide.

6 Discussion

Hereafter the results presented in the previous chapter are discussed individually and set in context to each other to evaluate implications for the objectives of this study. Furthermore the experimental design is examined regarding the suitability for the investigation of the biodegradation processes and the choosen analytical approach for the measurement of PFOA by GC-MS is assessed. Implications for further work, that could be conducted based on this study are mentioned throughout the discussion.

6.1 Soil Characterization

The experiments of the soil characterization intended to quantify soil properties of interest of the different samples, which are related to the partitioning behaviour observed for the different soils. Each soil had a specific characteristic of interest. Soil 1 contained a high amount of clay, soil 2 was rich in organic matter and soil 3 was characterized by the presence of iron oxides. Furthermore the potential applicability of a co-metabolic degradation of PFOA by methane oxdiation in the different soils was of interest. Hereafter the results are discussed briefly.

The results of the grain size distribution for the merged soil samples 2 and 3 are as comparable as the results of the XRD-analysis for the core horizons E and B. For both experiments the samples origin from consecutive horizons of the same core, which explains their similarity in these two analyses. For the XRD- and LPS-analysis organic matter was removed in the pretreatment, respectively specifically avoided. Respectively the analysis of organic matter the samples differed significantly, as soil sample 2 results from merging the OM-rich O-horizon with the subsequent E-horizon and soil sample 3 results from the E- and B-horizon, which are depleted in organic matter. The agricultural soil sample 1 contained an intermediate amount of OM, but differed significantly from the other soils regarding the mineralogical composition and the grain size distribution. While the core samples can be described as silty very fine to medium sands, soil 1 forms is classified as a fine to coarse silt - with a significantly higher content of clay. The mineralogical composition of soil 1 was lower regarding the quartz content compared to soil 2 and 3, but contained a significant amount of layered silicate minerals.

From an methodological perspective the estimation of the organic matter content via the LOI is of interest, because of the simple, fast and cheap approach to assess the total carbon content of a soil sample. Compared to the OEA, the estimation by LOI does not resolve compositional differences regarding the main components of organic material, but a distinguished estimations for TC and TOC could be performed with an acidic pretreatment (like for OEA). Due to the dependence of other soil properties (e.g. minerals with structural water, presence of carbonates), Chatterjee et al. (2009) lists several empirical equations for the LOI-TC relation resulting from various temperature treatments. The application of different treatments and estimating equations depends on the soil type and depth (Chatterjee et al., 2009). The derivation of an estimation equation from this study would not be reliable, because of the sedimentological differences of the agricultural, silty soil sample and the sandy, forrest soil sample. Far more replications of the experiment would have been necessary to derive a robust empirical equation. This is why the estim-

ation of TOC by LOI was computed under the general assumption, that soil OM consists to 58 % of carbon (Chatterjee et al., 2009).

6.2   Partitioning Experiment B

The partitioning experiment B intended to investigate the partitioning behaviour of the pollutants PCE and PFOA onto soil 1 to derive suitable sorption isotherms. The validation of the experimentally determined sorption isotherms would indicate the suitability of the experimental setup - especially the analysis of PFOA by GC-MS - for partitioning and possibly biodegradation experiments.

For PCE the partitioning on soils is described by the linear partitioning coefficient K_d, which is often computed by the organic carbon partitioning coefficient K_{oc} multiplied with the fraction of organic carbon f_{oc} present in the soil sample (Currie et al., 1994). The fraction of organic carbon in soil sample 1 was measured by OEA and amounts 2.85 %. In the DTSC report (1994) about PCE, experimental K_{oc} values range from 66 to 437 (from 11 different studies), with an arithmetic mean of 200. Thus, the K_d value for ?CE ranges from 1.88 to 12.45 with an arithmetic mean of 5.7. The experimental partitioning behaviour of PCE derived from partitioning experiment B is lineary approximated with a coefficient K_d of 9.34 (unitless by assuming density of water 1 $\frac{kg}{L}$), which would correspond to a K_{oc} of 327.6 for soil 1. Even though the value lays within the broad range given by literature, it deviates significantly from the arithmetic mean.

In Sima and Jaffé (2020) it is stated, that the general sorption behaviour of PFAS is nonlinear as the partitioning onto the solid phase decreases with increasing aqueous concentrations, which would imply the usage of a Freundlich isotherm to describe the partitioning. But for low PFAS concentration a linear isotherm can be approximated, e.g. for PFOA ¡0.2 μM = 0.083 ppm (Milinovic et al., 2015; Sima & Jaffé, 2020). The experimental values derived to describe the PFOA partitioning linency or nonlinear vary over a broad range depending on the used soil (Milinovic et al., 2015). Milinovic et al. (2015) proposes linear partitioning coefficients ranging from 2.2 $\frac{L}{kg}$ to 38 $\frac{L}{kg}$, and a range for the Freundlich coefficient K_F from 2 to 40 and from 0.9 to 1.1 for the Freundlich exponent n. From partitioning experiment B a better fit for the partitioning behaviour was achieved by a nonlinear approximation using a Freundlich isotherm with a Freundlich coefficient $K_F = 0.973$ and Freundlich exponent $n = 0.681$ ($R^2 = 0.83$). A linear approximation resulted in a coefficient $K_d = 0.307$ with an $R^2 = 0.731$. The linear fit could be improved by excluding the results for the high initial PFOA concentrations of 25 ppm and 50 ppm, resulting in a $K_d = 0.78$ with a $R^2 = 0.91$. Deriving a Freundlich isotherm under the exclusion of the high initial concentrations results in a $K_F = 0.82$ and $n = 0.92$ with a $R^2 = 0.81$. In Zareitalabad et al. (2013) logarithmic K_d values from different studies are presented ranging from $log(K_d) = -1.16$ to $log(K_d) = 0.96$ (after Ahrens et al., 2011, and Li et al., 2012). The $log(K_d)$ derived from partitioning experiment B is $log(K_d) = -0.51$, respectively $log(K_d) = -0.11$ for the exclusion of high initial concentrations. Thus, the experimentally determined linear partitioning coefficient falls in the range stated in Zareitalabad et al. (2013).

The comparison of the results of partitioning experiment B to other studies gives two

implications. On the one hand could the results describing the partitioning behaviour of PCE and PFOA in soil 1 be confirmed, eventhough the range of characterizing partitioning coefficients is wide. On the other hand, the necessesity to perform soil specific partitioning experiments in the course of biodegradation experiments is underlined by the wide range of soil and concentration specific linear and nonlinear partitioning coefficients. From the results of the porewater analysis no trend with the increasing initial PFOA and PCE concentration is apparent. As soil sample 1 is an agricultural soil the high concentrations of nitrate can be ascripted to the long-term application of fertilizers to support the crops growth, while the enhanced calcium concentrations result from the addition of calcite to the soil to lime it.

6.3   Partitioning Experiment C

In partitioning experiment C the phase distribution of the contaminants between the three soil samples was investigated with the goal to derive linear or nonlinear partitioning coefficients. Due to limited sample material of soil 2 and soil 3, the partitioning experiments were just performed for triplicated samples of the initial PFOA and PCE concentrations, which were intended to use in the biodegradation experiments (12.5 ppm PFOA and 2.5 ppm PCE). With the assumption of an intersection through the origin an isotherm was derived. Furthermore, the results were used to relate the partitioning coefficients with the measured soil properties to identify a potential correlation.

In partitioning experiment B a linear partitioning behaviour of PCE onto soil 1 is implied, which is why the isotherms were approximated lineary. The resulting partitioning coefficients K_d vary significantly between the soils, with $K_d = 1.18$ for soil 1, $K_d = 26.48$ for soil 2, and $K_d = 4.43$ for soil 3. The range of linear partitioning coefficients of PCE is 1.88 to 12.45 (Currie et al., 1994). Just the experimentally determined K_d of soil 3 falls in this suggested range. Furthermore, the derived partitioning coefficient for soil 1 in this experiment differs significantly from the the one determined in partitioning experiment B ($K_d = 9.337$).

For PFOA a linear partitioning coefficient K_d was derived for all three soils and the coefficient K_F and exponent n of the nonlinear Freundlich isotherm were computed for soil 1 and 3. The computed linear coefficient for soil 1 is $K_d = 0.476$, for soil 2 $K_d = 1.605$ and for soil 3 $K_d = 0.483$. The suggested range in Zareitalabad et al. (2013) varies from $K_d = 0.069$ to $K_d = 9.120$, which covers all three derived partitioning coefficients. The linear coefficient for soil 1 from partitioning experiment B including all initial concentrations was $K_d = 0.307$, but under exclusion of the high initial concentrations was computed with $K_d = 0.78$. The estimated value for soil 1 in partitioning experiment C falls in this artificial range. Regarding the nonlinear partitioning behaviour the Freundlich coefficient and exponent for soil 1 in partitioning experiment B were computed with $K_F = 0.973$ and $n = 0.681$, while in partitioning experiment C K_F was fixed to 1 and n was approximated with 0.582. In F. Li et al. (2019) the Freundlich parameters for the sorption of PFOA onto different soils ranges from 2.99 to 6.22 for K_F and from 0.55 to 0.70 for n. The estimated parameters in study are not covered by this range.

To examine a potential effect of soil properties on the partitioning behaviour of PCE and

PFOA in the soils, the linear partitioning coefficients were correlated with parameters from the soil characterization and with results of the corresponding porewater analyses. The results of some statistical models for PCE and PFOA are presented in Appendix 8.1.5. For the partitioning of both contaminants onto the solid phase, the TOC or OM content appears to be an important predictor, while the significance for PCE appears higher with a lower p-value (see Table 23, Table 24, Table 25 in Appendix 8.1.5). The coefficient of determination could be slightly improved for both contaminants by adding results from the porewater analysis. Regarding PCE a better statistical fit was achieved by adding the sum of major and minor cation concentrations (by ICP-MS) as a predictor, while for PFOA the calcium and iron concentration were added as covariates (see Table 26, Table 27, Table 28 in Appendix 8.1.5). However, the p-values of these added covariates just improved the R^2 value slightly. But the resulting p-values imply, that these parameters are not significant. The poor estimation of the linear partitioning coefficient by soil parameters probably results from the variation of the K_d values. In other studies (Milinovic et al., 2015; F. Li et al., 2019) better correlations of the linear partitioning coefficient of PFOA with the total organic carbon content were found.

The results of this experiment imply, that the estimation of the partitioning behaviour of PCE and PFOA with the choosen simplified approach of linear approximation is insufficient to describe the distribution of PCE and PFOA between a soil and the aqueous phase. Instead a range of initial concentrations should have been chosen, like for soil 1 in partitioning experiment B. Thereby, the chosen concentration range should be limited and not to high due to the increasing variation of results with high concentrations (see Figure 17, Figure 19).

6.4 Incubation Experiment A

The discussed results of the partitioning experiment C have direct implications on the results of incubation experiment A, because the derived partitioning coefficients were used to compute the solid phase concentrations from the measured aqueous concentrations of PCE and PFOA. Thus, insecurities in the partitioning coefficients propagate in the computation of the mass balances of incubation experiment A. An overestimation of the partitioning coefficient as for PCE in soil 2, leads to an overestimation of contaminant onto the solid phase like for soil 2 (Figure 21, Figure 26). The subsequent computation of a sink term in a corresponding mass balance would induce an underestimation of a potential sink term or lead to false mass balance. The underestimation of the partitioning onto the solid phase would consequently result in an overestimation of a sink term. Therefore, a reliable estimation of the partitioning coefficients is required to identify the biodegradation of contaminants in the used approach of parent contaminant analysis. An alternative approach would be the analysis of degradation products, which requires the knowledge of responsible degradation mechanisms. For PCE the degradation mechanisms and products are well studied, but for PFOA still to identify. Eventhough the estimated linear partitioning coefficients for PFOA from partitioning experiment C are within estimated ranges (Zareitalabad, Siemens, Hamer, & Amelung, 2013; Miao, Guo, Peng, Fan, & Yang, 2017), the insecurities propagate in the corresponding mass balances of incuba-

tion experiment A. This restricts certainty regarding the computed results of the phase distribution and the sink term.

Nevertheless, the measured results of the aqueous concentrations of PCE and PFOA (Figure 25, Figure 27) are not affected. A difference of the aqueous concentrations of PCE between the different treatments was just observed for soil 1 b). Comparing the absolute mass differences of PCE all treatments to corresponding results from partitioning experiment C implies a reduction of the mass present in the aqueous and gaseous phase for the methane treatment of soil 1 b) and the methane treatment of soil 3 (Figure 26, Figure 20). Even though the quantitation of a potential biodegradation by a mass balance is too uncertain, the mass differences indicate a mass reducing process. But it could also be caused by changes in the atmospheric conditions affecting the partitioning behaviour of PCE.

The comparison of the mean masses of PFOA present in the aqueous phase of partitioning experiment C and the different treatments in the incubation experiment appear to show some differences. But considering the corresponding standard deviations, the differences between the abiotic and biotic experiment disappear except for soil 3. In the partitioning experiment of soil 3 an amount of 27.69 $\pm$ 5.88 μg PFOA appears in the aqueous phase. This is comparable to the results of the biotic control treatment with 27.21 $\pm$ 3.14 μg, but higher than the measured mass in the methane treatment with 17.29 $\pm$ 2.21 μg. Considering the standard deviations, these differences might be significant, even though the number of samples of the incubation experiment is too small to be more certain. This difference in the aqueous occurence of PFOA could also result from changes of the partitioning behaviour induced by changes in the atmospheric conditions of the closed systems. Figure 50 shows the GC-monitoring results of the methane treatment of soil 3, where the CO_2 levels first increase for blanks and samples during the training period up to approximately 20000 ppmv, but subsequently decrease gradually. Until the end of the incubation period the CO_2 levels are slightly higher than the initial conditions, even though the variance of the results increases during the monitoring with the increased sampling frequency. This observation seems counterintuitive comapred to the simultaneously increasing methane concentrations, indicating anaerobic methanogenesis. Unfortunately the atmospheric conditions of the control treatment were not monitored. But increased concentrations of cations in the aqueous solution compared to the abiotic partitioning experiment and the methane treatment imply the dissolution of present minerals. This could be explained by more acidic conditions induced by enhanced CO_2 levels from biological activity, which would indicate anaerobic conditions (Table 14, Table 12). Especially higher iron concentrations in the control treatment than in the methane treatment are of interest regarding the appearant differnces in aqueous PFOA concentrations. As stated by Bolan et al. (2021), one suggested partitioning mechanism of PFOA onto the solid phase is the adsorption to iron-oxides and -hydroxides (Figure 5) . This suggests, that the enhanced aquoeus PFOA concentrations in the control treatment could result from the dissolution of iron-(hydr-)oxides, which was induced by the anaerobic conditions due to biological activity. The anaerobic iron dissolution could result from iron reduction as a metabolic mechanism of microorganisms. However, the iron concentration in the partitioning experiment exceed the observed concentrations in the control treatment, even though the measured PFOA concentrations are similar. This might be explained

by a relative change of the dominant sorption mechanism of PFOA. To evaluate this assumption, the organic matter content and the amount of iron oxides present would have to be examined before and after the abiotic and biotic experiments and related to measured aqueous PFOA concentrations. From the results of the used experimental setup no certain assumption can be derived.

A further evaluation of the presented results is difficult due to the uncertainty of required parameters. For example the interpretation of the differences in nitrate concentrations measured in the control and methane treatments of soil 1 a) and b) with a significant reduction of nitrate in the methane treatments is interesting. While the concentrations of the control treatment are comparable to the measured ones in the abiotic partitioning experiments, the results from the methane treatment imply a concentration decrease by two magnitudes (Table 14, Table 12). While this could be attributed to biological denitrification occuring as metabolic mechanism under sub-oxic conditions, it is questionable why this does not apply for the control treatments. A similar trend was observed for the measured iron concentrations for soil 1 a). One explanation could be the inhibition of the metabolic acitivity in the control treatments, e.g. due to the presence of toxic pollutants. The inhibition caused by PCE and PFOA can be excluded, as the CO_2 concentrations measured in the corresponding methane treatment imply a significant biologic metabolic activity. Both treatments were inoculated with the same initial solutions. Results from the ICP-MS analysis do not show minor or trace cations in sufficient concentration to inhibit the metabolic activity. As no certain cause could be identified or found in literature, the biological activity in the control treatment of soil 1 is unsure. A monitoring of the headspace composition of the control samples regarding the oxygen content and CO_2 content could have given further implications. Additionally to the headspace monitoring, the pH analysis of the samples of both treatments before and after the incubation would have given further information to resolve and explain the occuring changes in concentrations. By these and prior implications the methodological approach of the experimental design is reviewed in the following paragraph.

6.5 Methodology of Experimental Design

The experimental desing intended to characterize the abiotic partitioning behaviour of PCE and PFOA in different soil samples to derive mass balances from subsequential incubation experiments to quantify potential biodegradation. So far some methodological flaws were already pointed out, which will be reviewed to improve the presented experimental approach.

Soil The soil characterization could be refined and adjusted to the specific sorption mechanisms of the contaminants of interest. In the case of PFOA the content of Fe-(hydr-)oxides and alumina present on the mineral phase should have been quantified for the used soil samples as the visual inspection indicated the presence of oxide coatings. A characterization of the mineralogical composition was performed in form of a XRD-analysis, but this method is not capable of the identification or quantification of these oxides. For example an additional XRF-analysis would have given further insights

regarding the mineralogical composition and enable the correlation of the results with determined partitioning coefficients. Furthermore, it could be of interest to repeat certain soil analyses of samples after the usage in incubation experiments to examine potential changes. Differences in results regarding the content of organic matter or the amount of oxides present could be related with observations of other experiments like the chemical porewater composition or gaseous headspace composition to validate and quantify the occurrence of biogeochemical reactions. Regarding the choice of soil samples it would have been interesting to investigate a natural soil of known exposure to the contaminants (e.g. from firefighting training areas, military bases, airports), as the adjustment of indigenous microorganisms to the presence of pollutants is assumed (Prevedouros et al., 2006; Bolan et al., 2021). Differences in occuring biogeochemical reactions could be compared to unpolluted soil samples.

Partitioning Experiments As pointed out by the comparison between partitioning experiment B and C, the approach in the latter was insufficient for the derivation of reliable partitioning coefficients. Also for partitioning experiment B the application of high concentrations caused a higher variance of the results compared to low concentrations (Figure 19). On the other hand the wide range of initial PFOA concentrations in partitioning experiment B allow the identification of the nonlinear partitioning behaviour as suggested by other studies (Sima & Jaffé, 2020). Nonetheless, in order to describe the partitioning behaviour of a contaminant like PFOA to a specific soil, specific partitioning experiments should be performed as for soil 1. The variance of the range of initial concentrations of contaminants should match with the concentration range of interest. Over a small concentration range a nonlinear partitioning behaviour can be sufficiently approximated with a linear sorption isotherm (Sima & Jaffé, 2020). In this study the extension of partitioning experiment B to the soils 2 and 3 was restricted by the available amount of soil material. Otherwise it would have also been of interest to investigate the effect of the co-contamination on the partitioning behaviour. Comparing the results of separately contaminated samples with co-contaminated samples could given implications regarding adsorption competition onto the solid phase (?, ?). Additionally to investigation of equilibrium states a time resolved approach could have been chosen to investigate adsorption kinetics as many approaches and model were recently reviewed (Sima & Jaffé, 2020). Besides the derivation of the partitioning behaviour, the effect of the contaminants on the porewater chemistry could have been further investigated by measuring the porewater pH.

Incubation Experiments In respect of the biological incubation experiments, the GC-monitoring of the headspace composition should have been extended to the samples of the control treatments and the monitoring of the oxygen content. The inconsistency of the GC-monitoring, especially regarding the methane consumption, could have been improved by more frequent aeration of the samples to ensure a sufficient oxygen supply. Furthermore, the measurement of the pH values in the samples would have been crucial to characterized the biogeochemical processes and enable the opportunity of geochemical computational modelling of the enclosed systems. Theoretically the pH conditions in the

samples could be derived from the measurements of the atmospheric CO_2 pressure and the concentration of biocarbonate in the extracted porewater solutions. As a major anion the bicarbonate concentrations can theoretically be derived from the results of the IC-analysis for anions under neglection of other minor and trace anions and the results of cation concentrations in porewater. Presuming the ICP-MS analysis detects all major cations present, a charge balance could be computed under the presumption bicarbonate is the only significant anion not detected in the IC-analysis. With the CO_2 pressure and the bicarbonate concentrations, the carbonate system can be completely determined including the pH (Zeebe & Wolf-Gladrow, 2001).

All the suggested improvements serve the purpose of a more detailed characterization of the closed systems to identify differences and quantify occuring mechanisms in the experimental setup. This targets to allow a more reliable derivation of mass balances to quantify biogeochemical reactions and quantify potential degradation mechanisms. Improving the predictability of the adsorption onto the solid phase for specific soil samples with an extended analysis of the headspace composition and the measurement or monitoring of the pH conditions would allow a derivation of more reliable mass balances of the contaminants. In combination with a reviewed analytical approach, laboratory experiments examining the PFAS behaviour in soils in relation to biogeochemical reactions could be performed.

6.6   Analytical Approach

Except for the GC-MS analysis of PCE and PFOA and the OM estimation by LOI, the applied analytical methods are well established and frequently performed. As the OM estimation via the determination of the LOI has already been briefly discussed prior, hereafter the PCE and PFOA analyses are examined. Furthermore, the porewater extraction and potential insecurities from used laboratory equipment are evaluated.

The analysis of both contaminants were performed on the same GC-MS instrument (6890N GC with 5973N MSD by Agilent), which has not been operated recently (see Appendix 8.2), and also on the same GC-column (Zebron Phenomenex ZB5). The column of low-polarity was suitable for the analysis of PFOA (Scott et al., 2006), but less suitable for the chromatographic separation of compounds of higher polarity like PCE. This is why the analysis of PCE degradation products like TCE, (cis-, trans-) DCE, and VC was not performed in this study. The usage of a polar GC-column would allow the quantification of these degradation products of PCE and therefore validate assumed biodegradation processes. Besides instrumental variations, like the instrumental drift trend (see Figure 42), operational error caused by the manual sample injection are assumed to be a main cause for the variance of replicated samples. An automized sample injection system or more replica per sample could encounter this error source.

Besides the partitioning and potential degradation of PFOA by the proposed methodological approach, the evaluation of the PFOA analysis by per-analytical derivatization and subsequential GC-MS after Li and Sun, 2020, was a main objective of this study. The analysis allows a less-cost intensive measurement of PFOA in aqueous samples compared to the well established, but rarely available HPLC-MS/MS method (Z. Li & Sun, 2020). The analysis was successfully applied in this study, even though some adjustments regard-

ing the derivatization procedure have been made due to available laboratory equipment. The partially high variations, especially for high PFOA concentrations (see Figure 19), might improved by minor adjustments. For example the usage of small, gas-tight screw cap vials (preferably HDPE or glass) instead of PP snap cap vials. This could decrease the chance of potential evaporation of the analytical n-hexane solution between the derivatization and instrumental analysis. An occuring evaporation causes higher concentrations in the analytical solution, which leads to an overestimation of the corresponding porewater concentrations. The performance of the derivatization could be further improved by usage of an automized N_2-flow evaporator as well as using glass labware (Lath, Knight, Navarro, Kookana, & McLaughlin, 2019) to minimize losses of the analyte. A further source of uncertainty is the manual injection of the small sample volume in the GC-MS instrument, which could be encountered by usage of an autosampler. This would also encounter the time-consumption linked to the manual sample injection. An advantage of the analytical approach, which has not been emphasized, is the adjustability of the derivatization method to expected target concentrations in the water sample by the volume ratios choosen for the derivatization. Furthermore, low concentrated analytes can be enriched before the derivatization by solid phase extraction, if sufficient sample material is available (Scott et al., 2006; Z. Li & Sun, 2020). From an instrumental perspective the analyte signal could be enhanced by increasing the injection volume of the sample. However, this could also increase the background signal, respectively the signal-to-noise ratio of the target analyte, which would be counterproductive.

Additionally to the instrumental analysis, the porewater extraction procedure appears as potential insecurity due to the dilution with purified water before the isolation of the aqueous phase. The procedure was conducted, because of the limited water volume added to the soil samples. The partial porespace saturation was choosen to avoid a transport limitations of potential biodegradation reactions due to diffusive transport of oxygen as electron acceptor from the gaseous phase. To extract the porewater for subsequent analyses, purified water was added and a consequential dilution factor was computed from the initially injected volume and the final volume. For the incubation experiments the initial soil moisture content was not included in the correction, which could have been adjusted by prior determination of the moisture content for each soil. An uncertainty during the porewater extraction is the desorption of compounds adsorbed to the solid phase, especially regarding the analyte PFOA. This factor could be considered by correcting the amount of desorbed compound depending on the corresponding desorption kinetics. These, however, depend on the specific sorption mechanism (see Figure 5) (Sima & Jaffé, 2020). The practicality of such correction could be evaluated by derivation of the soil- and analyte-specific desorption kinetics.

The described analytical and methodological adjustments could improve the reliability of results derived by the described approach for the quantification of PFOA and other perfluoroalkylic acids in the course of partitioning and biodegradation studies. Some of the implied suggestions to improve the method would have to be evaluated in further studies.

7 Conclusion

The objective of this study was to investigate the co-metabolic biodegradability of PFOA under methane oxidizing conditions employing an methodological approach enabling the quantification of a potential mass reduction. The methodological approach was based on the quantification of the abiotic phase distribution behaviour in partitioning experiments and the subsequent transfer of the results to the biotic incubation experiments. The quantification of PFOA was performed by setting up an alternative analysis by GC-MS with a pre-analytical derivatization, after Li and Sun (2019). Furthermore the characterization of sorption mechanisms was investigated by correlating soil specific characteristics with results of the partitioning experiments for three different soils.

The results of the study imply a successful analysis of PFOA in porewater samples by GC-MS analysis. The suggested method by Li and Sun (2019) was slightly adjusted to available laboratory equipment. Further improvements of results are assumed to be feasible by minor adjustments to improve the analytical reliability. Regarding the methodological approach a more detailed analysis of the partitioning behaviour of PFOA between the different soil samples should have been employed, but limitations of available sample material of two soils restricted a more detailed investigation. Nevertheless, the results derived by a more extensive partitioning experiment for soil sample 1 were validated by literature values. On the one hand this validation implies the successful performance of the PFOA analysis by GC-MS, even though further improvements are expected to be achieved by minor changes. On the other hand it implies that detailed soil specific partitioning experiments are required to allow the reliable quantification of mass reducing processes in corresponding incubation experiments for the method chosen in this study. The quantification of a potential mass reduction was restricted by variations of the results of the partitioning experiment. These variation transfer in the subsequent mass balance computations, which is why no certain interpretations could be derived from the biodegradation experiments. However, the measurements of the porewater concentrations imply a potential mass reduction in one soil sample of enhanced iron content under methane treatment in the incubation experiment. The observed mass differences between the abiotic partitioning experiment, the biotic control treatment and the methane treatment could be accounted to biological process or to changes in the phase distribution behaviour. To attribute the observed mass reduction to biological processes further investigations regarding the soil specific partitioning mechanisms and a resolution of occurring biogeochemical reactions should be performed. Improvements of the methodological approach to quantify occuring biodegradation in soils are suggested by the results of this study. Especially the expansion of the gas phase monitoring during incubation to control treatments and the determination of further soil and porewater parameters is indicated. An application of the analytical and methodological adjustments in the framework of the further investigation of the behaviour of PFOA in soil sample 3 is suggested. A more extensive study on soil 3, which originates from the E- and B-horizon of a forrest soil core sample, would allow the further investigation of partitioning mechanisms and give more insights regarding a potentially occuring biodegradability.

8 Appendix

8.1 Supplemental

8.1.1 Grain Size Distribution

Hereafter the additional tables and figures of the grain size distribution results describing the arithmetic statistics of the grain size distribution (Table 16), the descriptive statistics from Grain Size Program GRADISTAT (Table 17, 18), the cumulative and differential grain size distribution (Figure 29) and the ternary clay-silt-sand diagram (Figure 30) are shown.

Table (16) Arithmetic volume statistics computed over range from $0.375 \mu m$ to $2000 \mu m$ for all soils with 2 replica in $[\mu m]$ with mean and standard deviation. Results exported from instrumental report.

Averaged	Soil 1 $[\mu m]$	Soil 2 $[\mu m]$	Soil 3 $[\mu m]$
Mean	21.73 ± 2.08	225.39 ± 5.96	281.54 ± 56.49
Median	6.60 ± 0.19	132.87 ± 3.59	136.01 ± 19.50
SD	42.11 ± 3.77	248.20 ± 7.35	352.41 ± 94.76
Skewness	3.19 ± 0.23	1.38 ± 0.02	1.64 ± 0.27
Kurtosis	10.07 ± 1.81	1.41 ± 0.02	2.29 ± 1.01

Table (17) Descriptive sample statistics and characterization from Grain Size Program GRADISTAT v9.1 by Simon Blott, 2020.

Soil	Soil 1	Soil 2	Soil 3
Sample type	Bimodal Poorly Sorted	Polymodal Very Poorly Sorted	Polymodal Very Poorly Sorted
Textural group	Mud	Muddy Sand	Muddy Sand
Sediment name	Fine Silt	Medium Silty Fine Sand	Very Coarse Silty Medium Sand

Table (18) Descriptive sample statistics after Folk Ward method from Grain Size Program GRADISTAT v9.1, Simon Blott, 2020.

Folk & Ward	Soil 1	Soil 2	Soil 3
Mean	Coarse Silt	Very Fine Sand	Very Fine Sand
Sorting	Poorly Sorted	Very Poorly Sorted	Very Poorly Sorted
Skewness	Coarse Skewed	Very Fine Skewed	Fine Skewed
Kurtosis	Mesokurtic	Platykurtic	Platykurtic
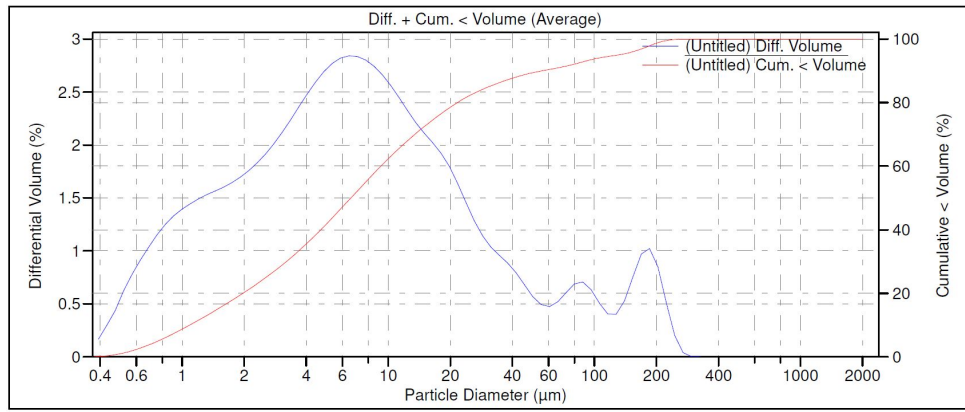
(a) Soil 1
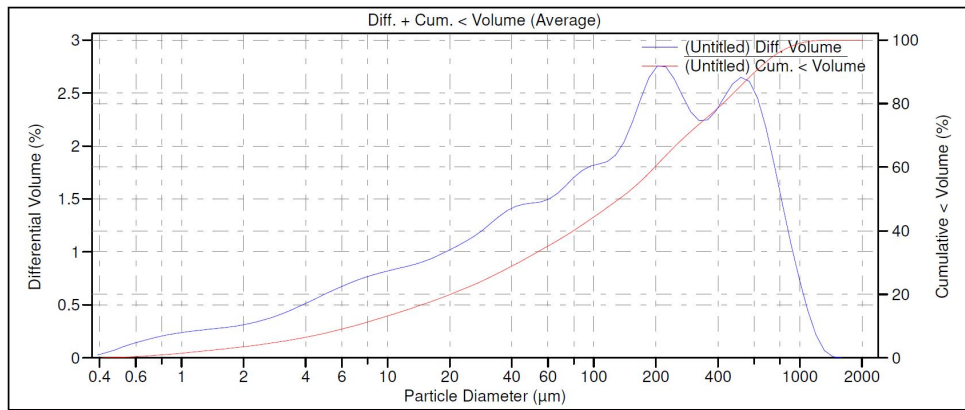
(b) Soil 2
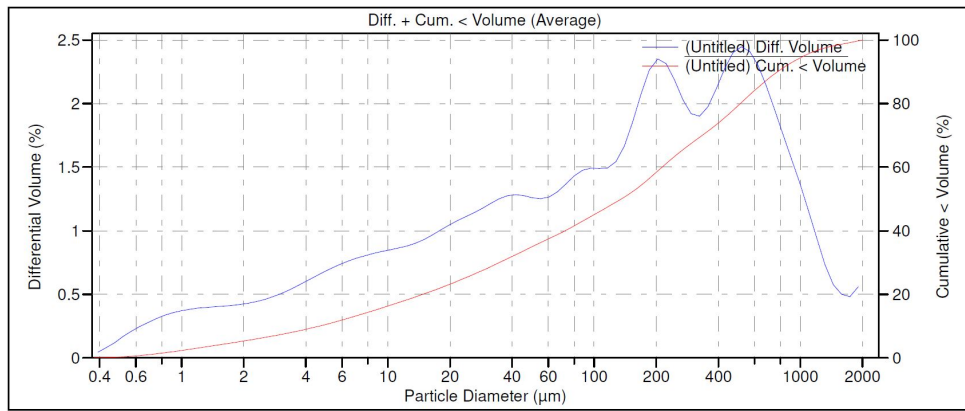
(c) Soil 3

Figure (29)   Differential (blue line) and cumulative (red line) volumetric grain size distribution from LPS analysis of soil 1, soil 2 and soil 3.
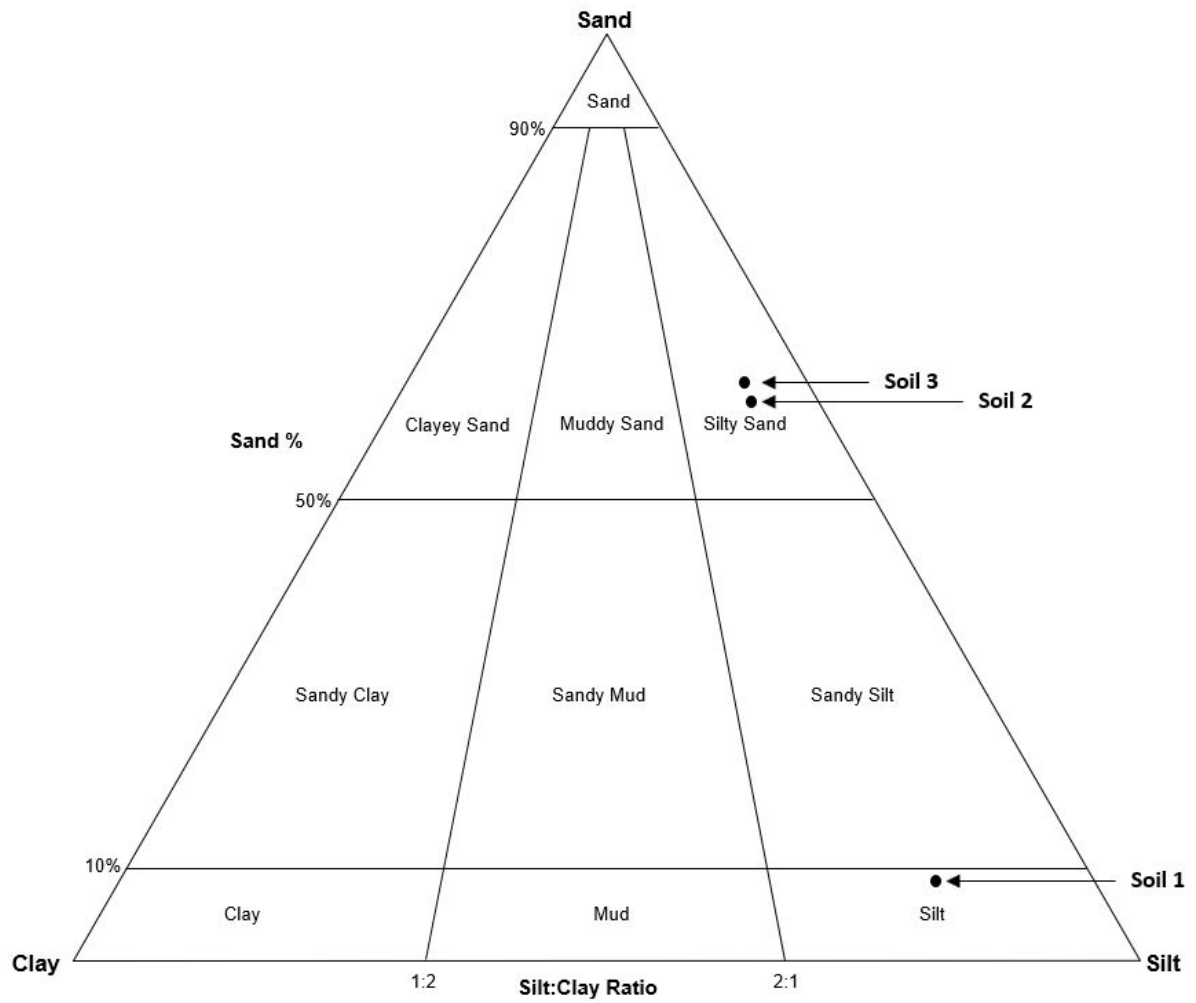
Figure (30) Characterization of grain size type of soil samples in ternary sand-silt-clay diagram using Grain Size Analysis Program GRADISTAT v9.1 (copyright (c) Simon Blott, 2020).

8.1.2 Organic Matter

Here the raw data of the OEA analysis are presented in Table 19 and the linear correlation of the relative TOC content measured by OEA and estimated by LOI in Figure 31 is illustrated.

Table (19) Raw data of OEA for soil samples with all blank and standard measurements performed. Initial standard and blank measurements treated as such, later treated like samples to validate measurements.

| Sample ID	Type	Weight [mg]	N [%]	C [%]	H [%]
Blank	Unknown	1	7.04	-0.34	1.91
Blank	Blank	0	0.00	0.00	0.00
Blank	Blank	0	0.00	0.00	0.00
Bypass	By-Pass	0	0.00	0.00	0.00
BBOT 72.58C 6.53N 7.41S	Standard	1.973	6.53	72.58	6.10
BBOT 72.58C 6.53N 7.41S	Standard	2.068	6.53	72.58	6.10
BBOT 72.58C 6.53N 7.41S	Standard	2.487	6.53	72.58	6.10
BBOT 72.58C 6.53N 7.41S	Standard	2.726	6.53	72.58	6.10
BBOT 72.58C 6.53N 7.41S	Standard	3.09	6.53	72.58	6.10
BBOT 72.58C 6.53N 7.41S	Standard	3.123	6.53	72.58	6.10
Blk3	Unknown	1	-0.78	0.79	-0.03
Blk4	Unknown	1	-0.83	0.82	-0.03
Peaty 15.95c 1.29N 0.43S	Unknown	12.962	1.30	15.70	0.00
BBOT 72.58C 6.53N 7.41S	Unknown	2.46	6.46	72.77	6.08
Peaty 15.95c 1.29N 0.43S	Unknown	13.768	1.29	15.90	0.00
Peaty 15.95c 1.29N 0.43S	Unknown	13.605	1.26	15.80	0.00
Soil 1 TC	Unknown	15.568	0.18	2.98	0.77
Soil 1 TC	Unknown	15.367	0.17	2.86	0.78
Soil 2 TC	Unknown	15.168	0.38	10.24	1.05
Soil 2 TC	Unknown	15.358	0.36	9.92	1.00
Soil 3 TC	Unknown	15.885	-0.02	1.24	0.25
Soil 3 TC	Unknown	15.453	-0.02	1.30	0.26
Soil 1 TOC	Unknown	15.482	0.18	2.85	0.72
Soil 2TOC	Unknown	15.48	0.33	9.53	0.96
Soil 3 TOC	Unknown	15.525	-0.03	0.82	0.17
Peaty 15.95c 1.29N 0.43S	Unknown	12.723	1.20	15.18	0.00
Peaty 15.95c 1.29N 0.43S	Unknown	13.191	1.24	15.96	0.00
BBOT 72.58C 6.53N 7.41S	Unknown	2.511	6.34	72.73	6.00
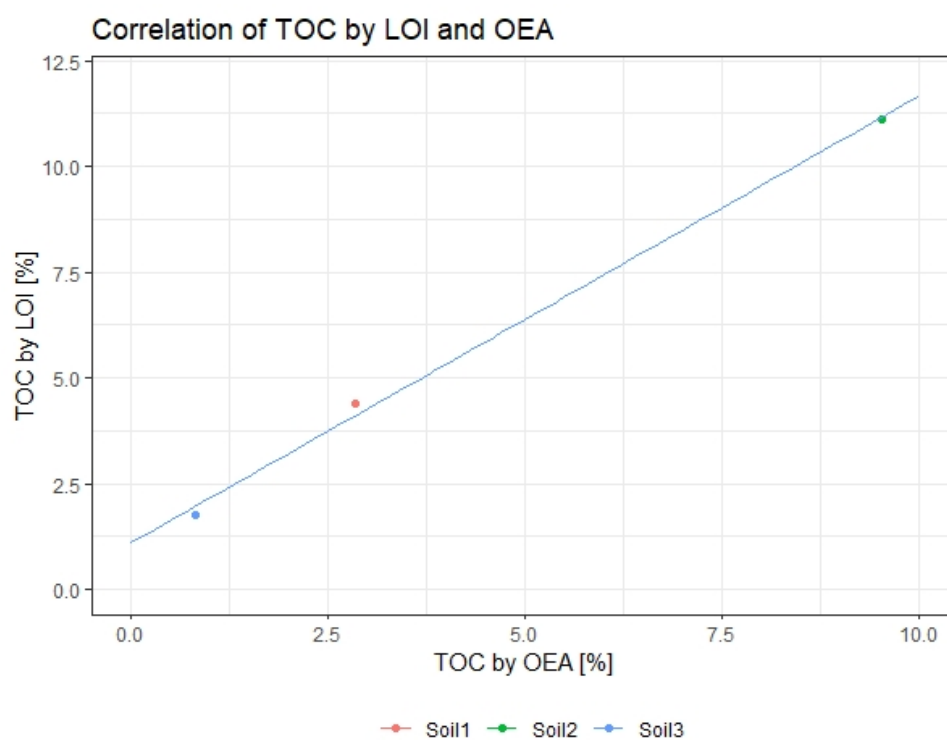
Figure (31) Linear correlation of TOC content [%] measured by OEA and estimated by LOI-analysis for soil samples 1, 2 and 3.

8.1.3 X-Ray Diffraction

As supplemental data the comparison of the measured diffractogram by XRD-analysis and the synthetic diffractogram using Profex for core horizon E (Figure 32) and horizon B (Figure 33) are shown as well as a comparative table of the chemical composition of the simulated mineral phase (Table 20) Measured versus simulated diffractograms for E- and B-horizon of core soil sample. The simulated mineralogical and chemical composition of soil 1, and the core soil horizons E and B are illustrated in Figure 34 and 35.
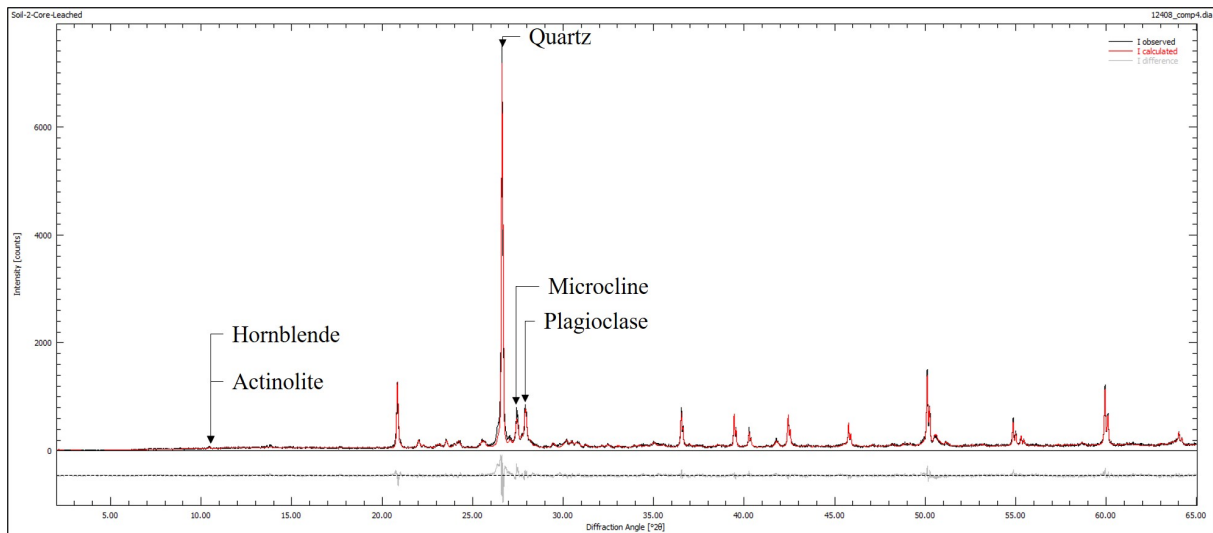
Figure (32) Measured diffractogram by XRD analysis (black line) and synthetic diffractogram simulated with XRD-analysis software Profex with identified peaks to main minerals for E-horizon of core soil sample.
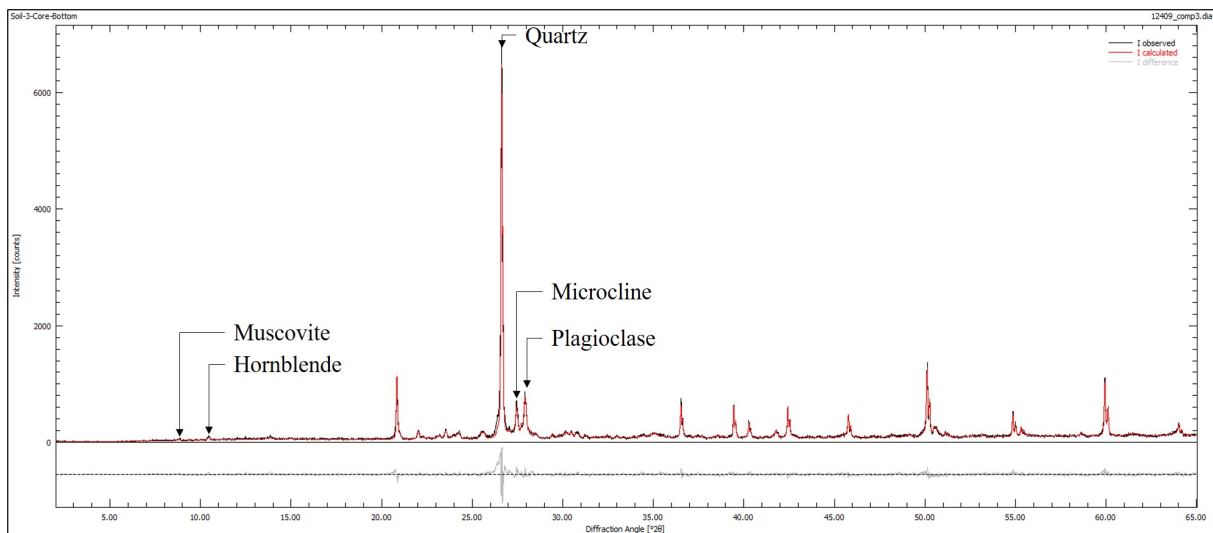
Figure (33) Measured diffractogram by XRD analysis (black line) and synthetic diffractogram simulated with XRD-analysis software Profex with identified peaks to main minerals for B-horizon of core soil sample.

Table (20) Relative chemical composition of mineralogical phase of bulk samples of soil 1, E-horizon and B-horizon of core sample. Derived by using analysis software Profex for XRD-results for soil samples.

Elements	Soil 1	E-horizon	B-horizon
Hydrogen	0.11	0.00	0.00
Oxygen	49.71	50.59	50.20
Sodium	1.49	1.62	1.68
Magnesium	0.66	0.15	0.30
Aluminium	9.83	4.56	5.49
Silicon	31.74	39.40	37.87
Potassium	3.47	2.70	3.16
Calcium	0.50	0.69	0.82
Titanium	0.00	0.04	0.10
Iron	2.51	0.24	0.37
Sum	100.0	100.0	100.0
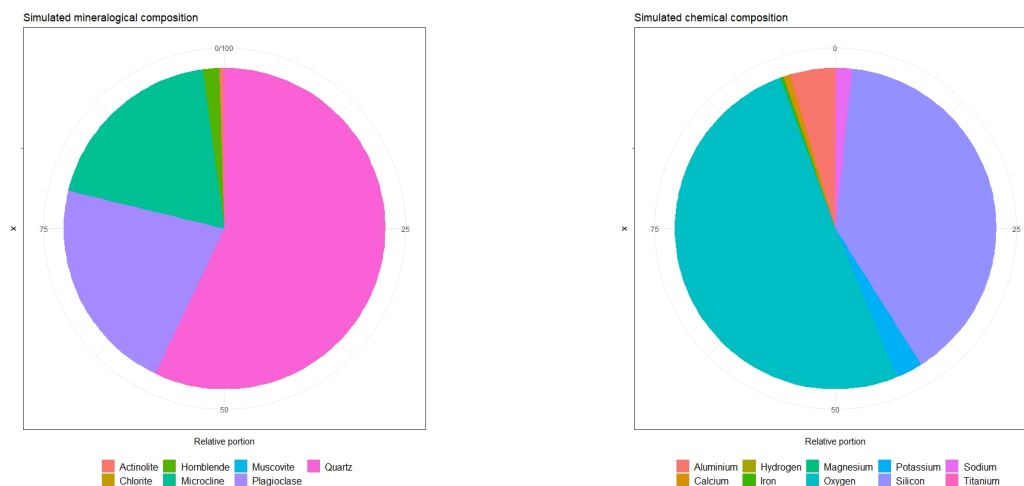
Figure (34) Computed mineralogical and chemical composition of E-horizon of core soil sample derived from simulated diffractogram using XRD-analysis software Profex, validated by comparison to measured diffractogram by XRD.

93
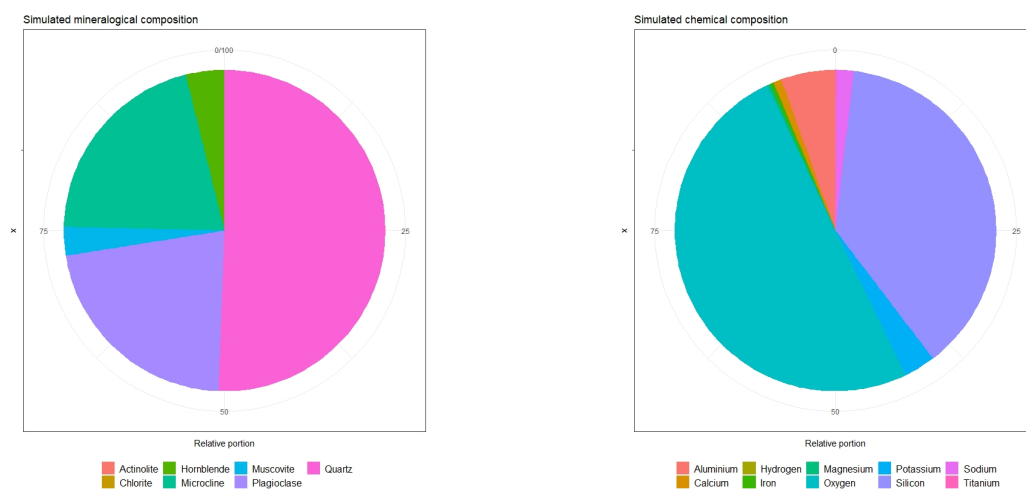
Figure (35) Computed mineralogical and chemical composition of B-horizon of core soil sample derived from simulated diffractogram using XRD-analysis software Profex, validated by comparison to measured diffractogram by XRD.

8.1.4 Partitioning Experiment B

For the partitioning experiment B the instrumental drift trends and calibration curves of the PCE measurements (Figure 36, 37) performed at the 29.06.2021 and 30.06.2021 are shown. Analogues for the PFOA measurements performed at the 05.07.2021 and 07.07.21 are shown in Figure 38, Figure 39 and Figure 40. In the calibration plots for PFOA the uncorrected, the blank corrected and the blank and drift corrected calibration curves are compared. For the derivation of the Freundlich isotherm, the ln-ln-plot of the solid to aqueous PFOA concentrations was used, which is depicted in Figure 41. Furthermore, the results of the IC analysis for cations is shown in Table 21.
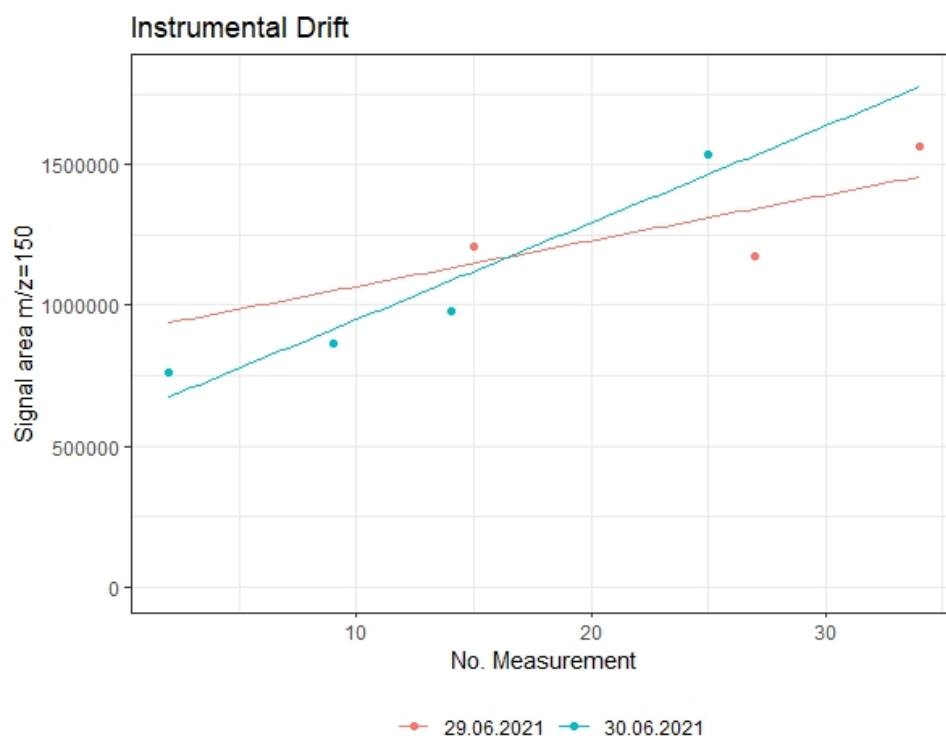
Figure (36) Instrumental drift during PCE analysis of partitioning experiment B by GC-MS, derived from blank measurements with integradted internal standard (1,2-Dichlorobenzene-d4) signal m/z=150 for two measuring sessions.
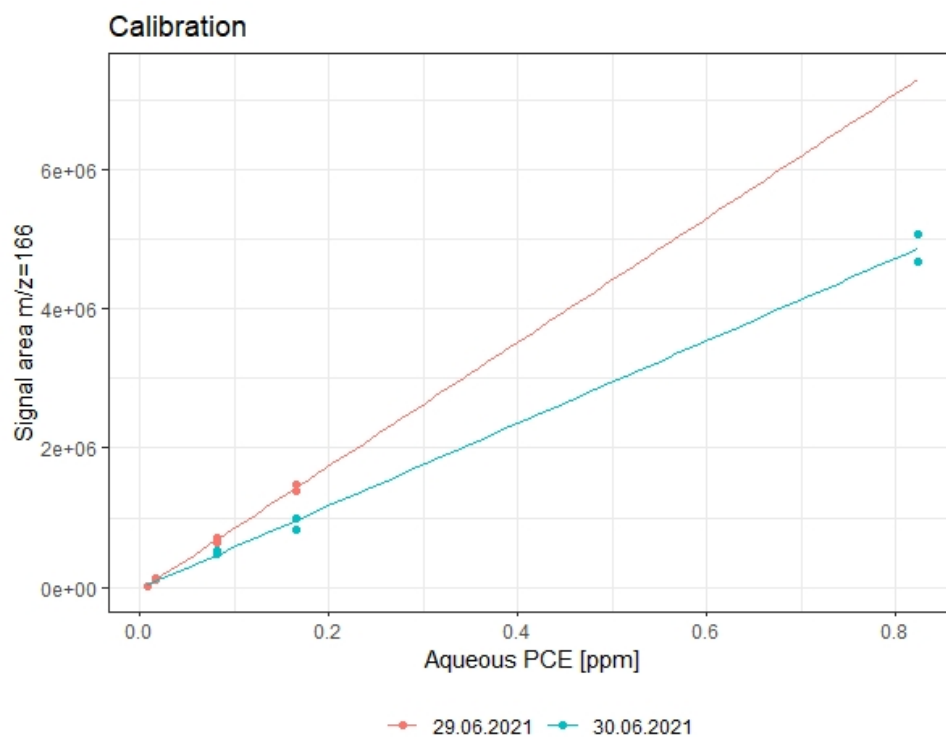
Figure (37) Calibration of GC-MS for PCE analysis of samples from partitioning experiment B with calibration standards. Aqueous PCE concentration of standards and samples computed by Henry's law with K_H=0.59867. Calibration standards corrected for instrumental drift and instrumental blank.

Figure (38) Instrumental drift during PFOA analysis of partitioning experiment B by GC-MS, derived from blank measurements with integradted internal standard (PCNB) signal m/z=293 for two measuring sessions.
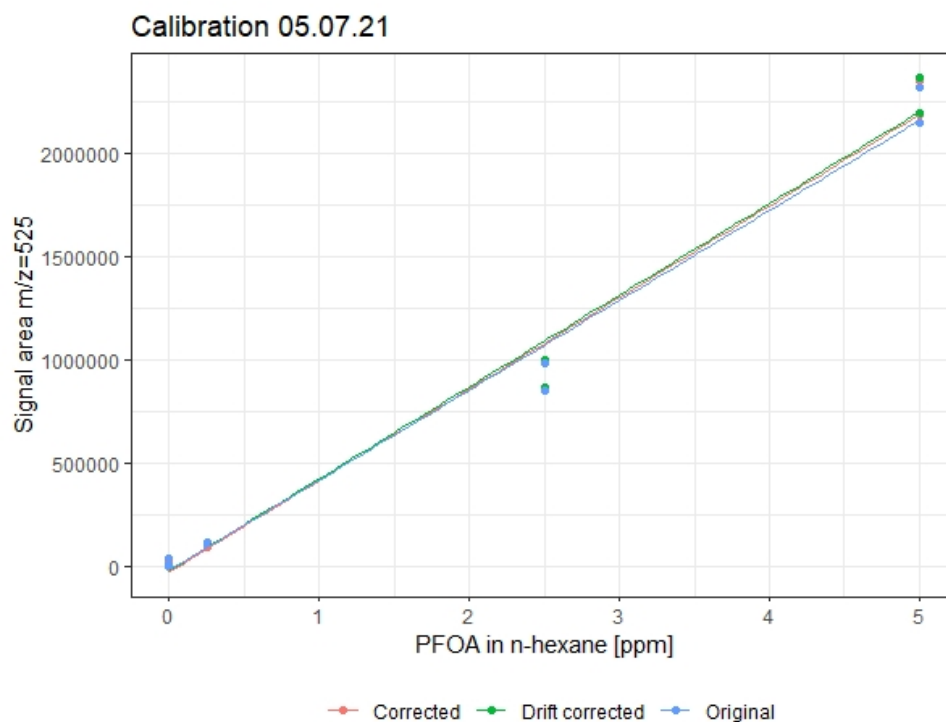
Figure (39) Comparisons of changes of calibration curves of GC-MS analysis for PFOA by correction for instrumental drift and processing blank measured 05.07.2021. Corrected calibration used for further processing of samples from partitioning experiment B with calibration standards in n-hexane analysis solution. Aqueous PFOA concentration of standards and samples computed by dilution factors during derivatization and porewater extraction.

Figure (40) Comparisons of changes of calibration curves of GC-MS analysis for PFOA by correction for instrumental drift and processing blank measured 07.07.2021. Corrected calibration used for further processing of samples from partitioning experiment B with calibration standards in n-hexane analysis solution. Aqueous PFOA concentration of standards and samples computed by dilution factors during derivatization and porewater extraction.
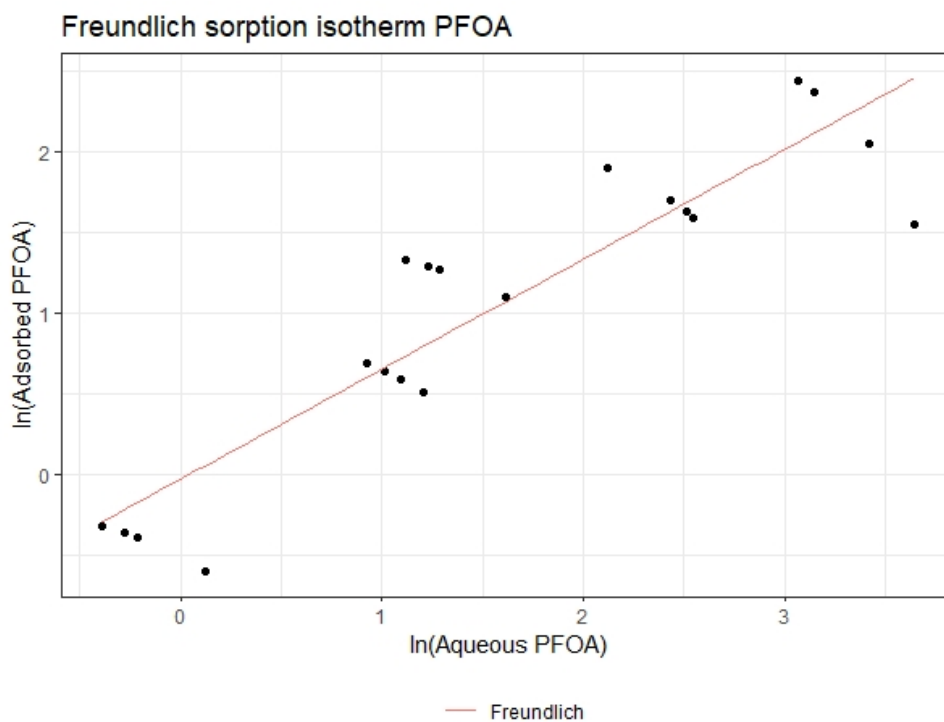
Figure (41) Double-natural-logarithm plot of the aqueous and the solid phase concentration of PFOA measured in partitioning experiment B to determine the coefficients of the Freundlich sorption isotherm. The slope in the lineary approximate ln-ln-plotted data described the exponent in the linear form (n), whereby the y-axis intersection describes the factor K_F of the linear form (here $ln(K_F)$).

Table (21) Porewater concentration of major anions with different initial concentrations of PFOA in soil one from partitioning experiment B analyzed by IC.

PFOA [ppm]	Na [ppm]	K [ppm]	Mg [ppm]	Ca [ppm]
0	7.666	8.407	2.572	192.904
2.5	8.187	6.030	5.024	276.969
7.5	8.596	8.414	5.890	298.104
12.5	8.747	7.494	7.093	340.207
25	8.486	7.920	5.151	260.997
50	8.224	7.004	3.785	230.009

8.1.5 Partitioning Experiment C

As for the other partitioning experiment the instrumental drift trend and the calibration curve for the PCE measurements of partitioning experiment are shown hereafter for the measurements performed on 15.07.2021 and 16.07.2021 in Figure 42 and Figure 43. Analogue figures are presented for the PFOA analyses performed on the 21.07.2021 and 23.07.2021 (Figure 44, Figure 45, Figure 46) as well as the double logarithmic plot of the PFOA concentrations for the derivation of the Freundlich isotherms in Figure 47. Furthermore the porewater concentrations of the major cations measured by IC and corrected for the dilution during the porewater extraction are shown in Table 22.
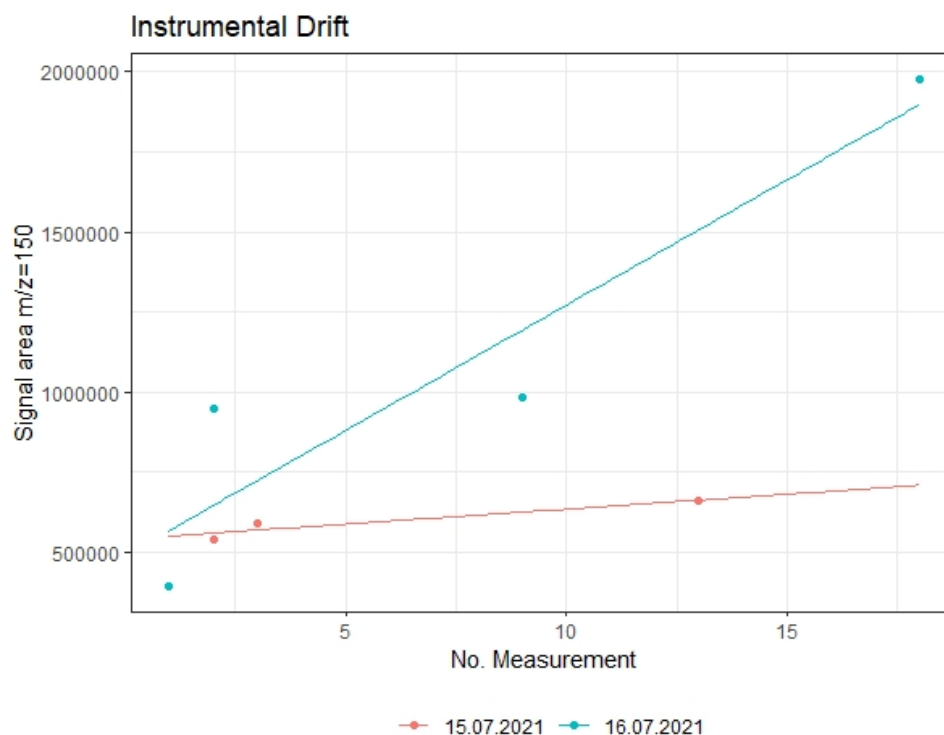
Figure (42) Instrumental drift during PCE analysis of partitioning experiment C by GC-MS, derived from blank measurements with integradted internal standard (1,2-Dichlorobenzene-d4) signal m/z=150 for three measuring sessions.
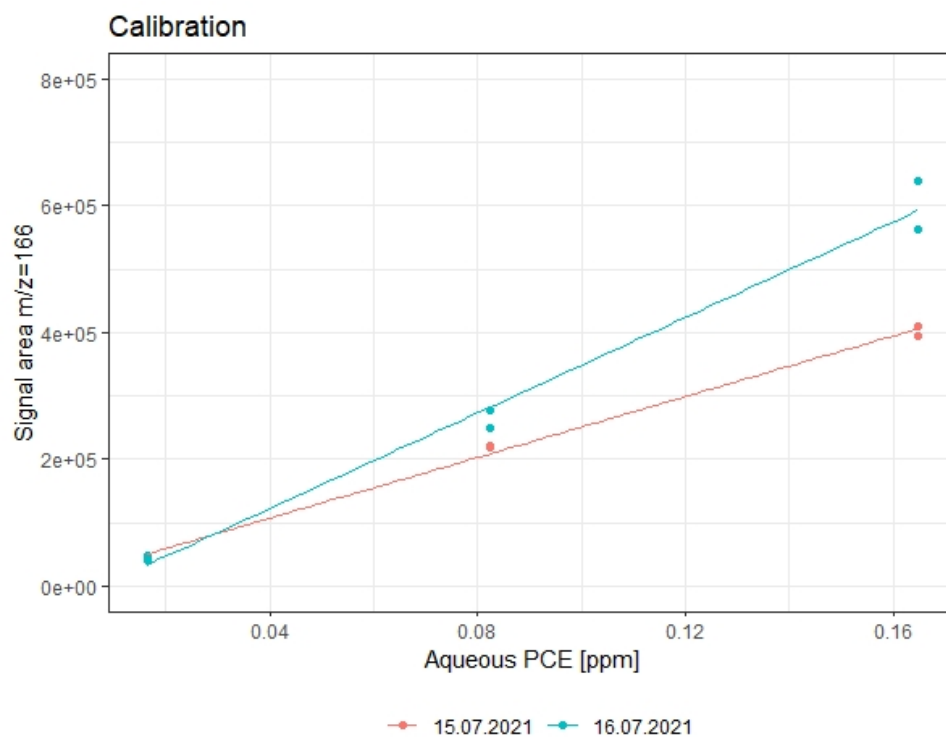
Figure (43) Calibration of GC-MS for PCE analysis of samples from partitioning experiment C with calibration standards. Aqueous PCE concentration of standards and samples computed by Henry's law with K_H=0.59867. Calibration standards corrected for instrumental drift and instrumental blank.
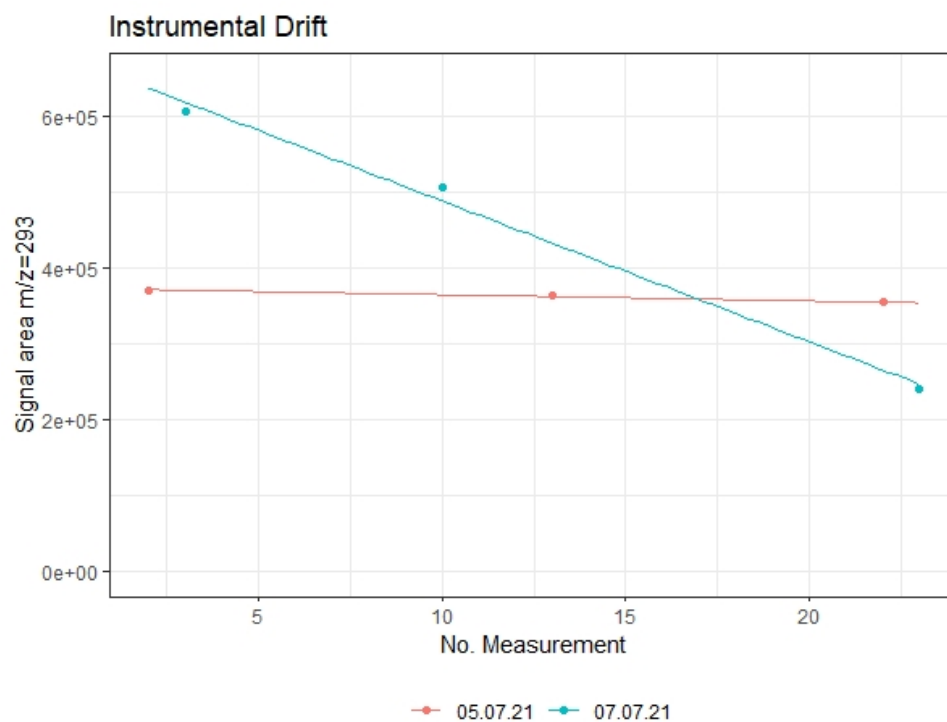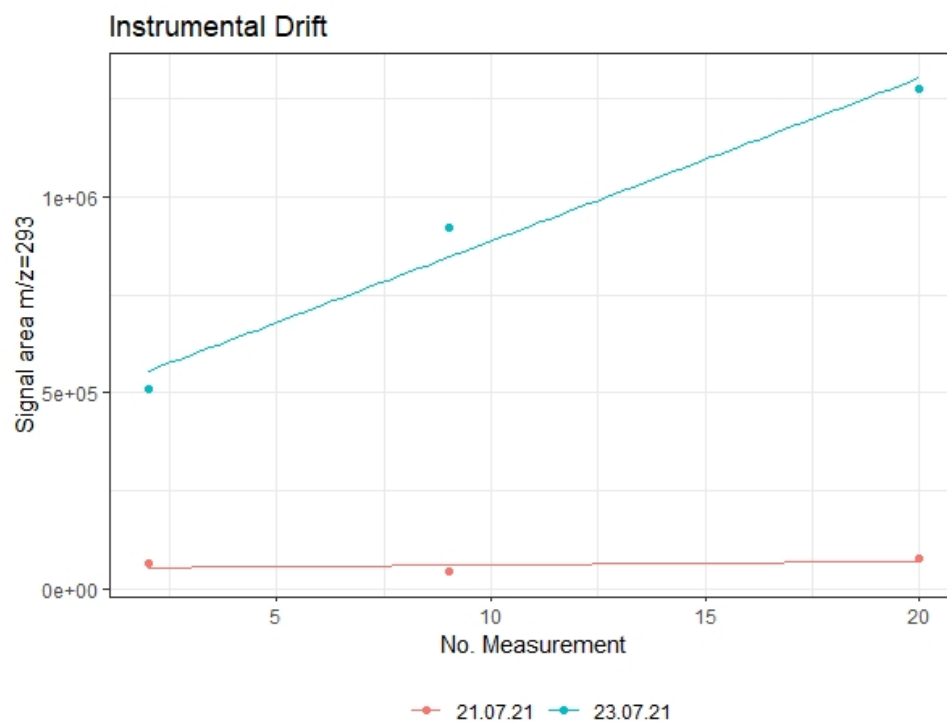
Figure (44) Instrumental drift during PFOA analysis of partitioning experiment C by GC-MS, derived from blank measurements with integradted internal standard (PCNB) signal m/z=293 for two measuring sessions.
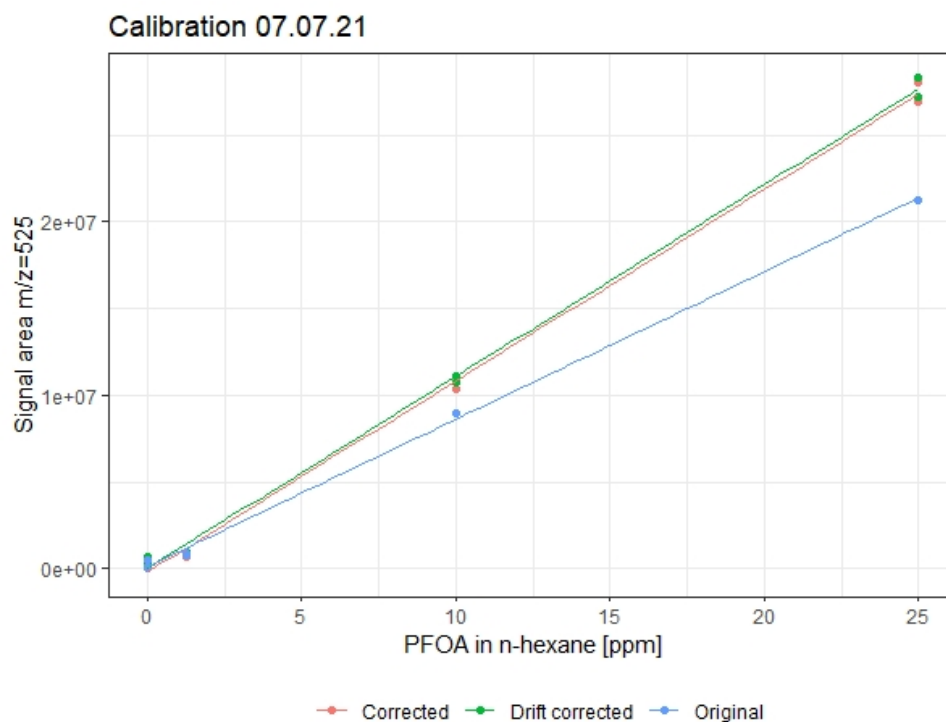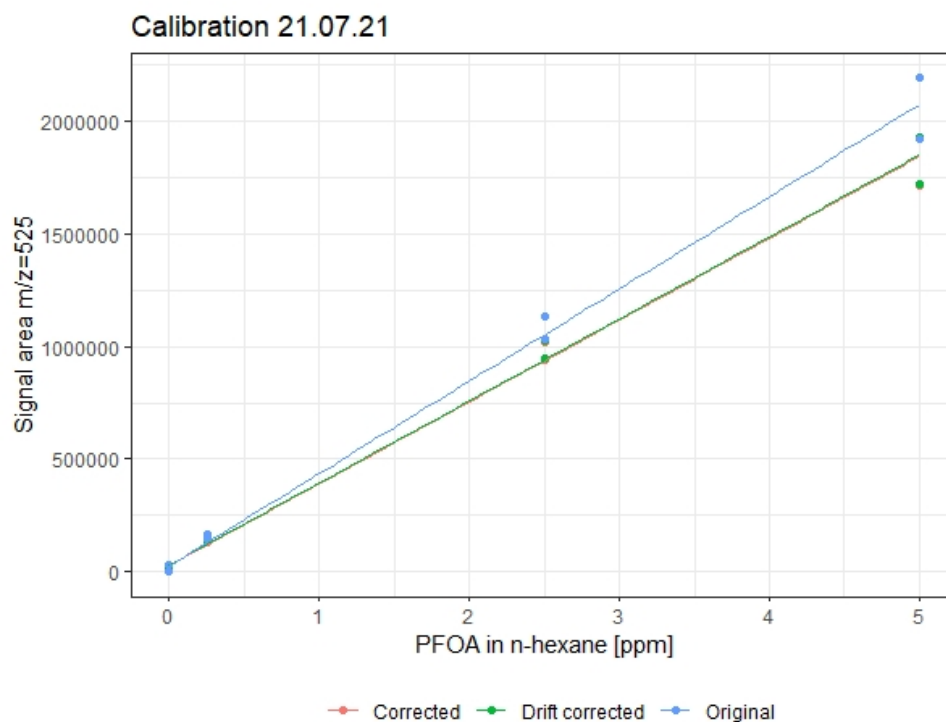
Figure (45) Comparisons of changes of calibration curves of GC-MS analysis for PFOA by correction for instrumental drift and processing blank measured 21.07.2021. Corrected calibration used for further processing of samples from partitioning experiment C with calibration standards in n-hexane analysis solution. Aqueous PFOA concentration of standards and samples computed by dilution factors during derivatization and porewater extraction.
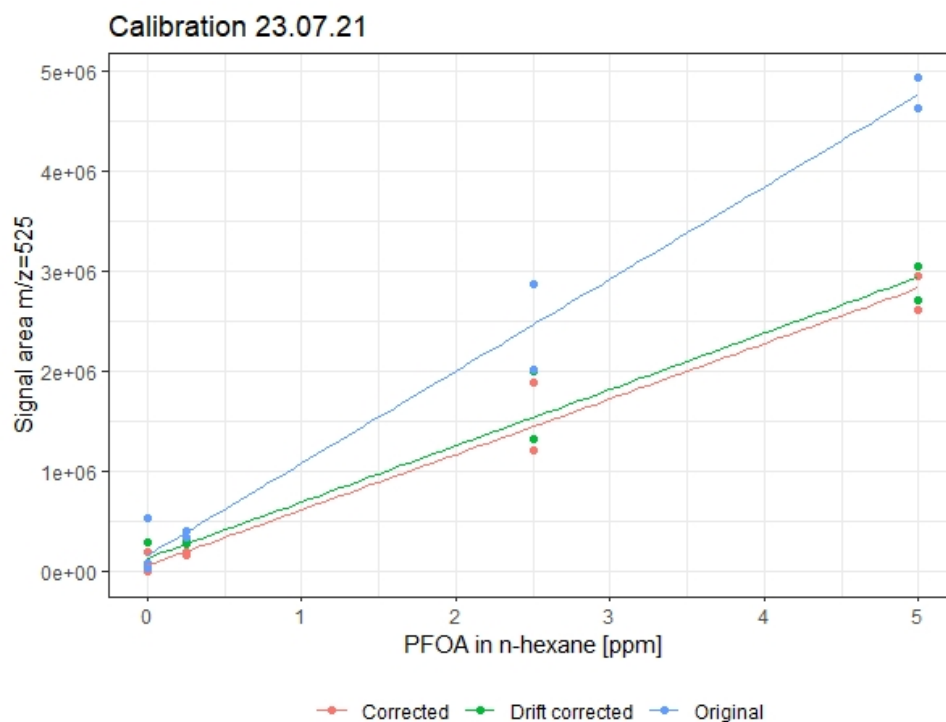
Figure (46) Comparisons of changes of calibration curves of GC-MS analysis for PFOA by correction for instrumental drift and processing blank measured 23.07.2021. Corrected calibration used for further processing of samples from partitioning experiment C with calibration standards in n-hexane analysis solution. Aqueous PFOA concentration of standards and samples computed by dilution factors during derivatization and porewater extraction.
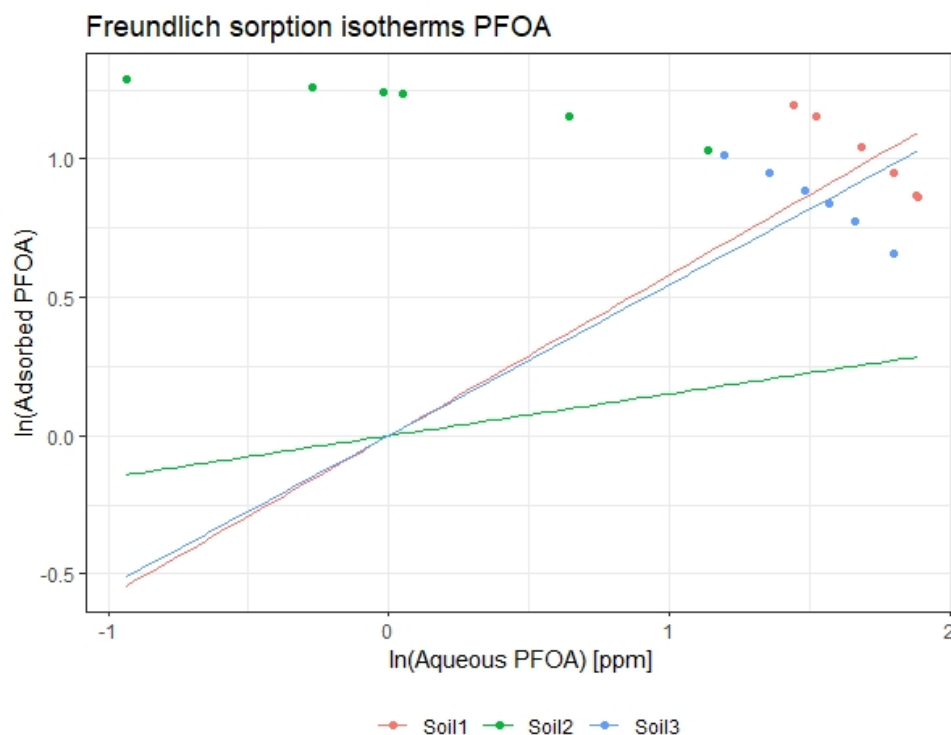
Figure (47) Double-natural-logarithm plot of the aqueous and the solid phase concentration of PFOA measured in partitioning experiment C to determine the coefficients of the Freundlich sorption isotherm. The slope in the lineary approximate ln-ln-plotted data described the exponent in the linear form (n), whereby the y-axis intersection is forced through the origin, which corresponds to a factor K_F of 1. The approximation for soil 2 is inadequate.

Table (22) Porewater concentration of major cations for blanks and contaminated of different soil samples from partitioning experiment C analyzed by IC.

	Element	Na	K	Mg	Ca
Soil	Type	[ppm]	[ppm]	[ppm]	[ppm]
Soil 1	Blank	7.649	3.148	5.412	255.768
	Sample	9.361	3.931	7.324	346.747
Soil 2	Blank	17.410	97.808	25.340	73.687
	Sample	16.011	90.446	19.989	59.482
Soil 3	Blank	7.903	6.103	1.911	3.502
	Sample	7.756	6.406	2.288	4.255

Table (23)   Linear correlation of soil parameter TOC as predictor for linear partitioning coefficients of PCE derived from results of partitioning experiment C. Statistical analysis performed with R using RStudio.

Model 1	Term	Estimate	Std.Error	Statistics	p-value
1	(Intercept)	-2.651882	2.213001	-1.198319	0.238622
2	TOC	3.630930	0.494650	7.340401	1.18E-08
		R2	0.5995	p-value:	1.18E-08

Table (24)   Linear correlation of soil parameter TOC and total cation concentration [*ppm*] as predictor for linear partitioning coefficients of PCE derived from results of partitioning experiment C. Statistical analysis performed with R using RStudio.

Model 2	Term	Estimate	Std.Error	Statistics	p-value
1	(Intercept)	3.589972	3.361746	1.067889	0.292881
2	TOC	3.656045	0.465913	7.847048	3.19E-09
3	Cations	-0.025062	0.010592	-2.366188	0.023638
		R2	0.6547	p-value:	8.28E-09

Table (25)   Linear correlation of soil parameter TOC and relative clay content [%] as predictor for linear partitioning coefficients of PCE derived from results of partitioning experiment C. Statistical analysis performed with R using RStudio.

Model 3	Term	Estimate	Std.Error	Statistics	p-value
1	(Intercept)	5.995872	5.472057	1.095726	0.280682
2	TOC	3.241658	0.532288	6.090041	5.88E-07
3	clay	-0.098421	0.057244	-1.719320	0.094390
		R2	0.6307	p-value:	2.69E-08

Table (26) Linear correlation of soil parameter TOC as predictor for linear partitioning coefficients of PFOA derived from results of partitioning experiment C. Statistical analysis performed with R using RStudio.

Model 1	Term	Estimate	Std.Error	Statistics	p-value
1	(Intercept)	-0.163465	0.621971	-0.262818	0.796045
2	TOC	0.412050	0.107891	3.819124	0.001511
		R2:	0.4769	p-value:	0.001511

Table (27) Linear correlation of soil parameter TOC and sum of cations [*ppm*] as predictor for linear partitioning coefficients of PFOA derived from results of partitioning experiment C. Statistical analysis performed with R using RStudio.

Model 2	Term	Estimate	Std.Error	Statistics	p-value
1	(Intercept)	0.160422	0.808251	0.198480	0.845334
2	TOC	0.423400	0.111311	3.803750	0.001730
3	Cations	-0.001811	0.002806	-0.645475	0.528370
		R2	0.491	p-value:	0.006314

Table (28) Linear correlation of soil parameter TOC and concentration of iron (Fe) and calcium (Ca) as predictor for linear partitioning coefficients of PFOA derived from results of partitioning experiment C. Statistical analysis performed with R using RStudio.

Model 3	Term	Estimate	Std.Error	Statistics	p-value
1	(Intercept)	-3.15562	3.22198	-0.97940	0.34400
2	TOC	0.59497	0.21365	2.78485	0.01461
3	[Fe]	0.22954	0.21492	1.06803	0.30358
4	[Ca]	0.00538	0.00755	0.71269	0.48775
		R2	0.5357	p-value:	0.01125

8.1.6 Incubation Experiment

As supplemental data for the incubation experiment the results of the monitored head-space content of methane and carbon dioxide during the soil training and incubation period for soil 1 a), soil 2 and soil 3 are presented in Figure 48, Figure 49 and Figure 50. Thereafter the instrumental drift trend and the corrected calibration curves for the PCE and PFOA measurements performed on the 03.08.2021, 04.08.2021, and 05.08.2021 for PCE and on the 11.08.2021, 13.08.2021, 16.08.2021 and 18.08.2021 for PFOA are depicted in Figure 51, Figure 52 and Figure 53 and Figure 54. Furthermore the relative mean mass balance derived for the Freundlich sorption isotherms is shown in Figure 55. Regarding the chemical porewater analysis the results for the major cations by IC are illustrated in Figure 29.
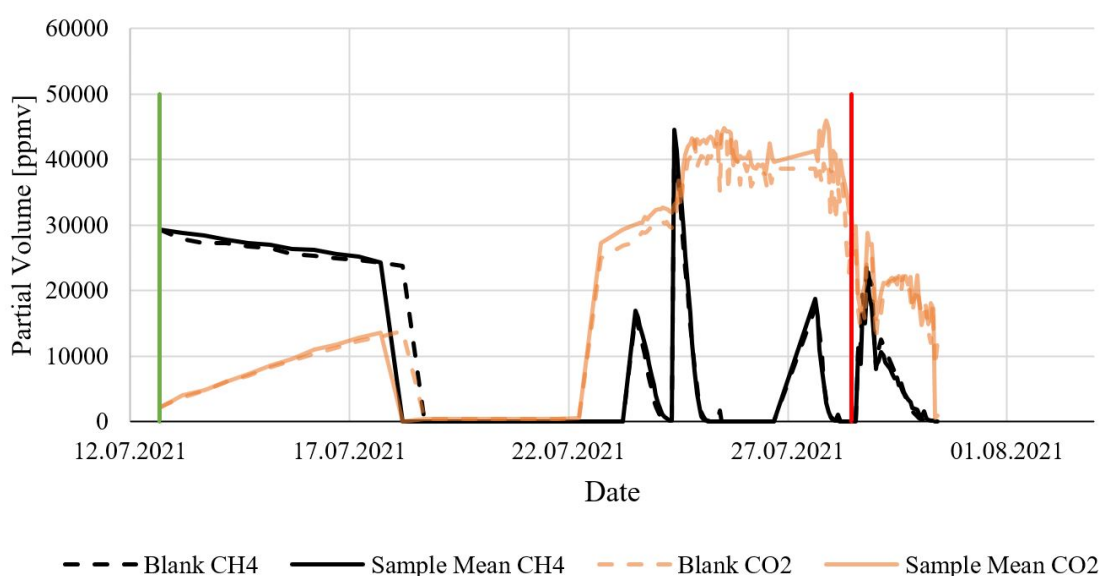
Figure (48) GC-monitored headspace content of methane and carbon dioxide for training period (12.07.2021 to 28.07.2021) and incubation period (28.07.2021 to 30.07.2021) for soil 1 a) for blank and mean of triplicated samples. The green line indicates the start of the methane consumption training, while the red line indicates the the addition of the contaminants.
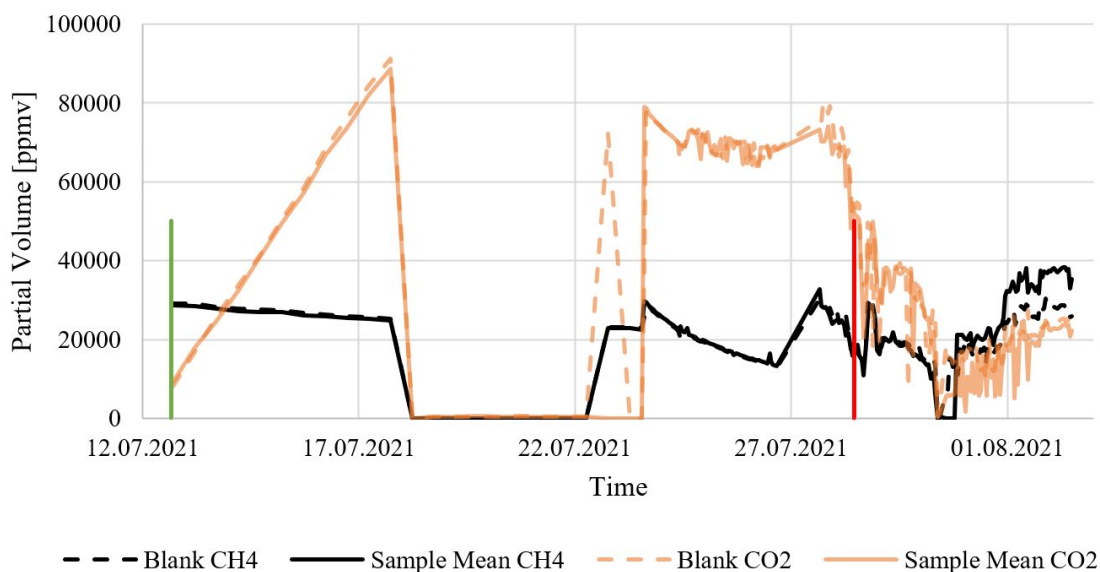
Figure (49) GC-monitored headspace content of methane and carbon dioxide for training period (12.07.2021 to 28.07.2021) and incubation period (28.07.2021 to 02.08.2021) for soil 2 for mean of dublicated blank and mean of dublicated contaminated samples. The green line indicates the start of the methane consumption training, while the red line indicates the the addition of the contaminants.
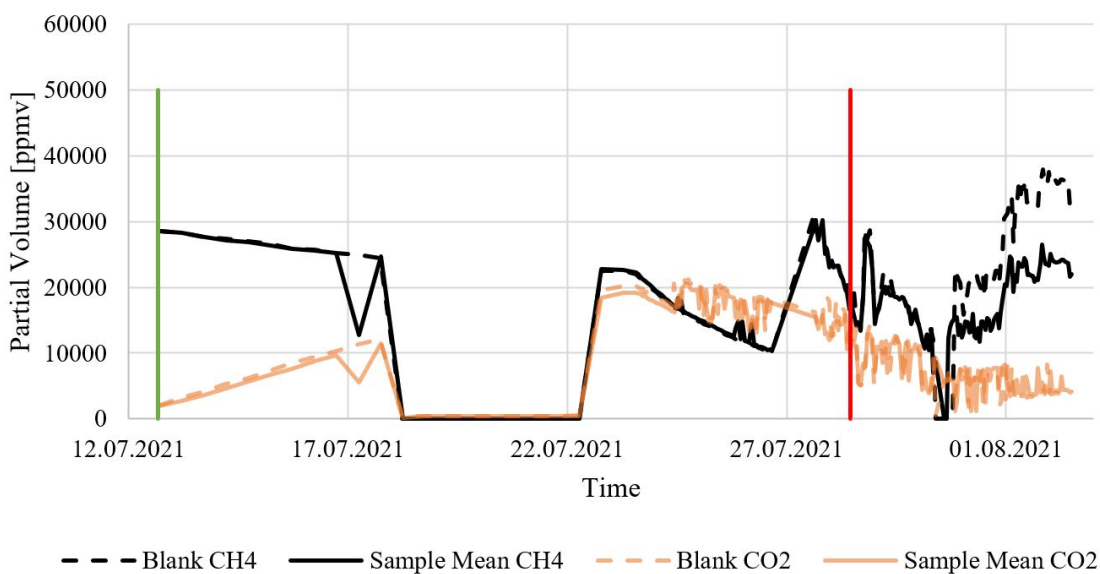
Figure (50) GC-monitored headspace content of methane and carbon dioxide for training period (12.07.2021 to 28.07.2021) and incubation period (28.07.2021 to 02.08.2021) for soil 3 for mean of dublicated blank and mean of dublicated contaminated samples. The green line indicates the start of the methane consumption training, while the red line indicates the the addition of the contaminants.
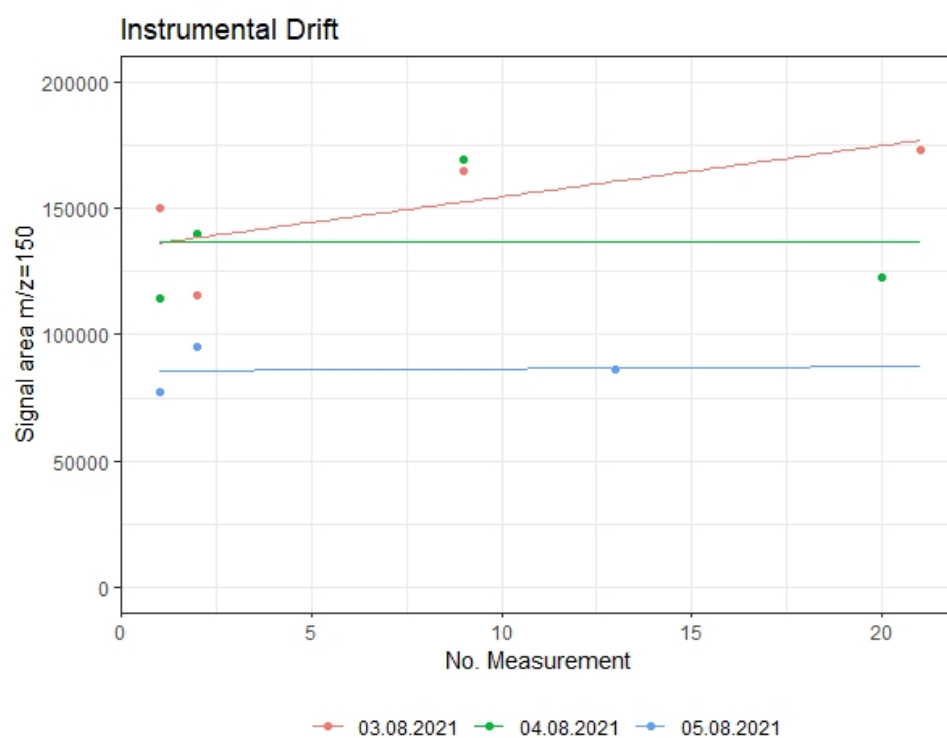
Figure (51) Instrumental drift during PCE analysis of incubation experiment A by GC-MS, derived from blank measurements with integradted internal standard (1,2-Dichlorobenzene-d4) signal m/z=150 for two measuring sessions.
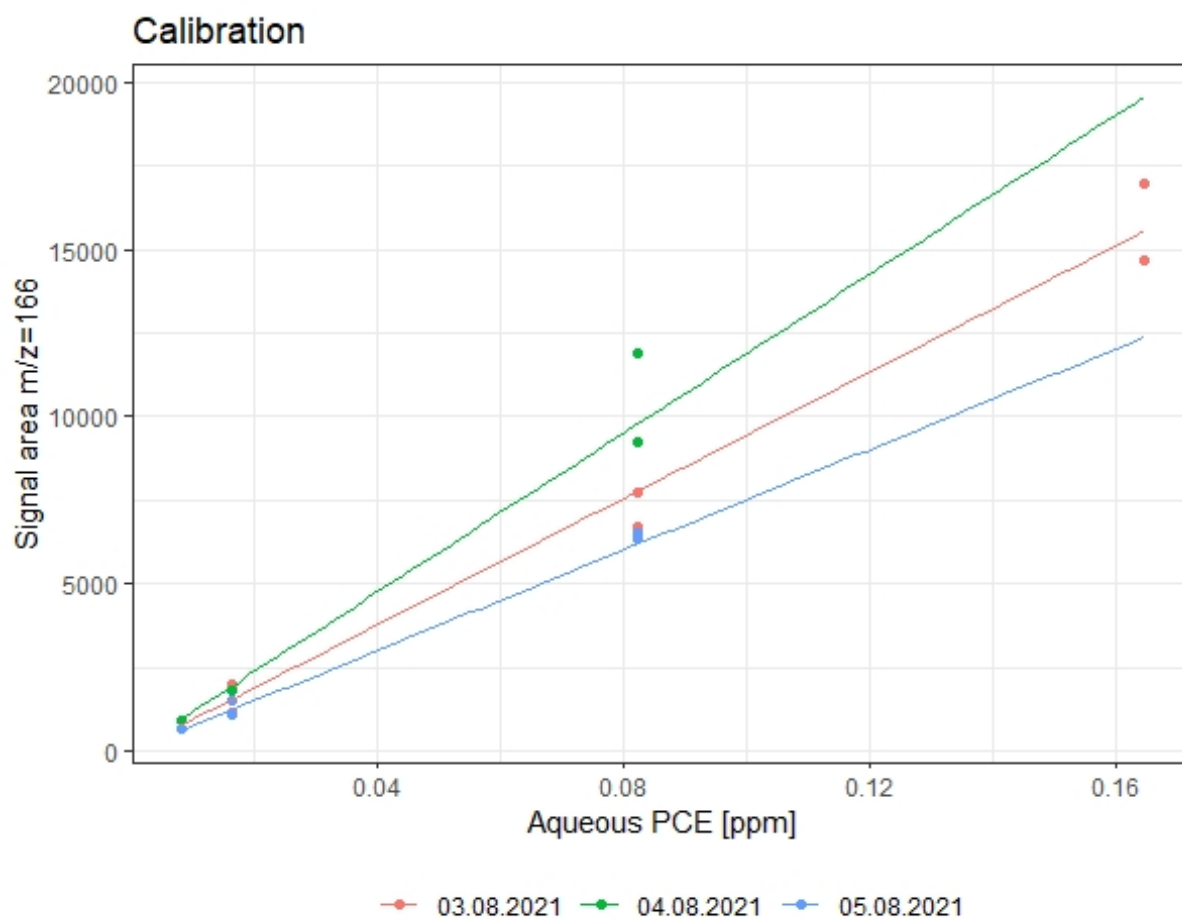
Figure (52) Calibration of GC-MS for PCE analysis of samples from incubation experiment A with calibration standards. Aqueous PCE concentration of standards and samples computed by Henry's law with K_H=0.59867. Calibration standards corrected for instrumental drift and instrumental blank.
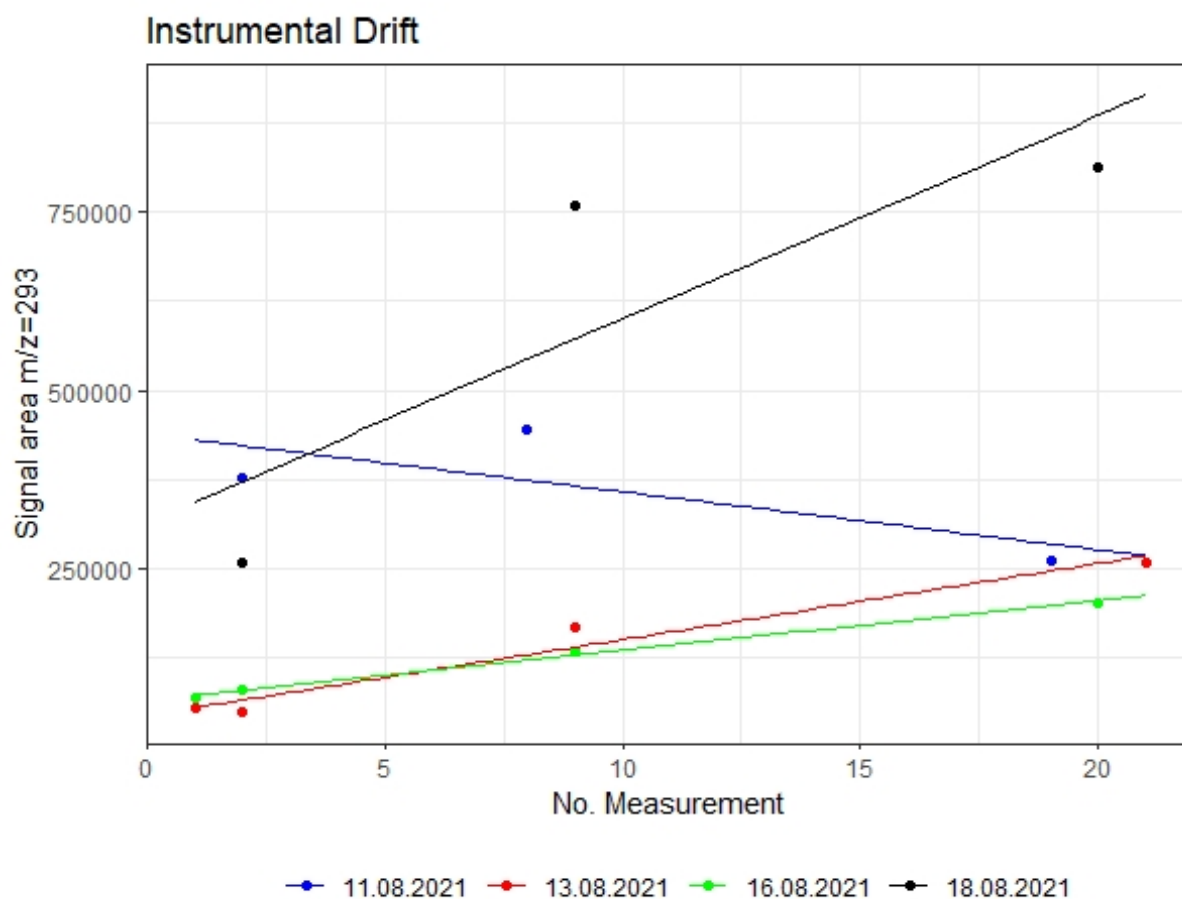
Figure (53) Instrumental drift during PFOA analysis of incubation experiment A by GC-MS, derived from blank measurements with integradted internal standard (PCNB) signal m/z=293 for four measuring sessions.
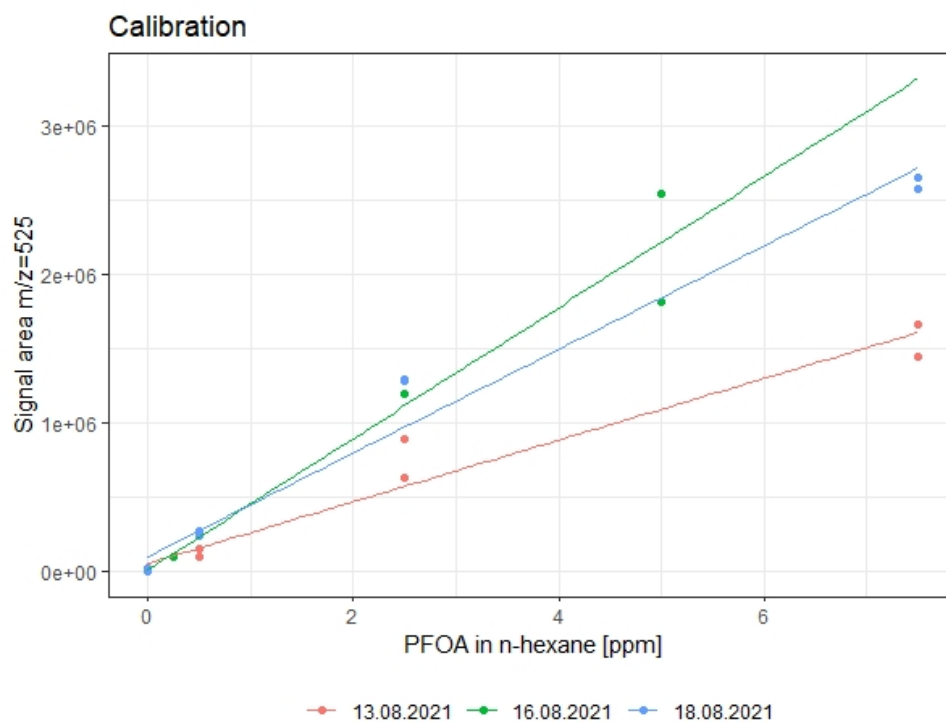
Figure (54) Corrected calibration curves for GC-MS analysis of PFOA of samples from incubation experiment A with calibration standards and samples in n-hexane analysis solution. Aqueous PFOA concentration of standards and samples computed by dilution factors during derivatization and porewater extraction. Calibration standards and samples corrected for instrumental drift and processing blank.
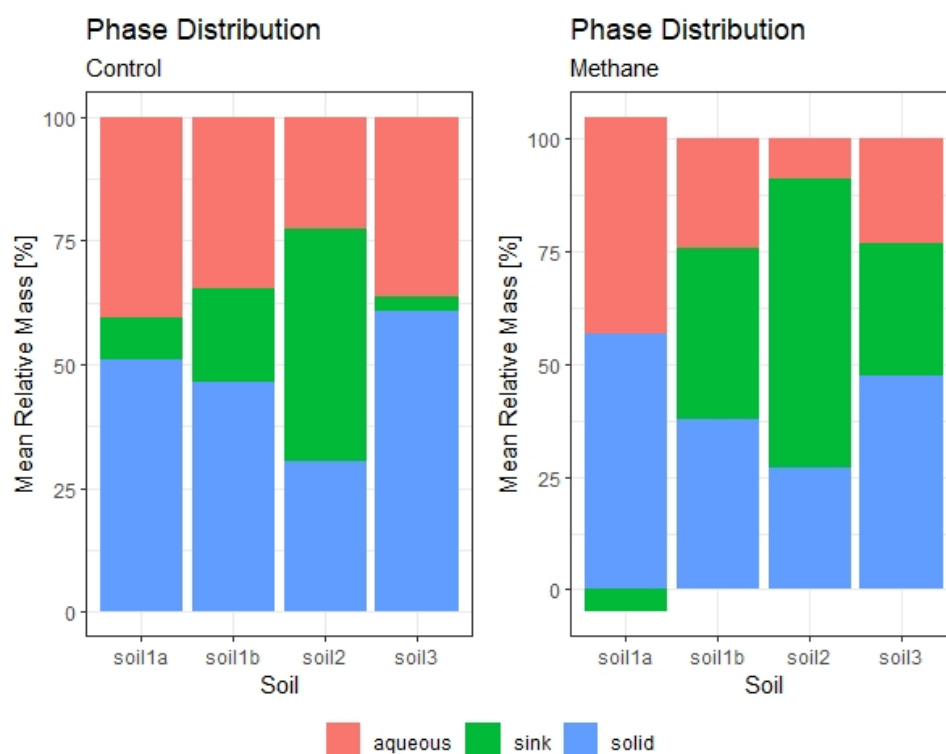
Figure (55) Relative mean mass distribution of PFOA between the aqueous and solid phase and the sink for the three different soil samples in the two different treatments of incubation experiment A. Solid phase concentrations computed from Freundlich isotherms derived in partitioning experiment C. Means were computed from replicated measurements of replica of same initial concentration.

Table (29) Porewater concentration of major cations for blanks and samples of incubation experiment A measured by IC.

Soil	Treatment	Element Type	Na [ppm]	K [ppm]	Mg [ppm]	Ca [ppm]
soil1a	Control	Blank	27.109	3.562	10.987	307.842
		Sample	26.503	3.043	10.511	286.416
	Methane	Blank	77.198	2.375	6.528	150.576
		Sample	23.425	3.093	6.710	164.904
soil1b	Control	Blank	25.424	2.819	10.616	309.804
		Sample	22.814	2.787	10.128	303.391
	Methane	Blank	5.027	1.747	3.955	164.654
		Sample	4.963	1.739	3.993	163.072
soil2	Control	Blank	42.829	75.879	13.018	52.174
		Sample	43.386	79.440	13.690	54.325
	Methane	Blank	8.602	65.984	5.015	20.821
		Sample	8.556	67.698	5.389	22.719
soil3	Control	Blank	34.484	7.617	3.623	13.341
		Sample	44.999	7.039	4.210	14.622
	Methane	Blank	6.969	7.639	0.763	1.781
		Sample	6.485	7.946	0.758	1.725

8.2 Instrumental setup and adjustments

Hereafter certain steps during the setup of the used GC-MS instrument are briefly described.

First of all the internal communication of the local network had to be adjusted to a static IP, which was given by the internal instrumental default settings to ensure a continuous communication of all instrument with the corresponding designated IP addresses. The motor oil of the vacuum pump for the MSD instrument was refilled to avoid the damaging of the pump and the computer system was replaced due to graphical communication errors. Beforehand the hard-drive was cloned to avoid losses of instrumental data, setting and access (e.g. product keys). Thereafter, a Miniature Helium Purifier (Vici Valco Instruments Co. Inc.) was installed in the carrier gas supply line to ensure a purification of the carrier gas and an improvement of the background signal. During the analyses an communication error in the local network occurred - caused by the malfunction of the network card in the GC instrument. The network card was substituted with an identical model without serial lock. Over several measuring sessions all available connections in the gas line were frequently retightend to encounter gas leakages. During the analysis the data acquisition rate was increased for the SIM-mode by adjusting the dwell tome from 1000 ms to 30 ms to improve the resolution.

Table (30) Comparison of GC-MS settings for analysis of PCE and PFOA.

	PCE	PFOA
GC-Settings		
Sample	Gas	Liquid
Injection	Manual	Manual
Injection volume	$50\mu l$	$1\mu l$
Injector Temp	$250°C$	$250°C$
Split/Splitless	Splitless	Splitless
Carrier Gas Flow	1ml/min, Helium	1ml/min, Helium
Column	Zebron Phenomenex ZB5	Zebron Phenomenex ZB5
Column dimensions	30m x $250\mu m$	30m x $250\mu m$
Film thickness	$0.25\mu m$	$0.25\mu m$
Oven Temperature	$35°C$ for 3min, $5°C$/min to $55°C$, hold 2min, $15°C$/min to $130°C$, hold for 1min	$50°C$ for 1min, $20°C$/min to $80°C$, hold for 2min, $10°C$/min to $150°C$, $50°C$/min to $300°C$, hold for 2min
Run time	15min	16.5min
MS-Settings		
Transfer Line Temp	$280°C$	$280°C$
Ion Source	EI (70eV)	EI (70eV)
Source Temp	$230°C$	$230°C$
Mass Analyzer	Quadrupole	Quadrupole
Acquisition Mode	SIM	SIM
Target m/z	166, 164, 150	525, 526, 293
Quadrupole Temp	$150°C$	$150°C$
Detector	HED	HED
Dwell time	30ms	20ms
Detector Temp	$240°C$	$240°C$
Tune file	atune	atune

References

Agency, U. E. P. (2016). *Health effects support document for perfluorooctanoic acid (pfoa).* Office of Water, May 2016, EPA 822-R-16-003.

Ahrens, L., Barber, J. L., Xie, Z., & Ebinghaus, R. (2009). Longitudinal and latitudinal distribution of perfluoroalkyl compounds in the surface water of the atlantic ocean. *Environmental science & technology*, *43*(9), 3122–3127.

Ahrens, L., Hedlund, J., Dürig, W., Tröger, R., & Wiberg, K. (2016). Screening of pfass in groundwater and surface water.

Anderson, R. H., Long, G. C., Porter, R. C., & Anderson, J. K. (2016). Occurrence of select perfluoroalkyl substances at us air force aqueous film-forming foam release sites other than fire-training areas: Field-validation of critical fate and transport properties. *Chemosphere*, *150*, 678–685.

Armitage, J. M., Schenker, U., Scheringer, M., Martin, J. W., MacLeod, M., & Cousins, I. T. (2009). Modeling the global fate and transport of perfluorooctane sulfonate (pfos) and precursor compounds in relation to temporal trends in wildlife exposure. *Environmental science & technology*, *43*(24), 9274–9280.

Bakken, L. (2020). *spreadsheet for gas kinetics.* (`https://www.nmbu.no/en/research/groups/nitrogen/spreadsheets-`)

Barber, J. L., Berger, U., Chaemfa, C., Huber, S., Jahnke, A., Temme, C., & Jones, K. C. (2007). Analysis of per-and polyfluorinated alkyl substances in air samples from northwest europe. *Journal of environmental monitoring*, *9*(6), 530–541.

Barry, V., Winquist, A., & Steenland, K. (2013). Perfluorooctanoic acid (pfoa) exposures and incident cancers among adults living near a chemical plant. *Environmental health perspectives*, *121*(11-12), 1313–1318.

Belisle, J., & Hagen, D. (1980). A method for the determination of perfluorooctanoic acid in blood and other biological samples. *Analytical biochemistry*, *101*(2), 369–376.

Blaine, A. C., Rich, C. D., Sedlacko, E. M., Hundal, L. S., Kumar, K., Lau, C., . . . Higgins, C. P. (2014). Perfluoroalkyl acid distribution in various plant compartments of edible crops grown in biosolids-amended soils. *Environmental science & technology*, *48*(14), 7858–7865.

Bolan, N. (2019). Pfas beyond defence. *Waste+ Water Management Australia*, *45*(6), 26–28.

Bolan, N., Sarkar, B., Yan, Y., Li, Q., Wijesekara, H., Kannan, K., . . . others (2021). Remediation of poly-and perfluoroalkyl substances (pfas) contaminated soils–to mobilize or to immobilize or to degrade? *Journal of hazardous materials*, *401*, 123892.

Bragg, W. H., & Bragg, W. L. (1913). The reflection of x-rays by crystals. *Proceedings of the Royal Society of London. Series A, Containing Papers of a Mathematical and Physical Character*, *88*(605), 428–438.

Brusseau, M. L. (2018). Assessing the potential contributions of additional retention processes to pfas retardation in the subsurface. *Science of the Total Environment*, *613*, 176–185.

Butt, C. M., Muir, D. C., & Mabury, S. A. (2014). Biotransformation pathways of fluorotelomer-based polyfluoroalkyl substances: A review. *Environmental toxicology and chemistry*, *33*(2), 243–267.

Buttet, G. F., Willemin, M. S., Hamelin, R., Rupakula, A., & Maillard, J. (2018). The membrane-bound c subunit of reductive dehalogenases: topology analysis and reconstitution of the fmn-binding domain of pcec. *Frontiers in microbiology*, *9*, 755.

Chatterjee, A., Lal, R., Wielopolski, L., Martin, M. Z., & Ebinger, M. (2009). Evaluation of different soil carbon determination methods. *Critical Reviews in Plant Science*, *28*(3), 164–178.

Chauhan, A., & Chauhan, P. (2014). Powder xrd technique and its applications in science and technology. *J Anal Bioanal Tech*, *5*(5), 1–5.

Cheremisinoff, N. P. (2016). *Perfluorinated chemicals (pfcs): contaminants of concern.* John Wiley & Sons.

Cousins, I. T., Goldenman, G., Herzke, D., Lohmann, R., Miller, M., Ng, C. A., ... others (2019). The concept of essential use for determining when uses of pfass can be phased out. *Environmental Science: Processes & Impacts*, *21*(11), 1803–1815.

Currie, R. C., Chiao, F., & McKone, T. E. (1994). Intermedia transfer factors for contaminants found at hazardous waste sites - tetrachloroethylene (pce). *The Department of Toxic Substances Control (DTSC) and the California Environmental Protection Agency in Support of the CalTOX model.* (`https://dtsc.ca.gov/wp-content/uploads/sites/31/2018/01/pce.pdf`)

Darlington, R., Barth, E., & McKernan, J. (2018). The challenges of pfas remediation. *The Military Engineer*, *110*(712), 58.

Darrow, L. A., Stein, C. R., & Steenland, K. (2013). Serum perfluorooctanoic acid and perfluorooctane sulfonate concentrations in relation to birth outcomes in the mid-ohio valley, 2005–2010. *Environmental health perspectives*, *121*(10), 1207–1213.

De Silva, A. O., Muir, D. C., & Mabury, S. A. (2009). Distribution of perfluorocarboxylate isomers in select samples from the north american environment. *Environmental Toxicology and Chemistry: An International Journal*, *28*(9), 1801–1814.

de Voogt, P., & Sáez, M. (2006). Analytical chemistry of perfluoroalkylated

substances. *TrAC Trends in Analytical Chemistry*, *25*(4), 326–342.

Doebelin, N., & Kleeberg, R. (2015). Profex: a graphical user interface for the rietveld refinement program bgmn. *Journal of applied crystallography*, *48*(5), 1573–1580.

Dreyer, A., Matthias, V., Weinberg, I., & Ebinghaus, R. (2010). Wet deposition of poly-and perfluorinated compounds in northern germany. *Environmental Pollution*, *158*(5), 1221–1227.

Dreyer, A., Weinberg, I., Temme, C., & Ebinghaus, R. (2009). Polyfluorinated compounds in the atmosphere of the atlantic and southern oceans: evidence for a global distribution. *Environmental science & technology*, *43*(17), 6507–6514.

Dufková, V., Čabala, R., Maradová, D., & Štícha, M. (2009). A fast derivatization procedure for gas chromatographic analysis of perfluorinated organic acids. *Journal of Chromatography A*, *1216*(49), 8659–8664.

Ellis, D. A., Martin, J. W., De Silva, A. O., Mabury, S. A., Hurley, M. D., Sulbaek Andersen, M. P., & Wallington, T. J. (2004). Degradation of fluorotelomer alcohols: a likely atmospheric source of perfluorinated carboxylic acids. *Environmental science & technology*, *38*(12), 3316–3321.

for Research on Cancer, I. A. (2016). *Perfluorooctanoic acid.* IARC Monographs-110.

Ge, J., Huang, S., Han, I., & Jaffé, P. R. (2019). Degradation of tetra-and trichloroethylene under iron reducing conditions by acidimicrobiaceae sp. a6. *Environmental Pollution*, *247*, 248–255.

Giesy, J. P., & Kannan, K. (2001). Global distribution of perfluorooctane sulfonate in wildlife. *Environmental science & technology*, *35*(7), 1339–1342.

Grandel, S., & Dahmke, A. (2008). Natürliche schadstoffminderung bei lckw-kontaminierten standorten methoden, empfehlungen und hinweise zur untersuchung und beurteilung. In *Christian-albrechts-universität zu kiel.*

Hansen, K. J., Clemen, L. A., Ellefson, M. E., & Johnson, H. O. (2001). Compound-specific, quantitative characterization of organic fluorochemicals in biological matrices. *Environmental science & technology*, *35*(4), 766–770.

Hellsing, M. S., Josefsson, S., Hughes, A. V., & Ahrens, L. (2016). Sorption of perfluoroalkyl substances to two types of minerals. *Chemosphere*, *159*, 385–391.

Higgins, C. P., Field, J. A., Criddle, C. S., & Luthy, R. G. (2005). Quantitative determination of perfluorochemicals in sediments and domestic sludge. *Environmental science & technology*, *39*(11), 3946–3956.

Hoff, P. T., Scheirs, J., Van de Vijver, K., Van Dongen, W., Esmans, E. L., Blust, R., & De Coen, W. (2004). Biochemical effect evaluation of perfluorooctane sulfonic acid-contaminated wood mice (apodemus sylvaticus). *Environmental*

health perspectives, *112*(6), 681–686.

Hoff, P. T., Van de Vijver, K., Van Dongen, W., Esmans, E. L., Blust, R., & De Coen, W. M. (2003). Perfluorooctane sulfonic acid in bib (trisopterus luscus) and plaice (pleuronectes platessa) from the western scheldt and the belgian north sea: distribution and biochemical effects. *Environmental Toxicology and Chemistry: An International Journal*, *22*(3), 608–614.

Horváthová, H., Lászlová, K., & Dercová, K. (2018). Bioremediation of pcb-contaminated shallow river sediments: the efficacy of biodegradation using individual bacterial strains and their consortia. *Chemosphere*, *193*, 270–277.

Houde, M., Martin, J. W., Letcher, R. J., Solomon, K. R., & Muir, D. C. (2006). Biological monitoring of polyfluoroalkyl substances: a review. *Environmental science & technology*, *40*(11), 3463–3473.

Huang, S., & Jaffé, P. R. (2019). Defluorination of perfluorooctanoic acid (pfoa) and perfluorooctane sulfonate (pfos) by acidimicrobium sp. strain a6. *Environmental science & technology*, *53*(19), 11410–11419.

ITRC, I. T. . R. C. (2021). *Pfas technical and regulatory guidance document and fact sheets pfas-1.* (https://pfas-1.itrcweb.org/)

Jahnke, A., Ahrens, L., Ebinghaus, R., Berger, U., Barber, J. L., & Temme, C. (2007). An improved method for the analysis of volatile polyfluorinated alkyl substances in environmental air samples. *Analytical and bioanalytical chemistry*, *387*(3), 965–975.

Jahnke, A., Ahrens, L., Ebinghaus, R., & Temme, C. (2007). Urban versus remote air concentrations of fluorotelomer alcohols and other polyfluorinated alkyl substances in germany. *Environmental Science & Technology*, *41*(3), 745–752.

Kärrman, A., Ericson, I., van Bavel, B., Darnerud, P. O., Aune, M., Glynn, A., ... Lindström, G. (2007). Exposure of perfluorinated chemicals through lactation: levels of matched human milk and serum and a temporal trend, 1996–2004, in sweden. *Environmental health perspectives*, *115*(2), 226–230.

Kelly, B. C., Ikonomou, M. G., Blair, J. D., Surridge, B., Hoover, D., Grace, R., & Gobas, F. A. (2009). Perfluoroalkyl contaminants in an arctic marine food web: trophic magnification and wildlife exposure. *Environmental science & technology*, *43*(11), 4037–4043.

Key, B. D., Howell, R. D., & Criddle, C. S. (1997). Fluorinated organics in the biosphere. *Environmental science & technology*, *31*(9), 2445–2454.

Langlois, I., Berger, U., Zencak, Z., & Oehme, M. (2007). Mass spectral studies of perfluorooctane sulfonate derivatives separated by high-resolution gas chromatography. *Rapid Communications in Mass Spectrometry: An International Journal Devoted to the Rapid Dissemination of Up-to-the-Minute Research in Mass Spectrometry*, *21*(22), 3547–3553.

Lath, S., Knight, E. R., Navarro, D. A., Kookana, R. S., & McLaughlin, M. J. (2019). Sorption of pfoa onto different laboratory materials: Filter membranes and centrifuge tubes. *Chemosphere*, *222*, 671–678.

Lau, C., Anitole, K., Hodes, C., Lai, D., Pfahles-Hutchens, A., & Seed, J. (2007). Perfluoroalkyl acids: a review of monitoring and toxicological findings. *Toxicological sciences*, *99*(2), 366–394.

Li, F., Fang, X., Zhou, Z., Liao, X., Zou, J., Yuan, B., & Sun, W. (2019). Adsorption of perfluorinated acids onto soils: Kinetics, isotherms, and influences of soil properties. *Science of the total environment*, *649*, 504–514.

Li, Y., Oliver, D. P., & Kookana, R. S. (2018). A critical analysis of published data to discern the role of soil and sediment properties in determining sorption of per and polyfluoroalkyl substances (pfass). *Science of the Total Environment*, *628*, 110–120.

Li, Z., & Sun, H. (2020). Cost-effective detection of perfluoroalkyl carboxylic acids with gas chromatography: optimization of derivatization approaches and method validation. *International journal of environmental research and public health*, *17*(1), 100.

Liu, J., & Avendaño, S. M. (2013). Microbial degradation of polyfluoroalkyl chemicals in the environment: a review. *Environment international*, *61*, 98–114.

Liu, J., Lee, L. S., Nies, L. F., Nakatsu, C. H., & Turco, R. F. (2007). Biotransformation of 8: 2 fluorotelomer alcohol in soil and by soil bacteria isolates. *Environmental science & technology*, *41*(23), 8024–8030.

Liu, J., Wang, N., Szostek, B., Buck, R. C., Panciroli, P. K., Folsom, P. W., ... Bellin, C. A. (2010). 6-2 fluorotelomer alcohol aerobic biodegradation in soil and mixed bacterial culture. *Chemosphere*, *78*(4), 437–444.

Lundström, U. S., van Breemen, N., & Bain, D. (2000). The podzolization process. a review. *Geoderma*, *94*(2-4), 91–107.

Mahinroosta, R., & Senevirathna, L. (2020). A review of the emerging treatment technologies for pfas contaminated soils. *Journal of environmental management*, *255*, 109896.

Martin, J. W., Kannan, K., Berger, U., Voogt, P. D., Field, J., Franklin, J., ... others (2004). Peer reviewed: analytical challenges hamper perfluoroalkyl research. *Environmental science & technology*, *38*(13), 248A–255A.

Martin, J. W., Smithwick, M. M., Braune, B. M., Hoekstra, P. F., Muir, D. C., & Mabury, S. A. (2004). Identification of long-chain perfluorinated acids in biota from the canadian arctic. *Environmental science & technology*, *38*(2), 373–380.

McMurry, J. E., Fay, R. C., & Robinson, J. K. (2008). Chemistry (5th ed.).

Miao, Y., Guo, X., Peng, D., Fan, T., & Yang, C. (2017). Rates and equilibria

of perfluorooctanoate (pfoa) sorption on soils from different regions of china. *Ecotoxicology and environmental safety*, *139*, 102–108.

Milinovic, J., Lacorte, S., Vidal, M., & Rigol, A. (2015). Sorption behaviour of perfluoroalkyl substances in soils. *Science of the Total Environment*, *511*, 63–71.

Mitchell, J. (1932). Origin, nature, and importance of soil organic constituents having base exchange properties. *Journal of the American Society of Agronomy*.

Montagnolli, R. N., Lopes, P. R. M., Cruz, J. M., Claro, E. M. T., Quiterio, G. M., & Bidoia, E. D. (2017). The effects of fluoride based fire-fighting foams on soil microbiota activity and plant growth during natural attenuation of perfluorinated compounds. *Environmental toxicology and pharmacology*, *50*, 119–127.

Moody, C. A., & Field, J. A. (2000). Perfluorinated surfactants and the environmental implications of their use in fire-fighting foams. *Environmental science & technology*, *34*(18), 3864–3870.

Munoz, G., Labadie, P., Botta, F., Lestremau, F., Lopez, B., Geneste, E., . . . Budzinski, H. (2017). Occurrence survey and spatial distribution of perfluoroalkyl and polyfluoroalkyl surfactants in groundwater, surface water, and sediments from tropical environments. *Science of the Total Environment*, *607*, 243–252.

Murray, A. M., Maillard, J., Jin, B., Broholm, M. M., Holliger, C., & Rolle, M. (2019). A modeling approach integrating microbial activity, mass transfer, and geochemical processes to interpret biological assays: An example for pce degradation in a multi-phase batch setup. *Water research*, *160*, 484–496.

Nadeem, S., Bakken, L. R., Frostegard, A., Gaby, J. C., & Dörsch, P. (2020). Contingent effects of liming on n2o-emissions driven by autotrophic nitrification. *Frontiers in Environmental Science*, *8*, 245.

Nakayama, H. (1967). Krafft temperatures of perfluoro-octanoic acid and of its salts. *Bulletin of the Chemical Society of Japan*, *40*(7), 1592–1595.

Olsen, G. W., Huang, H.-Y., Helzlsouer, K. J., Hansen, K. J., Butenhoff, J. L., & Mandel, J. H. (2005). Historical comparison of perfluorooctanesulfonate, perfluorooctanoate, and other fluorochemicals in human blood. *Environmental health perspectives*, *113*(5), 539–545.

Parsons, J. R., Sáez, M., Dolfing, J., & De Voogt, P. (2008). Biodegradation of perfluorinated compounds. *Reviews of Environmental Contamination and Toxicology Vol 196*, 53–71.

Pei, Y., & Chen, P. Y. (1977). Table of key lines in x-ray powder diffraction patterns of minerals in clays and associated rocks.

Post, G. B., Gleason, J. A., & Cooper, K. R. (2017). Key scientific issues in

developing drinking water guidelines for perfluoroalkyl acids: Contaminants of emerging concern. *PLoS biology*, *15*(12), e2002855.

Prevedouros, K., Cousins, I. T., Buck, R. C., & Korzeniowski, S. H. (2006). Sources, fate and transport of perfluorocarboxylates. *Environmental science & technology*, *40*(1), 32–44.

Rather, J. B. (1918). An accurate loss-on-ignition method for the determination of organic matter in soils. *Industrial & Engineering Chemistry*, *10*(6), 439–442.

Renner, R. (2001). Growing concern over: Perfluorinated chemicals. *Environmental science & technology*, *35*(7), 154A–160A.

Ross, I., McDonough, J., Miles, J., Storch, P., Thelakkat Kochunarayanan, P., Kalve, E., . . . Burdick, J. (2018). A review of emerging technologies for remediation of pfass. *Remediation Journal*, *28*(2), 101–126.

Rotander, A., Toms, L.-M. L., Aylward, L., Kay, M., & Mueller, J. F. (2015). Elevated levels of pfos and pfhxs in firefighters exposed to aqueous film forming foam (afff). *Environment international*, *82*, 28–34.

Sabaté, J., Vinas, M., & Solanas, A. (2004). Laboratory-scale bioremediation experiments on hydrocarbon-contaminated soils. *International biodeterioration & biodegradation*, *54*(1), 19–25.

Scott, B. F., Moody, C. A., Spencer, C., Small, J. M., Muir, D. C., & Mabury, S. A. (2006). Analysis for perfluorocarboxylic acids/anions in surface waters and precipitation using gc- ms and analysis of pfoa from large-volume samples. *Environmental science & technology*, *40*(20), 6405–6410.

Scott, B. F., Spencer, C., Marvin, C. H., MacTavish, D. C., & Muir, D. C. (2002). Distribution of haloacetic acids in the water columns of the laurentian great lakes and lake malawi. *Environmental science & technology*, *36*(9), 1893–1898.

Shahsavari, E., Rouch, D., Khudur, L. S., Thomas, D., Aburto-Medina, A., & Ball, A. S. (2021). Challenges and current status of the biological treatment of pfas-contaminated soils. *Frontiers in Bioengineering and Biotechnology*, 1493.

Shi, Y., Vestergren, R., Xu, L., Song, X., Niu, X., Zhang, C., & Cai, Y. (2015). Characterizing direct emissions of perfluoroalkyl substances from ongoing fluoropolymer production sources: A spatial trend study of xiaoqing river, china. *Environmental pollution*, *206*, 104–112.

Sima, M. W., & Jaffé, P. R. (2020). A critical review of modeling poly-and perfluoroalkyl substances (pfas) in the soil-water environment. *Science of the Total Environment*, 143793.

Sinclair, E., & Kannan, K. (2006). Mass loading and fate of perfluoroalkyl surfactants in wastewater treatment plants. *Environmental science & technology*, *40*(5), 1408–1414.

Skutlarek, D., Exner, M., & Färber, H. (2006). Perfluorierte tenside (pft) in der aquatischen umwelt und im trinkwasser. *Umweltwissenschaften und Schadstoff-Forschung*, *18*(3), 151–154.

Starling, A. P., Adgate, J. L., Hamman, R. F., Kechris, K., Calafat, A. M., Ye, X., & Dabelea, D. (2017). Perfluoroalkyl substances during pregnancy and offspring weight and adiposity at birth: examining mediation by maternal fasting glucose in the healthy start study. *Environmental health perspectives*, *125*(6), 067016.

Sunderland, E. M., Hu, X. C., Dassuncao, C., Tokranov, A. K., Wagner, C. C., & Allen, J. G. (2019). A review of the pathways of human exposure to poly- and perfluoroalkyl substances (pfass) and present understanding of health effects. *Journal of exposure science & environmental epidemiology*, *29*(2), 131–147.

Teaf, C. M., Garber, M. M., Covert, D. J., & Tuovila, B. J. (2019). Perfluorooctanoic acid (pfoa): environmental sources, chemistry, toxicology, and potential risks. *Soil and Sediment Contamination: An International Journal*, *28*(3), 258–273.

Van Loon, G., & Duffy, S. (2005). Environmental chemistry.: Oxford university press inc. *New York*, *308*.

Vierke, L., Möller, A., & Klitzke, S. (2014). Transport of perfluoroalkyl acids in a water-saturated sediment column investigated under near-natural conditions. *Environmental pollution*, *186*, 7–13.

Wang, Z., Boucher, J. M., Scheringer, M., Cousins, I. T., & Hungerbuhler, K. (2017). Toward a comprehensive global emission inventory of c4–c10 perfluoroalkanesulfonic acids (pfsas) and related precursors: focus on the life cycle of c8-based products and ongoing industrial transition. *Environmental science & technology*, *51*(8), 4482–4493.

Wang, Z., Cousins, I. T., Scheringer, M., Buck, R. C., & Hungerbühler, K. (2014). Global emission inventories for c4–c14 perfluoroalkyl carboxylic acid (pfca) homologues from 1951 to 2030, part i: production and emissions from quantifiable sources. *Environment international*, *70*, 62–75.

Wania, F. (2007). A global mass balance analysis of the source of perfluorocarboxylic acids in the arctic ocean. *Environmental science & technology*, *41*(13), 4529–4535.

Washington, J. W., Henderson, W. M., Ellington, J. J., Jenkins, T. M., & Evans, J. J. (2008). Analysis of perfluorinated carboxylic acids in soils ii: optimization of chromatography and extraction. *Journal of Chromatography A*, *1181*(1-2), 21–32.

Weathers, T. S., Harding-Marjanovic, K., Higgins, C. P., Alvarez-Cohen, L., & Sharp, J. O. (2016). Perfluoroalkyl acids inhibit reductive dechlorination

of trichloroethene by repressing dehalococcoides. *Environmental science & technology*, *50*(1), 240–248.

Wiedemeier, T. H., Rifai, H. S., Newell, C. J., & Wilson, J. T. (1999). *Natural attenuation of fuels and chlorinated solvents in the subsurface.* John Wiley & Sons.

Yeung, L., & Mabury, S. (2016). *Are humans exposed to increasing amounts of unidentified organofluorine? environ chem 13 (1): 102–110.*

Zareitalabad, P., Siemens, J., Hamer, M., & Amelung, W. (2013). Perfluorooctanoic acid (pfoa) and perfluorooctanesulfonic acid (pfos) in surface waters, sediments, soils and wastewater–a review on concentrations and distribution coefficients. *Chemosphere*, *91*(6), 725–732.

Zeebe, R. E., & Wolf-Gladrow, D. (2001). *Co2 in seawater: equilibrium, kinetics, isotopes* (No. 65). Gulf Professional Publishing.

Zhang, D., Zhang, W., & Liang, Y. (2019). Adsorption of perfluoroalkyl and polyfluoroalkyl substances (pfass) from aqueous solution-a review. *Science of The Total Environment*, *694*, 133606.

Zhang, Y., Lai, S., Zhao, Z., Liu, F., Chen, H., Zou, S., . . . Ebinghaus, R. (2013). Spatial distribution of perfluoroalkyl acids in the pearl river of southern china. *Chemosphere*, *93*(8), 1519–1525.

Zhao, S., Fan, Z., Sun, L., Zhou, T., Xing, Y., & Liu, L. (2017). Interaction effects on uptake and toxicity of perfluoroalkyl substances and cadmium in wheat (triticum aestivum l.) and rapeseed (brassica campestris l.) from co-contaminated soil. *Ecotoxicology and environmental safety*, *137*, 194–201.